FRICTION SURFACE DEVELOPMENT AND ITS STRUCTURE ON CARBON FIBRE REINFORCED SILICON CARBIDE DISC

Thesis submitted for the degree of

Doctor of Philosophy

at the Loughborough University

by

Yuan Wang

Supervisor: Dr. Houzheng Wu

Department of materials-Loughborough University

September 2011

Table of Content

Acknowledgements

I gratefully acknowledge the financial support by EPSRC/TSB through Rebrake project. I also would like to acknowledge the academic supports of my supervisor, Dr. Houzheng Wu. Thanks should be given to Mr John Bates, Dr. Zhaoxia Zhou, and Dr. David Ross for their technical support on FEGSEM, TEM and MEF3 optical microscopy.

Abbreviations

MMC: Metal matrix composite

CCC: Carbon fibre reinforced carbon composite

C_f/C-SiC: Carbon fibre reinforced silicon carbide composite

Al-SiC : silicon carbide reinforced aluminium composite

COF: Coefficient of friction

FEGSEM: Field emission gun scanning electron microscopy

TEM: Transmission electron microscopy

DBFIB: Dual beam focused ion beam microscopy

NAO: Non-asbestos organic

CVI: Chemical vapour infiltration

PIP: Liquid polymer infiltration

LSI: Liquid silicon infiltration

CFRP: Carbon fibre reinforced polymer

RTM: Resin transfer moulding

UCD: Unidirectional carbon fibre

CC: Chopped carbon fibre

List of tables

List of figures

Abstract

Carbon fibre reinforced ceramic composites (C_f/C-SiC) have been explored as lightweight and durable disc in a friction brake. This composite was manufactured through infiltration of liquid silicon into a C_f/C perform. It has heterogeneous microstructure, composed of three key phases, silicon carbide, C_f/C, and un-reacted residual silicon. The development of the transfer layer on the friction surface of C_f/C-SiC was studied through microstructural image registration of the surface after a range of braking stops on a laboratory-scale dynamometer test rig. When an organic pad was used as the counter face brake pad, it was found that a steady transfer layer was developed in silicon regions right after initial stops; in carbon-fibre/carbon (C_f/C) regions and most of the silicon carbide region, the friction surfaces were unsteady and any possible friction transfer layers were hardly built up. Large voids and cracks/crevices likely became pools to quickly and efficiently collect the transferred materials generated by the friction, but the compacts formed inside the pools were susceptible to be stripped off by further braking operation. Three types of friction surfaces were generalized: type I, the friction transfer layer had a steady relationship with the matrix and respectable longevity; type II, the transfer layer had an unstable relationship with the matrix and poor durability; type III, the friction transfer layer had a steady relationship with the matrix but short lifetime.

After testing against organic pads under the laboratory scale dynamometer testing condition, the friction surface of each key phase in C_f/C-SiC composites disc was studied by transmission electron microscopy (TEM). It was found that the transfer layer developed on Si consists of fine particles of metal silicides, silicates and minerals. The substrate damage of Si was not observed, while the precipitates having high oxygen content were found in the substrate. Formation of an interfacial bonding between transfer layer and silicon substrate is believed to be the key factor for the formation of a stable transfer layer on Si. However, the interfacial bonding between transferred materials and SiC was not detected. Kinks are common features developed on the friction surface of SiC. The interface between carbon fibre and carbon matrix was experienced mechanical damage, in form of microcracks, and the transferred material was developed in the interface. Instead of transfer layer, a thin amorphous film, produced by friction induced amorphisation of carbon fibre, was developed on top of carbon fibre.

Keywords: Friction, transfer layer, friction layer, friction film, brake disc, friction material, C_f/C-SiC, friction surface analysis, dynamometer testing, deformation of friction surface, microcracks

Chapter 1 Introduction

1.1 Background

Brake systems are important safety devices to slow down moving cars, trains and airplanes. The major components of the disc-type brake systems are brake disc and brake pad. Since its first invention, massive efforts were made to improve the brake performance. From the friction material point of view, researchers and engineers have been focusing on materials selection for disc and pad as well as understanding of their tribological behaviour.

It is known that a transfer layer with a thickness of several to tens of micrometres is developed when brake pads are set to against traditional brake discs, made of grey cast iron[1]. This transfer layer originates from accumulation and compaction of wear debris (materials removed from the contact surface of friction pair). In the development of pad materials for grey cast iron discs, one major focus is on the development and sustainability of friction transfer layer on the contact surfaces of both pad and disc. It is generally believed that it is these layers, rather than the bulk materials themselves, that give the friction couple the expected level and stability of coefficient of friction.

Carbon fibre reinforced ceramic composites have progressively been used as discs for friction brakes in vehicles in order to benefit from the light weight and long durability that the combination of carbon fibres (as reinforcements) and ceramic constituents (as matrix) can provide when they are appropriately engineered together through controlling the microstructure of the composites [2]. So far, few studies, however, have

been published on the development of friction surface on the ceramic composites disc, and its impact on friction performance of brakes[3]. It has been noticed that the friction performance of these composites is generally different from metallic materials. Such a distinction could lead to some difficulties in implementing knowledge and experiences that have been accumulated for a long period of time in the development of pad materials for metallic discs. As a consequence, it creates the potential problem of fulfilling the full benefits that C_f/C-SiC can provide. A further understanding is therefore needed to underpin possible mechanisms of friction surface development on C_f/C-SiC, which could govern the friction behaviour of C_f/C-SiC composites when they are engaged with pad materials. Such an understanding is likely to provide guidelines not only for the development of the pad materials, but also for any further attempts to optimise the microstructure of the C_f/C-SiC composites or their friction bearing surfaces in order to achieve the required friction performance of these friction brakes.

1.2 Aim and Objective

The aim of this research is to experimentally study the development of the friction surface on a C_f/C-SiC composite disc during the friction process, and to understand the impact on friction performance of brakes. Objectives of the research include:

(1) Experimental observation of the development process of the friction surface on a C_f/C-SiC disc.

(2) Studying the microstructure of the friction surface on the C_f/C-SiC disc, including: transfer layer; near-surface substrate, and; the interface between transfer layer and near-surface substrate.

(3) A study of the influence of the transfer layer development on the coefficient of friction values of the C_f/C-SiC disc paired with selected organic pad.

Chapter 2 Literature review

2.1Introduction

2.1.1 Why is a brake needed in a broader area?

Brake systems are invented and created to slow down a car, a train and an airplane etc… There are two types of brake system, drum brake and disc brake. There are several major components of a modern disc brake system: the brake disc, calliper, hydraulic actuation system and brake pad assemblies which consist of friction lining material, backing plates and other components. The brake disc is rigidly mounted onto the axle hub and rotates with the wheel (Figure 2-1).

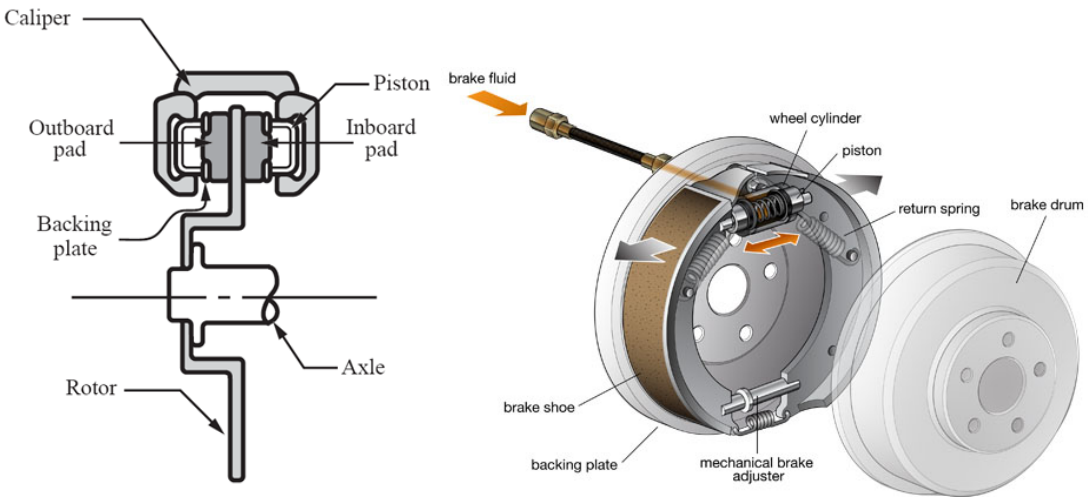

Figure 2-1 (a) Cross-section of a simplified disc brake. The wheel (not shown) is attached to the axle flange. The disc brake shown in this Figure has a fixed caliper[4] (b) assembling of drum brake[5]

When the driver pushes the brake pedal, the master cylinder converts the motion of the brake pedal to hydraulic pressure. Through the hydraulic line, the pressure is applied to the calliper piston, which is in contact with the brake pads. The movement of the calliper piston will then actuate a pair of pads pressed against the disc[6]. When

the brake disc and pad contact with each other, the kinetic energy of a vehicle travelling with some speed are converted into thermal energy within the sliding interface, via friction, by which the vehicle is decelerated. Due to the configuration of the brake disc and pads in a disc brake system, the location of the point of contact where the friction is generated also provides a mechanical moment to resist the turning motion of the rotor[6]. Brake discs are critical components within a frictional disc brake system as they provide contact surfaces for brake pads which are required to provide the stopping power. Pads pass a hydraulic compressive force via the brake callipers onto the brake disc allowing the vehicle to reduce speed as a result of the frictional force.

In drum brake systems, the drum brakes consist of a backing plate, brake shoes, brake drum, wheel cylinder, return springs and an automatic or self-adjusting system, as schematically illustrated in Figure 2-1(b). When the brakes is applied, brake fluid is forced under pressure into the wheel cylinder, which in turn pushes the brake shoes into contact with the inside surface of the drum, which is attached to the wheel, causing the wheel to stop. When the pressure is released, return springs pull the brake shoes back to their rest position[5].

Compared to drum brake, disc brakes offer better stopping performance, because the disc is more readily cooled. As a consequence, discs are less prone to the brake fade, caused when brake components overheat. In addition, disc brakes recover more quickly under wet conditions. Water tends to stay there until it is heated sufficiently to vaporize, at which point braking efficiency is fully restored. These features make disc brakes popular on sports cars, where they were first introduced, since these vehicles require more demanding brake performance. Disc brakes have now became the more common form in most passenger vehicles, although many use drum brakes on the rear wheels to keep costs and weight down. As the front brakes take most of the braking effort, this can be a reasonable compromise[7].

2.1.2 History of the disc brake

Disc-style brakes began in England in the 1890s; the first ever automobile disc brake was patented by Frederick William Lanchester in his Birmingham factory in 1902[8]. The early brake designs were substantially modified during the twentieth century. In particular, both the materials and actuation methods used have been much improved. Brake technology in the aerospace industry was developed quickly during the Second World War. The disc brake used in aircraft is of a clutch type, friction pads contact the disc in an annular region which extends over most of the disc (the angular extent). In contrast, in spot-type disc brakes, which are now used in car, the angular extent of the friction pads ranges from 30° to 50° [6]. Reliable modern spot-type disc brakes were developed in the UK by Dunlop[6], their disc brakes were similar to those present in automotive vehicles today.

2.1.3 Materials for brake discs

The role of brake disc is to react with brake pads and convert the kinetic energy of motion into thermal energy (heat) by means of friction. The amount of heat produced depends on the vehicle weight and speed at the moment that the brakes are applied. For example, when a vehicle weighing 1500 kg, is braked from 90 mile per hour to 0 mile per hour, the friction can cause the brake discs to reach, in a very short periods of time, surface temperatures in the region of 800°C. This can result in a thermal gradient between the surface and the core of the brake disc – sometimes in excess of 500°C [9]. Therefore, to reduce the thermal stress resulting from the repeated thermal cycling experienced during brake applications, the large amount of heat generated must be absorbed and dissipated as quickly as possible. Thus, a brake disc material should have a combination of the following properties: good specific heat capacity, good thermal conductivity, relatively low thermal coefficient of expansion, reasonably high strength at elevated temperatures and easy to manufacture[10].

Manufacturers choose disc brake materials according to their brake application. For normal cars and light trucks, the most popular disc material is grey cast iron. In racing and very high performance road cars, other disc materials have been employed, such as metal matrix composite (MMC) and carbon fibre reinforced ceramic disc.

2.1.3.1 Metal based brake disc

The vast majority of normal road car brake discs have been produced in grey cast iron, which has a pearlitic matrix[11] and graphite flakes in the pearlitic matrix[12]. It has the advantage of having a good combination of properties, e.g. relatively high thermal conductivity (40-72 W/m. ^{o}C), tensile strength (100-450 MPa)[13], and a working temperature range of 400-600^{o}C[14]. Grey cast iron is a type of low cost material and easy to manufacture by a casting process. However, the disadvantage of this material is the high density, typically 6.9-7.35 g/cm^{3} [2]. Improvements in fuel economy have led to interest in the replacement of the traditional cast iron brake disc with lighter weight alternatives[15].

Compared with grey cast iron, aluminium-based MMCs have densities of 2.8-3.0 g/cm^{3} , which can lead to a much lighter weight brake disc with a thermal conductivity two to three times higher than grey cast iron. The operating temperature for Al-MMC discs is limited to 400 °C[15], ventilation fins have to be designed to increase the air flow and cooling, which ensures the operation temperature is no longer exceeding the maximum service temperature[15]. The price of Al-MMC brake disc is approximately 2-3 times of grey cast iron disc due to the cost of material and less easy manufacture process[16]. These disadvantages restrict the wider application of Al-MMC.

2.1.3.2 Ceramic based disc materials

Carbon fibre reinforced carbon composite, called C_f/C composite, brake discs have been used in both aircraft and formula sports cars [15, 17]. This type of composite consists

of a carbonaceous matrix reinforced by carbon fibres, which lead to a low density (of about 1.8g/cm^3) brake disc material[15]. This type of composite combines the advantage of high specific strength and the stiffness of carbon fibres with the refractory properties of the carbon matrix[15].

The cost of C_f/C composite is nearly 100 times that of grey cast iron disc partly due to its high manufacturing cost[16]. Moreover, it suffers from oxidation when temperatures exceeds 500^{o}C in air, although a protective coating can improve the operation temperature[18,19]. Another drawback is that the coefficient of friction is unstable and insufficient below 150°C, which is heavily affected by humidity[2].

Carbon fibre reinforced silicon carbide (C_f/C–SiC) is a new generation of brake disc material. Compared with C_f/C composites, C_f/C-SiC composites provide improved oxidation resistance, a more stable coefficient of friction in humid and in a broard temperature regime[2,20]. This type of composite has a density of about 2 g/cm^3 [20]. The combination of these properties makes this type of material desirable for brakes in heavy duty and high speed conditions. As examples of successful application in brakes, SGL Group-The carbon company have been equipped C_f/C-SiC composite disc on luxury road cars, such as the Audi S8 and the Veyron[21].

2.1.4 Development of pad materials

The first brake lining material was a cotton-based material impregnated with bitumen solution, invented by Herbert Frood in 1897. They were later replaced with moulded materials containing crysotile asbestos fibres in the 1920's. In the 1950's, resin-bonded metallic linings were introduced. In the past decade, a multitude of different brake pads, having their own unique composites, have been developed[22] .

A commercial brake lining usually contains more than 10 different constituents. They are often categorized into four classes of ingredients: (a) binders, which hold

components of brake lining together, e.g. phenolic resin, cyanate ester resin, thermoplastic polyimide resin; (b) fillers, which reduce the cost and improve the manufacturability of brake lining material, e.g. barium sulphate, calcium carbonate, mica, vermiculite, rubber dust, cashew dust; (c) friction additives, which determine the frictional properties of brake pads and comprise a mixture of abrasives and lubricants, e.g. graphite, metal sulphides (tin sulphide, lead sulphide), metal oxides (aluminium oxide, quartz), metal silicates(zirconium silicate); (d) reinforcements, which provide mechanical strength for brake lining material (e.g. steel fibre, iron powder, brass chips, carbon fibre, glass fibre, Kevlar fibre, ceramic fibres, ceramic particles)[23,24]. Types of pad, as often called, are listed as follow:

(a) Asbestos organic lining: Asbestos fibres are used as reinforcement in the formulation. However, asbestos was banned to use in brake lining material in 1993, as medical research showed that it can lodge in the lungs and induce adverse respiratory conditions [25];
(b) Nonasbestos organic lining (NAO), which use a variety of fibres as alternatives of asbestos[25], e.g. nylon fibres;
(c) Semi-metallic lining (or resin-bonded metallic): Semi-metalic linings typically comprise about 65 wt% total iron content, 10-25 wt% steel wool, about 15 wt% graphite and 10 wt% organic binder[25].
(d) Metallic brake linings: Metallic brake linings can be based on either copper or iron, often with inorganic additives to improve performance. Most of them are solid-state sintered. These have been developed and used for heavy duty brakes and racing car[25].

(e) Carbon based brake linings: Carbon based brake linings, such as carbon-carbon, were developed for friction against C_f/C brake disc material. For example, aircraft disc brakes and racing cars, where light weight brake lining materials are needed [25].

2.2 C_f/C-SiC composites brake disc

The manufacturing method and microstructure of C_f/C-SiC composite brake discs are briefly reviewed in this session before introducing their friction surface and friction performance.

A C_f/C-SiC composite is composed of SiC matrix reinforced with carbon fibres. The composites can be manufactured through three main classes of processing method, chemical vapour infiltration (CVI) [26, 27, 28, 29, 30], liquid polymer infiltration (PIP) [31,32,33, 34, 35, 36, 37] and liquid silicon infiltration (LSI) [38, 39, 40, 41, 42, 43, 44]. In the CVI route, gaseous precursors, e.g. CH_3SiCl_3, infiltrate into a porous carbon fibre architecture and decompose into SiC at moderate temperatures (900-1100^{o}C)[26,30]. During the CVI process, also a densification process, the SiC is deposited on the fibre surface. To avoid the rapid sealing of the pore entrance by the deposition, the rate of densification is maintained at a relatively low level [45,46].

In the first step of PIP-process, the carbon fibre preform is impregnated with a polymer precursor through, for instance, resin transfer moulding (RTM), a technique commonly used for polymer matrix composites. Different polymer precursors can be used in PIP-process, such as, polycarbosilanes and polyvinylsilanes [35,36,37]. In the second step, the impregnated fibre preform is cured thermally to obtain a carbon fibre reinforced polymer (CFRP) green body. Then, the CFRP is pyrolysed at a temperature ranging from 1000 ^{o}C to 1200^{o}C to form C_f/C-SiC composite [31-37]. Normally, the C_f/C-SiC composites have porous structure after pyrolysis and the porosity largely open as the gaseous by-products produced by pyrolysis of cured polymer escape from composites. Hence, several impregnation/pyrolysis sequences have to be performed, in order to achieve a high enough densification level [31-37].

In the LSI-process, a porous carbon fibre preform is first infiltrated with carbon by CVI process to produce C_f/C composite[20, 38-42], or impregnated with polymer by PIP process to produce CFRP[39,43,44]. In this PIP process, liquid polymer precursor, such as phenolic resin or pitch, is utilised to impregnate the network of the C_f perform. The CFRP is then converted into porous C_f/C by pyrolysis at 900°C to produce carbon[39,43,44]. In the second step, the residual open porosity in C_f/C is filled with liquid silicon (melting temperature is 1414°C) which is infiltrated by capillary forces in the porous network of C_f/C and reacts with pyrolytic carbon to generate SiC matrix [39,43,44]. Among these methods, the LSI is the attractive method for manufacture of C_f/C-SiC disc as it is a time and cost effective process[47]. The manufacture methods of C_f/C-SiC composites are schematically illustrated in Figure 2-2.

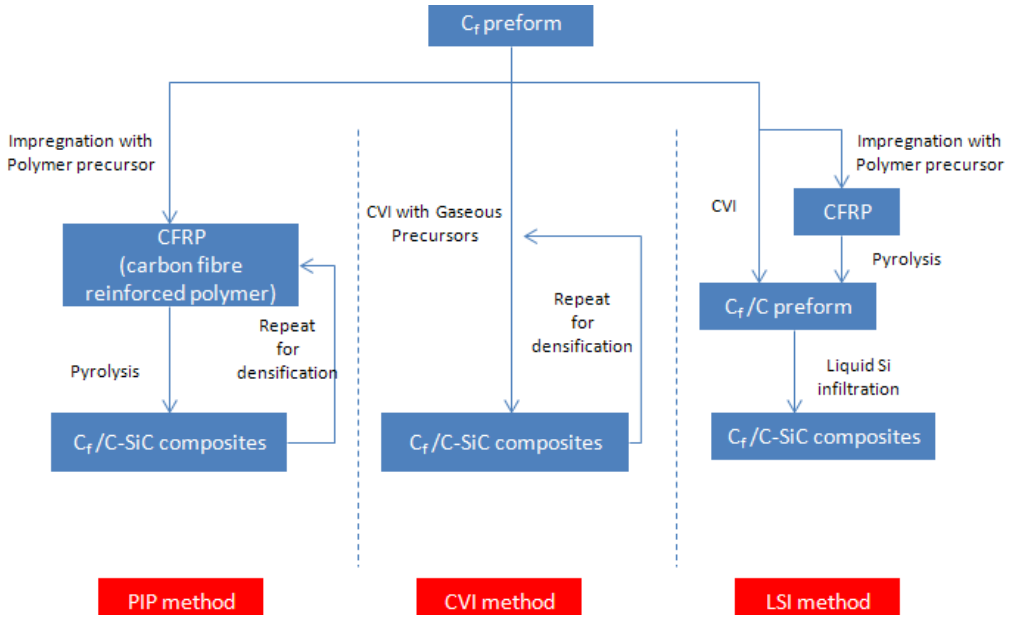

Figure 2-2 Schematic illustration of the manufacture method of C_f/C-SiC composite

The microstructure of C_f/C-SiC depends on the processing method used. Generally, the matrix produced by LSI often contains residual silicon compared to those manufactured through CVI and PIP processes[38-44]. Figure 2-3 shows the optical image of C_f/C-SiC, manufactured through LSI method [42]. There are three regions in the composites, C_f/C, SiC and Si, as marked in Figure 2-3. Carbon fibres are coated with carbon and a layer of SiC matrix is developed between C_f/C and residuals Si through the reaction of Si and carbon.

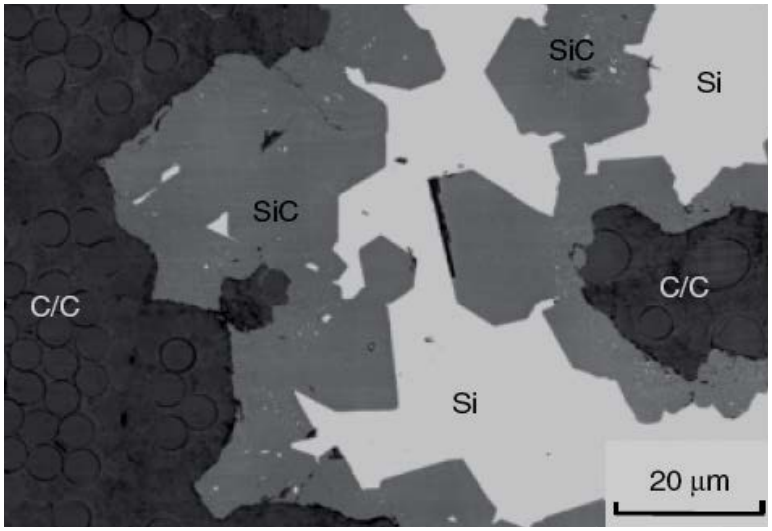

Figure 2-3 The microstructure of C_f/C-SiC composite manufactured by LSI method [42]

Usually, two types of carbon fibre architecture were utilised for manufacturing C_f/C-SiC brake disc, 2D and 3D architectures[38-44]. Woven C_f cloths or non-woven short C_f cloths are stacked layer by layer to form 2D C_f architecture [39]. In 3D architecture, non-woven C_f cloths and short-cut webs are alternatively stacked and two successive non-woven cloths were oriented at an angle of 90^o. Then vertical carbon fibres are needled through these layers to hold them together [20, 28, 42, 44]. The arrangement of carbon fibres are schematically illustrated in Figure 2-4 [42].

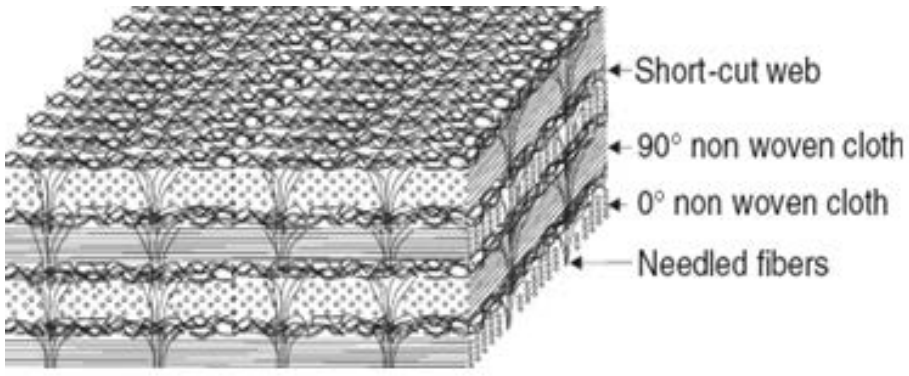

Figure 2-4 Schematic illustration of the arrangement of 3D carbon fibre perform [42]

C_f/C-SiC composites have 2D structure when carbon fibre preform with 2D architecture is used, whereas C_f/C-SiC composite have 3D structure when carbon fibre preform with 3D architecture is used. Figure 2-5 (a) and Figure 2-5 (b) show the cross-section microstructure of C_f/C-SiC composites with 2D woven C_f cloth and non-woven short C_f architecture, respectively. In the microstructure, the regions with dark contrast are C_f and the regions with bright contrast are ceramic matrix, including Si and SiC.

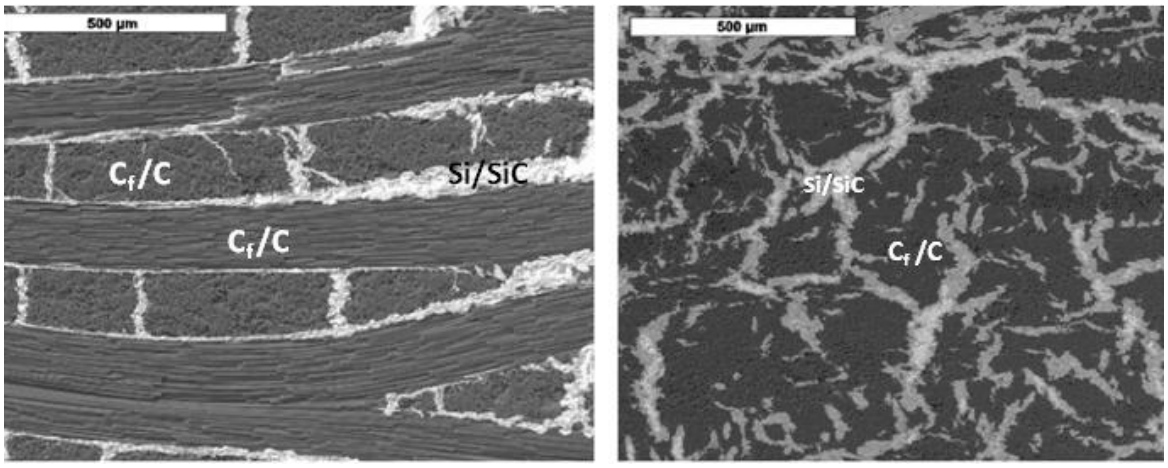

(a) (b)

Figure 2-5 Representative microstructure of C_f/C-SiC composite manufacture from stacked 2D woven C_f clothes (a) and non-woven short carbon fiber perform (b) (LSI method) [39]

Figure 2-6 (a) shows cross-section microstructure of 3D C_f/C-SiC composites manufactured through LSI method, and Figure 2-6 (b) and (c) show the in-plane microstructure of C_f/C-SiC on the laminar with non-woven carbon fibre architecture and the laminar with short-cut carbon fibre web, respectively[41,42]. In the microstructures, the dark contrast regions are C_fs while the bright contrast regions are ceramic matrix. The Si and SiC phases are not able to be differentiated clearly from these images due to the low magnification. Figure 2-6 (b) and (c) may suggest that the short-cut web layers contain more ceramic matrix than non-woven cloth layer.

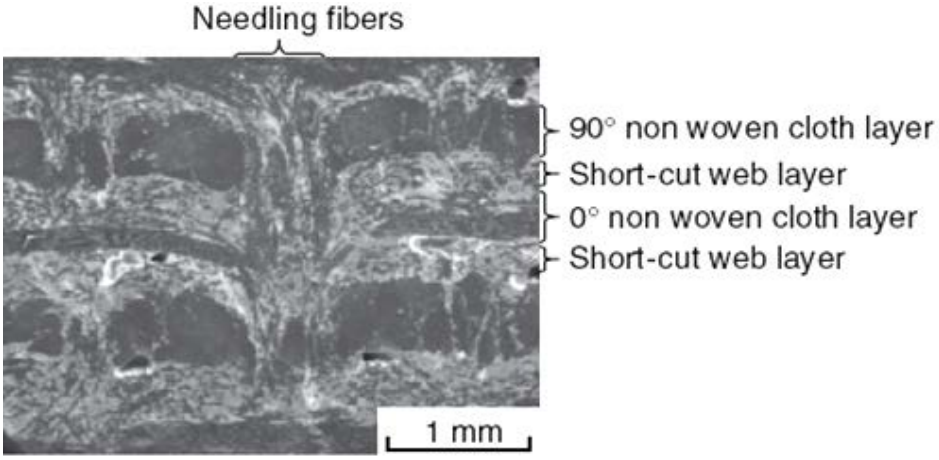

(a)

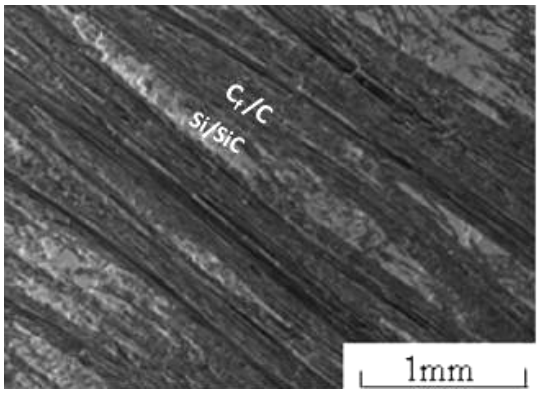

(b)

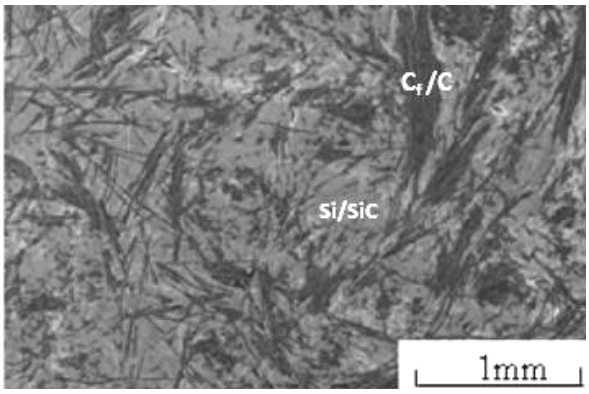

(c)

Figure 2-6 (a) Representative cross-section microstructure of 3D C_f/C-SiC composite[42]; (b) the in-plane microstructure of C_f/C-SiC composite on the lamina of non-woven carbon fibre archtecture[41] and, (c) The in-plane microstructure of C_f/C-SiC composite on the lamina of short-cut carbon fibre web[41]

2.3 Friction surface

The friction surfaces of brake pairs are the places where friction is originated. Studying friction surface generation will improve the understanding of friction performance of brake pairs. Investigations have been carried out on the friction surfaces of conventional brake disc materials (e.g. grey cast iron, Al-MMC, C_f/C composite) and

pad lining material. Generally, the studies of friction surfaces on these materials involved the following two major aspects:

(1) The mechanism of transfer layer generation on the contact surface. (The concepts of transfer layer are introduced in section 2.3.1);
(2) The microstructure and chemical composition of transfer layer

The existing knowledge on these two aspects will be reviewed in section 2.3.2 and 2.3.6.

It is believed that the transfer layer generated on the friction surface and it mediated the interaction of the contact surfaces during friction. Formation and removal of transfer layer will affect the chemical and microstructual conditions of contact surfaces, which could influence the friction performance of brake pair [48, 49, 50, 51, 52] (the influences of transfer layer on the friction performance will be reviewed in section 2.4).

However, as a new generation of brake disc material, the friction surface of C_f/C-SiC composite disc has not yet received enough studies; little information is available (see section 2.3.2) [41, 44, 53, 54]. Studies of the friction surface on C_f/C-SiC composites discs is required to improve the understanding of the friction performance of C_f/C-SiC brake disc, tailoring the microstructure of C_f/C-SiC composite and engineering pad lining material to optimise the friction performance of C_f/C-SiC brake disc.

2.3.1 The concept of transfer layer, transfer film and transferred material

It is generally accepted that a layer of material is generated on the tribological surfaces of a friction pair through rubbing of their contact surfaces. The chemical composition of such a layer of material differs from the substrates; therefore it is called third body material (or transferred material). In the early works [52, 55, 56], researchers realised that the adhesion and compaction of wear debris (produced from fragmentation of materials) had a great influence on the formation of third body layer on the contact

surfaces. Recently, other researches also confirm that formation of third body layer on the friction surface is a result of wear particles compaction [49 51 57 58 59 60 61].

No generally accepted nomenclature exists at the moment concerning the third body layer developed on brake pads or discs. Some researchers defined it as friction (or transfer) film [49, 52], others a friction (or transfer) layer [55, 57]. Filip et al.[61] used both terms in their research, since they observed a carbonaceous film on top of the friction layer—the latter consisted of compacted wear debris—but also at regions where no friction layer was present. Österle et al. [62] also used both terms as they detected a friction film with a uniform thickness and a transfer layer with variable thickness which was formed by debris compaction on a rough surface. They demonstrated that the variation between friction layer and friction film was dependant on their thickness and uniformity, the thickness of the friction layer varied locally over a wide range, especially where wear debris were deposited in grooves or pores, whereas the friction film had a uniform thickness of an order of a few nanometres with a smeared smooth appearance.

In my research, the term 'transfer layer (or friction layer)', has been used to define the accumulated and compacted wear debris that chemically bonded on the disc contact surface. It could have variable thickness, in a range of micrometres. Whereas, 'third body material' is used to define the transferred materials, which only mechanically compact on friction surfaces and which lack chemical bonding with the friction surface. 'Transfer film (or friction film)' was used to define a film developed on contact surface with uniform thickness in order of few nanometres.

2.3.2 Friction surface on C_f/C-SiC brake disc

There are only a few references in the literature reporting the microstructure and chemical composition of transfer layer developed on the friction surface of C_f/C-SiC composite disc. Li et al. [53] studied the microstructure of a friction surface on a C_f/C-SiC disc, paired with steel plate and demonstrated that the transfer layer had a non-uniform distribution on the friction surface of the composite. It seems that there is no sustainable transfer layer affiliated to C_f/C; any transfer layer developed has a direct link with the non-carbon ceramic matrix. Representative surface morphology is shown in Figure 2-7. However, there are no further studies on the transfer layer and the ceramic matrix. Further study by Jang et al. [44] demonstrated a similar friction surface, but again no more details on transfer layer. They compared the friction surfaces of two C_f/C-SiC discs having similar SiC content, but different C_f/C and Si contents. The study showed that the disc having low C_f/C but high Si content is covered evenly by transfer layer, while the one with high C_f/C but low Si content was covered by non-uniform transfer layer[44]. Such observations imply that the transfer layer is prone to develop on the Si and/or SiC substrates rather than on C_f/C substrate.

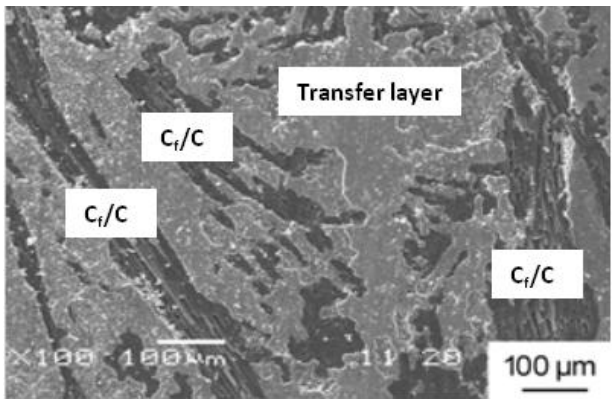

Figure 2-7 Friction surface developed on the surface of C_f/C-SiC when it is paired with steel plate[53]

The transfer layer developed on C_f/C-SiC disc is demonstrated to be very fine, composed of wear debris around tens nanometres, as shown in Figure 2-8 [41]. The typical chemical elements of C, Fe, O and Si are identified when a steel plate is paired with the composite[53]. Clearly, Fe is transferred from steel plate, Si from the substrate and O was from the air[53]. The transfer layer, found on friction surface of C_f/C-SiC after

self-mated friction test, included C, Si and O, but no Fe[54]. These findings indicate that apart from wear debris, further oxidation is included in the development of transfer layer.

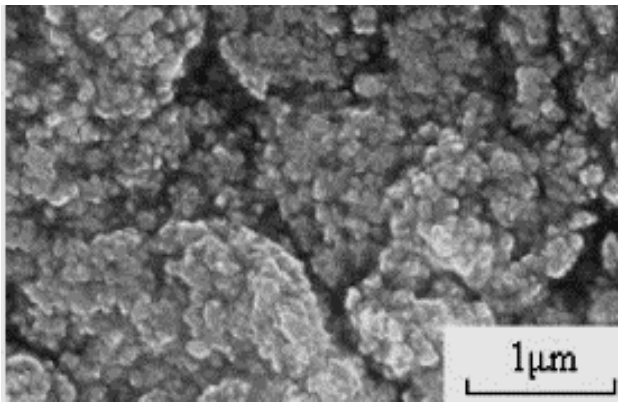

Figure 2-8 SEM image shows the transfer layer is composed of fine wear debris around tens nanometers[41]

2.3.3 Friction surface on grey cast iron disc

During friction, the contact surface of grey cast iron experienced plastic deformation and cracks may generate in the plastic deformed zone, leading to removal of materials from its surface. These metallic wear particles could be further mixed with the wear debris generated from the contact surface of pad. Under the brake pressure, these wear debris are compacted in the friction interface and form a transfer layer. Meanwhile, the transfer layer could be sheared into two parts, one part stays on the surface of grey cast iron disc, the other part on the surface of counterface [1,48, 63, 64-69].

The formation and stability of transfer layer developed on grey cast iron disc is dependent on the cohesive strength of the transfer layer itself as well as the adhesive bond strength between transfer layer and the friction surface. Jacko et al. [52] studied the friction surface of grey cast iron disc paired with polymer pad. They demonstrated that the transfer layer strongly adhered to the grey cast iron disc and polymer pad when the temperature at interface was below the decomposition temperature of

polymer pad. In contrast, when temperature exceeded the decomposition temperature of the polymer pad, the transfer layer was no longer adhered to the friction surface of polymer pad, but a thick transfer layer developed on the grey cast iron disc surface. Similar phenomena were also reported by Rhee et al. [48] through studying the friction surface of a grey cast iron disc paired with an organic pad. These results suggest that the transfer layer tends to be split and develop on both disc surface and pad surface if adhesive bond between disc and transfer layer, and between the pad and transfer layer remains stronger than the cohesive bond of transfer layer. If the cohesive bond of transfer layer and the adhesive bond to the disc are both strong, but the adhesive bond to the pad is weak, a massive material transfer to the disc surface occurs. If either the cohesive bond or the adhesive bond is weak, transfer layer cannot develop on the friction surface of both disc and pad.

Except for the bonding strength between transfer layer and grey cast iron disc, the surface roughness also influences the transfer layer formation. Rhee et al. [48] found that an increased surface roughness can promote the development of transfer layer. Terheci et al.[65] observed that the wear debris trapped in the wear tracks on the friction surface of grey cast iron disc. Libsch et al. [66] and Österle et al. [63] found that the machining, turning or grinding grooves on the surface of grey cast iron disc were no longer visible after friction test against organic pad, as the wear debris compacted in these lowlands to form a transfer layer and covered these grooves. The observations suggest that the formation of transfer layer can be promoted by providing mechanical support for wear debris compaction.

The friction surface of grey cast iron disc consists of a multi-layer structure; an example of such multi-layer structure is presented in Figure 2-9 (a). The transfer layer develops on grey cast iron discs contain material transferred from both disc and pad. Österle[63,64] studied the friction surface of grey cast iron paired with organic pad. They found the friction surface on grey cast iron disc consists of a multi-layer structure. A continuous

transfer layer with non-uniform thickness developed on the outermost friction surface. The transfer layer contains wear debris with tens nanometres. The key constituents in the friction layer are proved to be nanocrystallised Fe_3O_4, mixed with other elements which are originated from pad. Underneath the transfer layer, there is a severe plastic deformation zone, composed of a thin layer of fine grained fragmented structure (1-2 μm thick) and a shear deformed layer of cementite lamellae (2μm). Rhee et al. [67] also found a similar multi-layer friction surface in their research. Liu et al.[1] observed the transfer layer of grey cast iron disc paired with organic pad. In their research, not only constituents in pad were found embedded in the transfer layer but also fragmented bits of iron oxides from disc. Other researchers also found the transfer layer developed on the grey cast iron disc consisted of iron oxides and elements transferred from pad material [66, 68, 69]. These findings indicate that substrate deformation, fragmentation and oxidation are included in the development of transfer layer on friction surface of grey cast iron disc. Apart from the iron oxides from disc, the chemical composition of transfer layer on grey cast iron disc is depended on the constituents in pad.

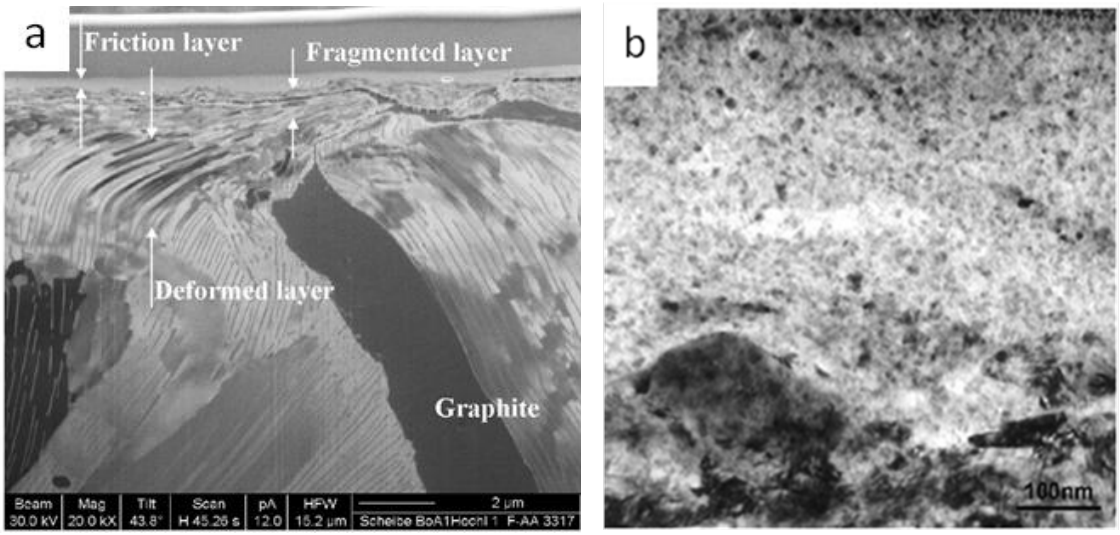

Figure 2-9 (a) Representative TEM cross-section image of grey cast iron disc after friction: continuous transfer layer compensates the roughness of the metallic surface profile with non-uniform thickness on outermost friction surface; a thin layer of fine grained fragmented structure (1μm); a region of sheared cementite lamellae (2μm) underneath the friction layer (b) transfer layer is composed of nano-sized particles [63 64]

2.3.4 Friction surface on Al-MMC disc

Aluminium metal matrix composite discs (Al-MMC) are composed of an aluminium matrix and ceramic particles as reinforcement. When Al-MMC disc is contacted by organic pad, Al matrix is easily worn away to form lowlands due to its much lower hardness than the ceramic particles in Al-MMC. Whereas the ceramic particles are only slowly abraded and blunted. This leads to the protrusion of ceramic particles from contact surface of disc. The protruded ceramic particles bear most of the loads and the Al matrix is protected from abrasion. In addition, the protruded ceramic particles penetrate into pad scratching the pad surface. As a result of scratching, a lot of wear debris generates from the pad. As friction proceed, wear debris are accumulated and compacted in the lowlands on Al matrix to form transfer layer. On the other hand, the ceramic particles in Al-MMC disc and hard abrasive particles in pad could be dislodged from the substrates. These dislodged abrasive particles enter into the friction surface, which could lead to removal of transfer layer through three body abrasion[70,71, 72,73]. The transfer layer is a balanced result of wear debris compaction and removal. An example is schematically illustrated in Figure 2-10.

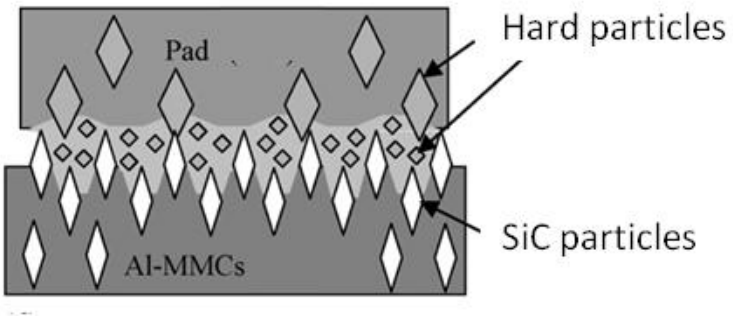

Figure 2-10 Schematic illustration of friction surface development of friction pair of Al-MMC disc and pad[71]

The transfer layer formation on Al-MMC is strongly influenced by: the amount of abrasive particles in pad; the size of abrasive particles in Al-MMC disc; the ratio of the size of the hard particles in the Al-MMC brake disc to those of the hard particles in the pad, and; the interfacial strength between Al matrix and ceramic particles. Zhang and

Wang [70] demonstrated that the thickness of transfer layer, developed on friction surface of Al-MMC disc, increased by increasing the amount of abrasive particles in pad from 4 vol% to 8 vol%. In another research, Zhang and Wang [71] found that transfer layer developed on Al-MMC having ceramic particles with size of 34 μm is thicker than that developed on Al-MMC having ceramic particles size of 3.5μm. It is believed that the small-size SiC particles can only support the thin transfer layer due to the unapparent protrusion of SiC particles and therefore shallow lowlands on Al matrix, whereas the large SiC particles could accommodate large amount of wear debris between the friction pair. Laden et al. [79] reported that the thickness of transfer layer increased by enhancing the interfacial strength between Al matrix and abrasive particles in Al-MMC disc. It is believed that the abrasive particles are dislodged from Al matrix and enter into the contact interface as a result of weak interface bonding, which leads to the distortion of transfer layer by three body abrasion. Nakanishi et al [73] found that the thickness of transfer layer reduced by increasing the ratio of size of the hard particles in the Al-MMC brake disc to those of the hard particles in the pad. It is believed that the hard particles protruded from the surface of the disc and prevented the pad from scratching off the transfer layer covering over the whole friction surface of the disc, when particle diameter ratio (disc/pad) is high. Thus the repeated braking operations thicken the accumulated transfer layer. By reducing the particle diameter ratio, the thickness of transfer layer developed on the disc surface could be reduced, as the large abrasive particles in the pad could penetrate into transfer layer and scratch off the transfer layer developed on disc. Meanwhile, the large particles in the pad could also protect the pad from wearing of hard particles in disc to prevent generation of excessive wear debris.These observations imply that the size and amount of abrasive particles in pad, the size of abrasive particles in Al-MMC disc, the ratio of the size of the hard particles in the Al-MMC brake disc to those of the hard particles in the pad and the interfacial strength between ceramic particles and matrix need to be engineered for the formation of a transfer layer on Al-MMC disc and optimising its thickness.

The transfer layer developed on Al-MMC disc contains materials transferred from the disc and the pad. Li and Tandon [74] observed Al rich layer and Fe rich layer existed alternately on friction surface of Al-SiC disc after friction against steel counterface (Figure 2-11). In addition, the sandwich structure experienced further fragmentation, mixing and compaction in further friction. They also observed the transfer layer contained fine debris of iron oxides, aluminium and the intermetallic compound, FeAl, which was formed by alloying of Al and Fe under the friction induced heat. Alpas et al.[72] and Tjong et al.[75] found that the transfer layer consisted of iron oxides, aluminium and fine SiC particles after sliding against steel counterface. Sallit et al. [76] observed a transfer layer with similar sandwich microstructure developed on the friction surface of the Al-SiC disc when organic pad was used. They found that the Al matrix and materials transferred from organic pad lining material existed alternately on the friction surface. Other researches[77,78,79,80] reveal that the transfer layer, developed on the friction surface of Al-MMC disc, consists of the materials transferred from Al-MMC disc (e.g. SiC, Al and Al oxide), and materials transferred from organic pad. These observations indicate that oxidation, substrate fragmentation, mechanical mixing, and mechanical alloying are included in the transfer layer development on Al-MMC disc.

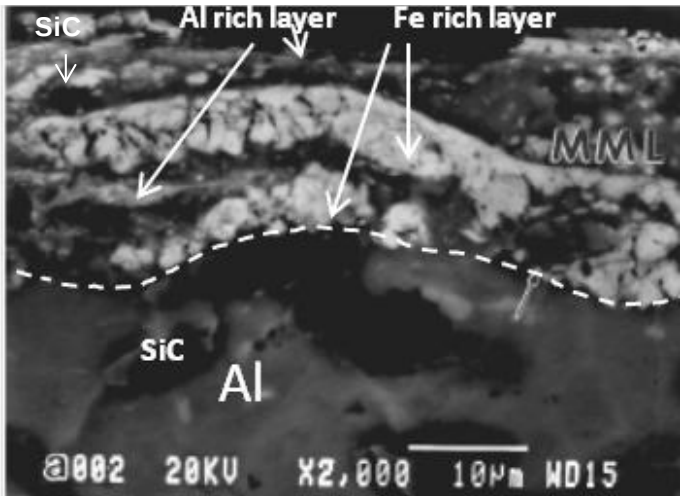

Figure 2-11 An illustration of sandwich structure of transfer layer developed on Al-SiC disc after friction against steel conterface[74]

2.3.5 Friction surface on C_f/C composite disc

C_f/C composites are composed of carbon fibres, e.g. pitch fibre and PAN fibre, and matrix, such as CVI carbon and pitch. On a polished surface of C_f/C composite with 3D microstructure, longitudinal carbon fibres (parallel to the friction surface), Z direction needled carbon fibres (perpendicular to the wear surface) and carbon matrix can be distinguished under optical microscopy. An representative microstructure of PAN carbon fibre reinforced CVI matrix C_f/C composite shows in Figure 2-12(a) [81]. When contact occurs on the surface of C_f/C composites, the carbon matrix and carbon fibres are fractured and dislodged from the friction surface. The fragments of carbon fibres and carbon matrix are further milled down into wear debris between the contact surfaces. These wear debris are compacted and adhered to the surface of C_f/C composite to form transfer layer. Repeated braking could lead to delamination of part of the transfer layer, which causes the formation of fresh wear debris. Most of the debris could be compacted again and regenerate the transfer layer[81,82,83,84, 85, 86].

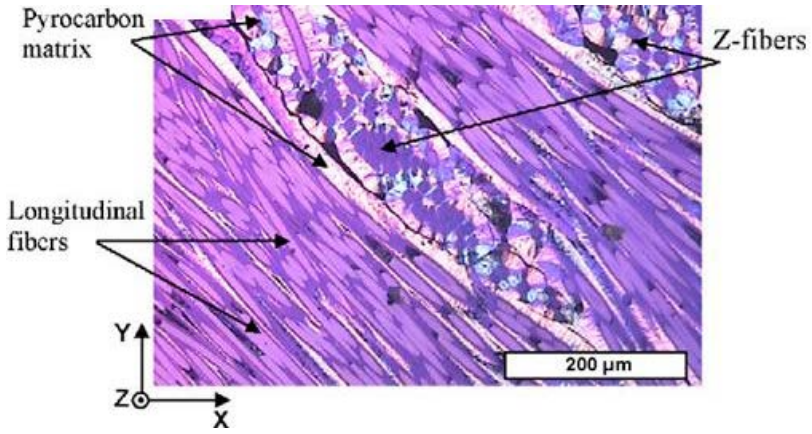

Figure 2-12 Representative microstructure of as-polished PAN-CVI C_f/C composite [81].

The development of transfer layer is influenced by the fibre orientation on the friction surface of C_f/C composite. Ju et al. [87] studied the friction surface of 2D PAN carbon fibre reinforce pitch matrix C_f/C composite with longitudinal orientated carbon fibres appeared on the friction surface and 3D C_f/C composite with both longitudinal oriented and Z direction carbon fibres appeared on the friction surface. They observed

that the formation of transfer layer on 2D C_f/C composite were much faster than the formation of transfer layer the 3D C_f/C composite, under same testing condition. Hutton et al. [94] observed the friction surface of PAN fibre reinforced CVI matrix C_f/C composite with 3D structure. They found that carbon fibre orientations parallel to the friction surface favoured the formation of transfer layer. Under same testing condition, the transfer layer was not preferred to develop in the Z direction carbon fibre region. Murdie et al. [88] investigated the friction surface of pitch fibre reinforced resin-CVI matrix C_f/C composite and observed that the coverage of transfer layer occurred over the longitudinal carbon fibre regions than over the Z direction carbon fibre regions. The greater coverage of transfer layer on the longitudinal carbon fibre regions is due to the collection of wear debris in the shallow grooves formed by dislodging of carbon fibres, through the fracture of interfaces between fibres and matrix which are generally weak. Kasem et al [81] investigated the friction surface of 3D PAN carbon fibre reinforced CVI carbon matrix C_f/C composites. They found that the transfer layer preferred to develop in the longitudinal carbon fibre regions, but not Z direction carbon fibre regions. They also demonstrated that the interface debonding and dislodging of carbon fibres preferred to occur in the longitudinal carbon fibre regions where the entire fibre/matrix interface exposed on the friction surface. Whereas the interface debonding in Z direction carbon fibre regions only occurred in the near surface region and the rest of Z direction carbon fibres are still remained adhesions with matrix below the rubbing surface. This could prevent dislodging of Z direction carbon fibres from the friction surface, and therefore the formation of grooves for wear debris collection [81]. It seems that existing of mechanical supports on friction surface, such as grooves, assists the transfer layer development. Engineering the orientation of carbon fibres in C_f/C composites is important for the development of transfer layer on their friction surfaces.

According to the microstructure, transfer layers developed on C_f/C composite are divided into three catalogues[89]: Type Ⅰ transfer layer is a thin, smooth and bright film. Type Ⅱ transfer layer is characterized by a thick, rough and dark powdery debris layer.

Type III transfer layer is identified as a smooth, dense, and bright film. Type III transfer layer is thicker and more stable than the type I transfer layer. Type I and type III transfer layer is preferred for stabilization of coefficient of friction (COF). The type of transfer layer could be influenced by the type of matrix, type of carbon fibres, the interfacial strength between carbon fibre and matrix, and the density of C_f/C composite. Chen et al. [90] investigated the friction surface of 2D PAN fibre reinforced CVI carbon matrix C_f/C composite with three different densities, under same testing condition. On the friction surface of C_f/C composite with intermediate density, the smooth type I transfer layer was disrupted into powdery type II transfer layer with the increasing of sliding distance. Then the type II transfer layer was compacted again to form type III transfer layer with further increase of sliding distance. For the one with highest density, microstructure transitions of transfer layer from type I to II occurred on its friction surface, but type III transfer layer was not found. Only type II transfer layer developed on the friction surface of C_f/C composite with lowest density, no microstructure transition occurred. They also observed that the type I and III transfer layers tended to develop on 2D PAN carbon fibre reinforced C_f/C composite with CVI carbon matrix, but not on the one with pitch-resin matrix. Lee et al. [91] compared the friction surface of PAN carbon fibre reinforced pitch matrix C_f/C composite and PAN carbon fibre reinforced pitch-resin matrix C_f/C composite, under same testing condition. They concluded that the dense and smooth transfer layer preferred to develop on the PAN carbon fibre reinforced pitch matrix C_f/C composite. Chen et al. [92] studied the CVI matrix C_f/C composite with PAN carbon fibres and PAN-oxidised carbon fibres. They observed that the type II transfer layer developed on friction surface of the C_f/C composite with PAN-oxidized carbon fibres which had higher fibre/matrix interfacial strength. In contrast, dense and smooth transfer layer developed on the friction surface of C_f/C composite with PAN fibres. These observations suggest that the microstructure of C_f/C composite, such as type of matrix, the type of carbon fibre, the fibre/matrix interfacial strength and the density of C_f/C composite, should be optimised for formation of type I or type III transfer layer, which are preferred for stabilising COF.

Apart from the influence of microstructure of the C_f/C composite, the type of the transfer layer developed on C_f/C composite disc is greatly influenced by the friction speed, brake pressure, sliding distance and temperature at the friction interface. Chen et al.[89] investigated the friction surface of PAN fibre reinforced pitch carbon matrix C_f/C composite and observed microstructure transitions of transfer layer. With increasing of the sliding distance or sliding speed, type Ⅰ transfer layer became unstable and disrupted to form a powdery type Ⅱ transfer layer. Then the powdery debris were compacted again and formed type Ⅲ transfer layer. In another research[93], they demonstrated that the type Ⅰ transfer layer can exist on the friction surface of PAN fibre reinforced pitch carbon matrix C_f/C composite when temperature at interface was below 150^{o}C. The type Ⅰ to Ⅱ type transition occurred when interface temperature increased. It is believed that desorption of water by friction induced heat could lead to distortion of type Ⅰ transfer layer and induce the transition from type Ⅰ to type Ⅱ transfer layer. However, the detailed mechanism of the transition remains uncertain. Murdie et al.[88] observed that a type Ⅱ transfer layer formed on the friction surface of pitch fibre reinforced resin-CVI matrix C_f/C composite at low sliding speed and low brake pressure testing conditions, whereas the type Ⅲ transfer layer was developed on the friction surface at high sliding speed and high brake pressure. They claimed that the smooth transfer layer was composed of plastically deformed and fractured components of the composite, including CVI carbon and fibres. They argued that the high pressure and high speed applied on the rubbing surfaces assist deformation of wear debris and also the production of a higher surface temperature to enhance the plastic deformation of wear debris to form the transfer layer. Hutton et al.[94] studied the friction surface of PAN fibre reinforced CVI matrix C_f/C composites, which were tested under various friction speeds. They observed a type Ⅱ transfer layer generated under low friction speed (Figure 2-13 (a)), and type Ⅲ transfer layer generated at high speed friction (Figure 2-13 (b)). Yen et al.[95] monitored the temperature change at friction surface of C_f/C composite during friction process. They found that increasing of interface temperature, induced by friction, led to the microstructure change of transfer layer: Type Ⅰ transfer layer generated at

temperature below 150°C; type Ⅰ to type Ⅱ transition occurred in the temperature range of 150-200 °C; type Ⅲ transfer layer generated at temperature range 200-650 °C. When the interface temperature is higher than 650°C, cracks at interface of the carbon fibres and carbon matrix could be generated on the friction surface of C_f/C composite, as a result of oxidation. Further oxidation leads to the growth and penetration of cracks into the matrix, which finally induces the delamination of substrate materials from the surface. In addition, the type Ⅲ transfer layer could be peeled off as a result of substrate delamination. These observations illustrated: type Ⅰ transfer layer tends to generate when temperature at interface is below 150°C; type Ⅰ transfer layer could be destroyed into type Ⅱ transfer layer when interface temperature is above 150°C; type Ⅲ transfer layer tends to generate at increased sliding distance, sliding speed, brake pressure and interface temperature. Oxidation occurs when interface temperature is further increased, which induces delamination of substrate and removal of transfer layer.

Except for the three types of transfer layer, a thin amorphous film with non-uniform distribution could generate on the friction surface of carbon fibres and carbon matrix (Figure 2-14). It is believed that the area covered by amorphous film has experienced a microstructural distortion [86, 88, 96].

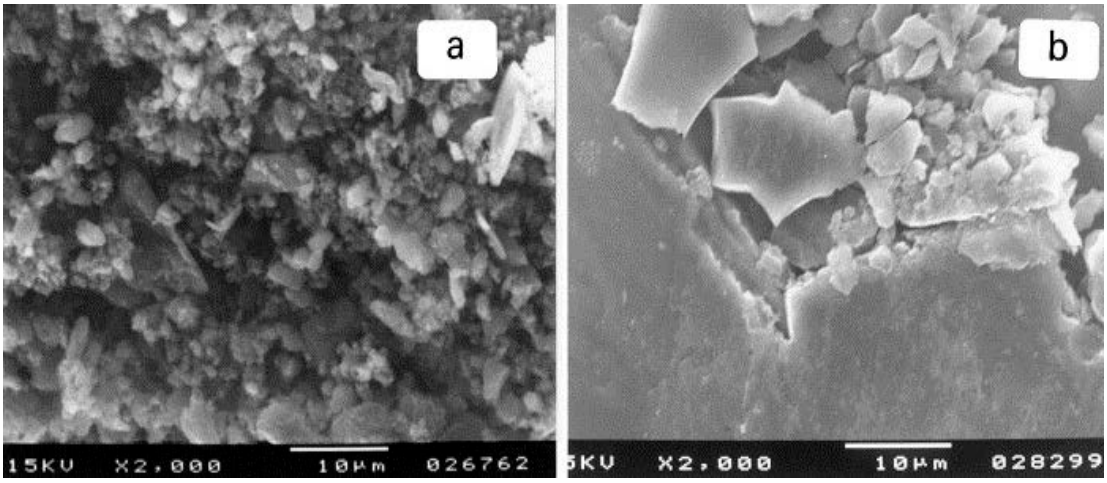

Figure 2-13 The powdery type of transfer layer on PAN fibre reinforced CVI matrix C_f/C composite, generated at low sliding speed (1800 rpm) (b) the dense and smooth transfer layer generated at high sliding speed (6000rpm) [94]

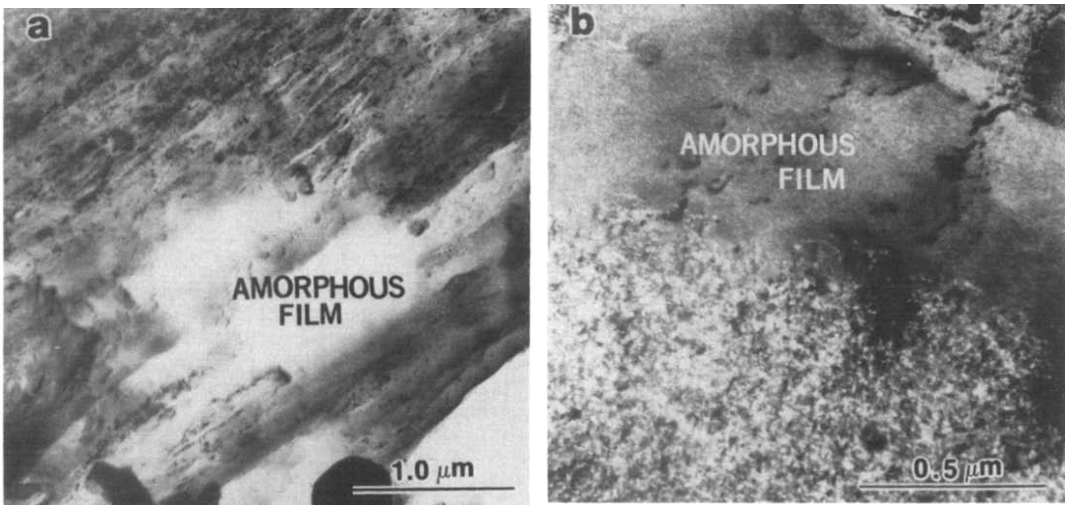

Figure 2-14 The amorphous layer developed on the friction surface of pitch fibre reinforced resin-CVI matrix C_f/C composite (a) carbon fibre (b) carbon matrix[88]

2.3.6 Friction surface on pad

It is generally accepted that the friction surface on pad consists of many small discontinuous micro-contact areas, also called contact patches[97], or contact plateaux[51], or plates[62, 63, 98]. These micro-contact areas are characterised by flat protrusions rising above the rest of the surface [50, 51, 59, 99]. The concept of micro-contact area was first introduced by Eriksson et al. [51] by examining the friction surface on an organic pad after friction test by pairing with a grey cast iron disc. In their study, they differentiate the micro-contact areas as primary plateaux and secondary plateaux. The reinforcing components of the pad, like steel or glass fibres, represent primary contact plateaux. Whereas, the secondary plateau is referred to the compacted wear debris deposited on the friction surface[51]. Through in-situ observation of the friction processes, they claim that the micro-contact areas experience a dynamic growth process, including creation, growth and deterioration during friction[99]. The authors also outline the mechanism to explain the formation and damage mechanisms of the micro-contact areas[51,59,99]. Similar dynamic process of friction surface generation on organic pad is also observed in Österle's researches [58, 62 , 63, 98]. The proposed mechanisms of friction surface generation are reviewed below.

Normally, pad lining materials consist of materials with different properties. The weakest and soft components include the resins and solid lubricants, while the abrasive particles and fibres are examples of the hard components. In addition, the components have a correspondingly wide range of wear resistance. As a result, areas which are rich in hard abrasive particles are worn slower than other areas containing less wear resistant components during friction. These hard abrasive particles protrude on the surface due to the lower wear rate[51]. The lowlands surrounding the protruded regions consist of less wear resistant constituents, such as polymeric resin, fillers, and friction modifiers (Figure 2-15). They were mechanically weak and worn mainly by wear debris through rolling and whirling in the labyrinth between disc and pad[99]. Repeating of such a process leads to a gradual milling down of the lowlands and the hard abrasive regions stay at a higher level than the surroundings. In addition, during this process, the wear debris are reduced in size by fragmentation and wearing. When the particles are small enough, they either leave the contact or take part in the forming of secondary plateaux[51]. It is believed that the normal pressure, shear forces and friction heat are combined to assist the compacting and sintering of the debris to form the secondary plateaux[99]. The formation of secondary plateaux should be a gradual process, because of the following constrains: (a) supply of wear debris; (b) space between surface of pad and disc; (c) friction heat to raise the temperature

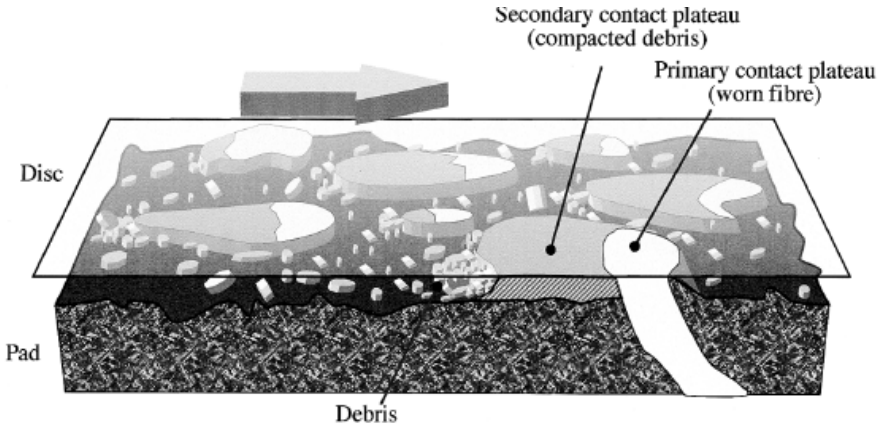

Figure 2-15 Schematic illustration of the contact situation between an organic pad and a brake disc proposed in [51] to illustrate the development of micro-contact areas on protruding regions (called primary contact plateaux) and in the front of these primary contact areas (called secondary plateaux)

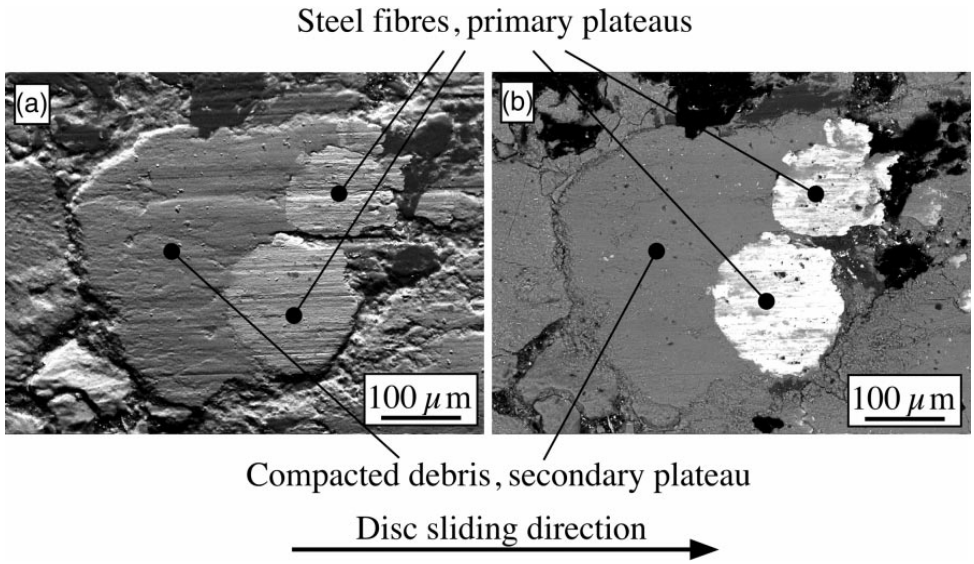

Figure 2-16 Contact plateaux on an organic pad. Two primary plateaux, steel fibres, support the debris compacted to their left to form secondary plateau (SEM). (a) Enhanced topographical contrast; (b) enhanced compositional contrast[51].

The sustainability of the secondary plateaux is related with the structure of pad lining material. They cannot survive without the support of structural components of the pad, like the primary plateaux. They would degrade within a second after losing their support, after wearing out or detachment of the fibres in the pad lining material[99]. They can be removed mechanically by irregularities on the disc surface[51], and loose wear debris between the disc and pad surface[99]. When these deterioration mechanisms dominate over the formation mechanisms, the secondary plateaux could degrade, even with the support of primary plateaux. In addition, the secondary plateaux require a sufficient normal force to exist. Large parts of the compacted areas could peel off in flakes by reducing the brake pressure[51]. Those observations indicate that there is neither strong chemical bond between the secondary plateaux and the pad substrate, nor strong substrate to support the secondary plateaux.

Österle et al.[58] outlined a mechanism of dynamic growth of friction surface on organic pad, but instead of steel fibres, abrasive quartz crystals form the primary contact areas.

The model is presented in Figure 2-17. In a first stage of friction, soft material is worn off preferentially, while a hard quartz crystal is elevated from the surface as long as it is bound firmly to the pad. The sharp edge of quartz scratched material from the disk surface, which is transformed to wear debris. The wear debris release from the pad and disc surface may adopt the function of milling balls leading to further wear of disc and pad. Meanwhile, the wear debris are deposited in wear troughs around quartz crystals and compact there by being pressed against the elevated edges of quartz. The contact plates are developed through this mechanism. However, further wear of the micro-contact plates and their surrounding materials may lead to pull out of quartz and degradation of the contact plates. The authors conclude that the formation of micro-contact plates is not a stable process during friction, but a dynamic equilibrium between initiation, growth and degradation of contact plates would take place [62, 63, 98]. It can be seen that the model outlined by Österle et al. [58] supports the one outlined by Eriksson et al. [51]

A refined model of transfer layer development on friction surface of organic pad (Figure 2-18) is further outlined by Österle et al.[62] through combining the model (Figure 2-15) which was initially provided by Eriksson et al. [59] and the model (Figure 2-17) from their earlier research[58]. In this model, both quartz crystals and steel fibres are hard abrasive constituents in pad lining materials. During friction, these constituents are worn slowly compared with other constituents, such that they protrude from surface and become primary contact plateaux. The loose wear debris then accumulate around these primary contact plateaux to form compacted contact plates (so called transfer layer). This model also shows the distortion of the compacted contact plates, e.g. the plates are fragmented and transferred to wear debris again.

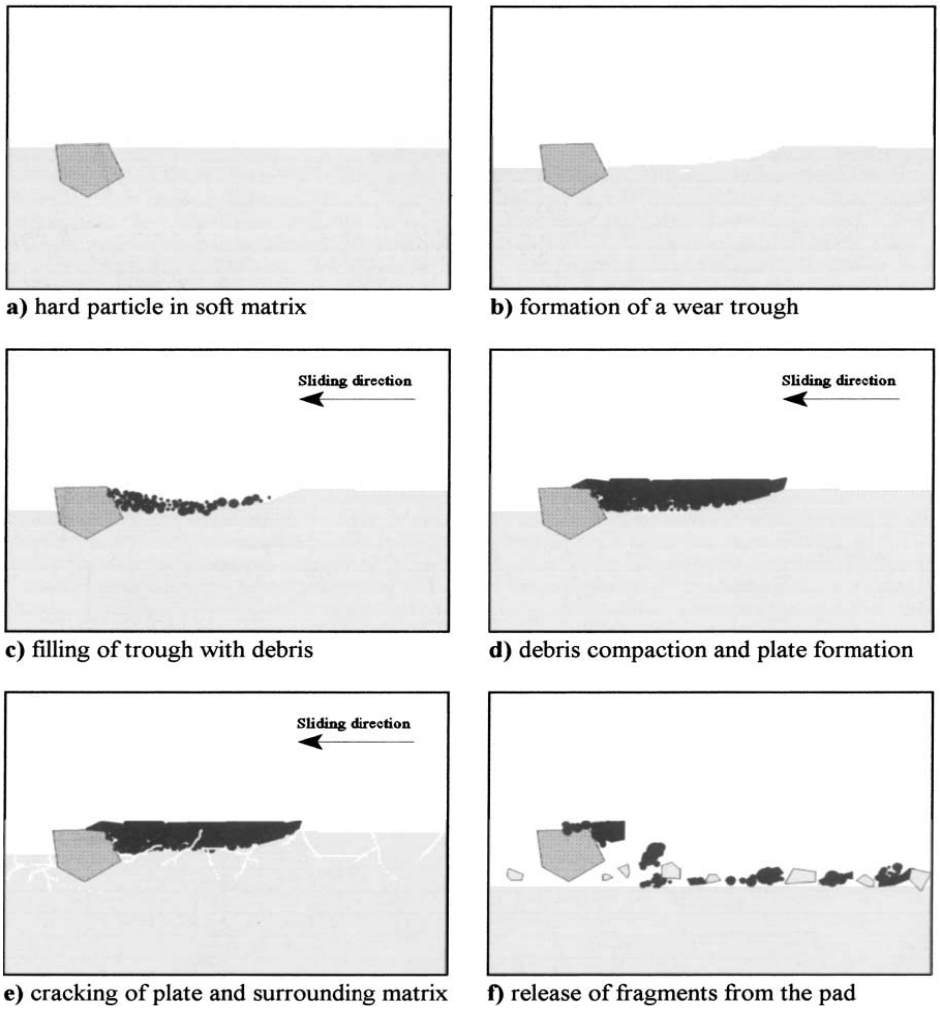

Figure 2-17 Generation, growth, and degradation of a micro-contact at the surface of a pad [58].

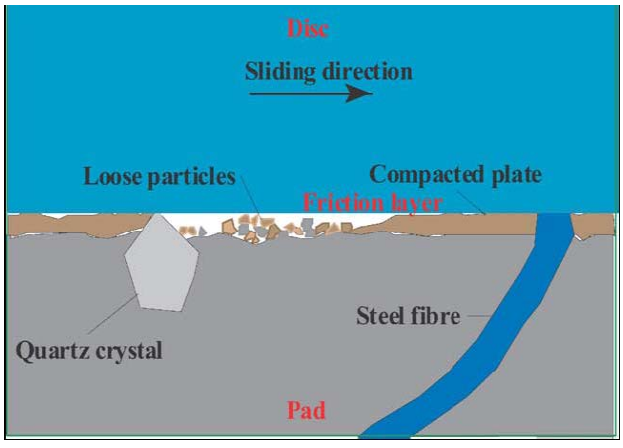

Figure 2-18 Schematic illustration of transfer layer formation on a brake pad when both quartz crystal and steel fibre are included as abrasives[62]

Generally, friction surface on pad consists of an outermost carbonaceous transfer film [61] or nano-crystallised metal oxide transfer film with uniform thickness[62], a discontinuous transfer layer forms by wear debris compaction [49, 50, 51, 55-61, 100] and severely deformed near surface region [62, 64]. Filip et al. [61] found a carbonaceous transfer film, consisted of randomly oriented grains of crystalline carbon, developed on the pad lining material after rubbing against a cast iron disc. The crystal size of carbon varied from 5 to 18 nm. The thickness of the film varied between 2 and 7 nm. The source of the carbonaceous friction film is not clear from the literature, but two possible resources are proposed: a decomposition product from the organic binder resin and/or graphite flakes in the grey cast iron. Österle et al. [62] reported a continuous transfer films, about 100 nm thickness without any visible grain structures, developed on the outmost friction surfaces of brass (Figure 2-19(a)) and steel fibres (Figure 2-19(b)) in organic pad. The transfer films have a different microstructure and chemical composition compared with the underneath transfer layers, which consist of compacted wear debris particles with variable thickness. In addition, the transfer film contains an oxidation product of metal sulphur, which is originated from pad lining material, whereas the underlying friction layer mainly contain metal oxides, e.g. Cu_2O in transfer layer developed on brass surface, and Fe_3O_4 and Fe_2O_3 in transfer layer developed on steel surface.

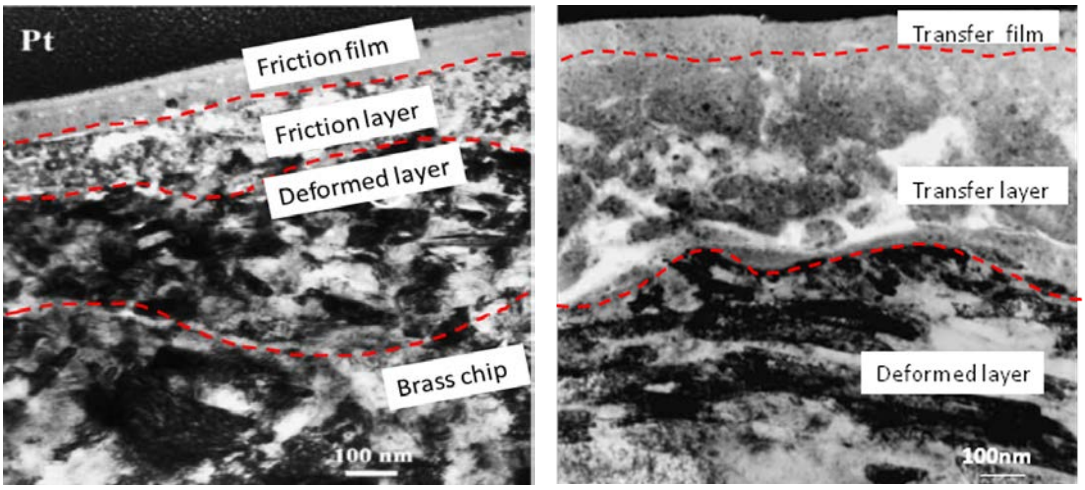

(a) (b)

Figure 2-19 Cross section TEM image of the friction surface on (a) brass fibre and on (b) iron fibre [62]

Eriksson et al. [51] reported a homogeneous fine grained (5-10nm) dense film (<1 μm) developed on the outermost friction surface. Below this thin film, coarser wear debris (few hundred nanometres) compact together forming a thick and porous transfer layer (Figure 2-20). The transfer film and transfer layer are dominated by FeO/or Fe_3O_4, which are originated from grey cast iron disc and/or iron chips in organic pad lining material. It is believed that the homogenisation of the transfer film resulted from the high shear stress and temperature at the outmost friction surface.

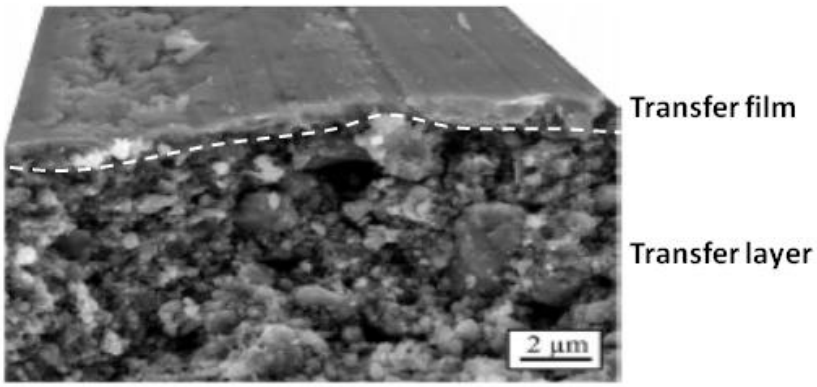

Figure 2-20 Friction surface of organic pad. The thin homogeneous top transfer film and the transition to transfer layer with a coarser structure[51].

In other researches[58, 62, 98], chemical species, such as solid lubricant and fillers (e.g. sulphides, graphite) which originated from the pad formulation, have been found in the transfer layer. Furthermore, a few researchers have also detected new chemical compounds which are not from either the disc or pad. The chemical decompositions and reactions, induced by friction heat, contributed to the development of these new chemical compounds in the transfer layer [49, 61]. For example, Wirth et al. [49] reported that molybdenum sulphide experiences decomposition and oxidation at high interface temperatures, and can further interact with iron oxide, Fe_2O_3 to produce a complex oxide compound $Fe_2(MoO_4)$. Decomposition of solid lubricant Sb_2S_3 and alloying of Cu by Sb can take place during friction, and sulphur interaction with Cu can result in the formation of Cu_2S[61].

A deformed metallic subsurface layer below the transfer layer is observed in the subsurface of metal fibres in organic pad and the substrate of metallic pad [62, 64, 101]. Figure 2-19 shows that the deformed brass and steel located underneath the transfer layer. Within the deformed layer, most of the grains are orientated along the sliding direction. Under braking pressures, the shear stress between the two sliding surfaces induces plastic deformation of metals, and thereby results in the change of their microstructure[62, 64, 101].

These observations indicate that friction induced the oxidation, mechanical milling and chemical reactions occurred on the friction surface, leading to the formation of wear debris with various chemical compositions. In addition, the chemical composition of transfer layer is greatly influenced by the ingredients in pad.

2.4 The influence of transfer layer on coefficient of friction of brake pairs

During friction, the COF values of a friction couple change with sliding time, sliding distance or number of brakes. Generally, the COF values become stabilised after a so called 'bed-in', 'run-in', 'break-in' or 'wear-in' period[103]. Steady state refers to the stage in which the COF values have reached and maintained a relatively constant level, regardless of the increasing of sliding time, distance or number of stops. Whereas, run-in process occurs before steady-state and is usually accompanied with changes in COF values[102, 103]. Researchers have revealed that the COF values are significantly influenced by transfer layer developed on friction pairs although the mechanisms are still not fully understood. The influences of transfer layer on friction performance are reviewed here.

2.4.1 Grey cast iron disc paired with an organic pad

It is agreed that COF values increase as the real contact areas increase. Such type of contact areas should be a consequence of wearing off of surface asperities or the formation of transfer layer. An example is illustrated in Figure 2-21 (a). Eriksson et al. [51, 59] demonstrated the increasing of the averaged COF values with number of stops during run-in stage when grey cast iron was tested against organic pad. They found that the averaged COF values increased when the surface was worn smooth and the transfer layer was developed. Rhee et al. [48] also recorded the similar run-in procedures of grey cast iron from repeated brake testing against semi-metallic pad. They claimed that the rise of COF values in run-in stage was related to the transfer layer formation.

The transfer layer development also influence the increasing of COF within each single brake, this is referred to 'mico-run-in' [51,59]. An example is given in Figure 2-21 (b). This phenomenon was explained by Eriksson et al. [59 99], who observed that the transfer layer could partly deteriorate when the brake pressure reduced at the end of each stop, and argued that the deterioration of transfer layer lead to the reduction of real contact areas. The reduced area of contact leads to a low COF value at the beginning of each stop. However, the real contact area will be enlarged again by building up of transfer layer at new position on friction surface when next brake is applied. The COF values recover as a result of transfer layer re-building. Therefore, the COF values show an increased trend during each stop. Even when the steady state COF are reached, this phenomenon could still be seen during each stop.

In addition, the formulation of pad could influence the chemical composition and microstructure of transfer layer, and consequently influence the level of COF and its stability. Hee et al. [104] reported that the stability of COF could be improved by adding potassium titanate into pad formulation, which enhanced the formation of transfer layer during friction. Gudmand-Høyer et al. [105] found that the existence of Sb_2S_3 in pad

lining material and transfer layer could stabilise the COF, but led to the reduction of the level of COF at evaluated temperature. Cho et al.[100] claimed that the stability of COF could be improved by increasing the thickness of transfer layer, e.g. increasing the contents of lubricant or iron powder, or reducing the contents of abrasive ingredients with higher hardness in pad. These observations illustrate that the pad need to be properly formulated for obtaining a desired level of COF and maintaining the stability of COF.

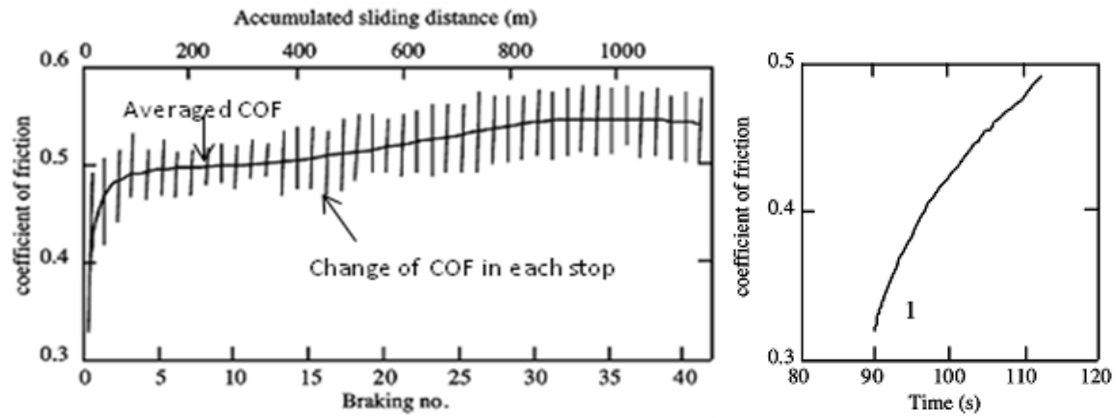

Figure 2-21 (a) COF values increased during run-in procedures, (b) change of COF values inside the first stop[59]

2.4.2 Al-MMC disc paired with pad

Although the influence of transfer layer on the change of COF values in run-in stage of Al-MMC brake disc has not yet been well understood, the influence of transfer layer on the level of COF and the stability of COF have already been reported. Laden et al.[79] reported that the removal of transfer layer from the friction surface of Al-MMC disc resulted in reduction of the level of COF and instability of COF. Ravikiran et al.[106] reported that the formation of transfer layer increased the level of COF. Nakanishi et al.[73] reported that generation of transfer layer with a constant thickness on the disc surface is important for stability of COF. In their research, the thickness of transfer layer is controlled through varying the diameter ratio of hard particles in disc and pad. They found the thickness of transfer layer on Al-MMC disc surface continuously

increased through the repeated braking and led to a reduction of the level of COF after the run-in stage by using high disc/pad particle diameter ratio. By using lower particle diameter ratio, the thickness of transfer layer could be maintained constant during friction and therefore the COF values could be maintained in a stable state after run-in stage (Figure 2-22). It seems that the formation of transfer layer with a constant thickness on Al-MMC disc could increase the level of COF and improve the stability of COF.

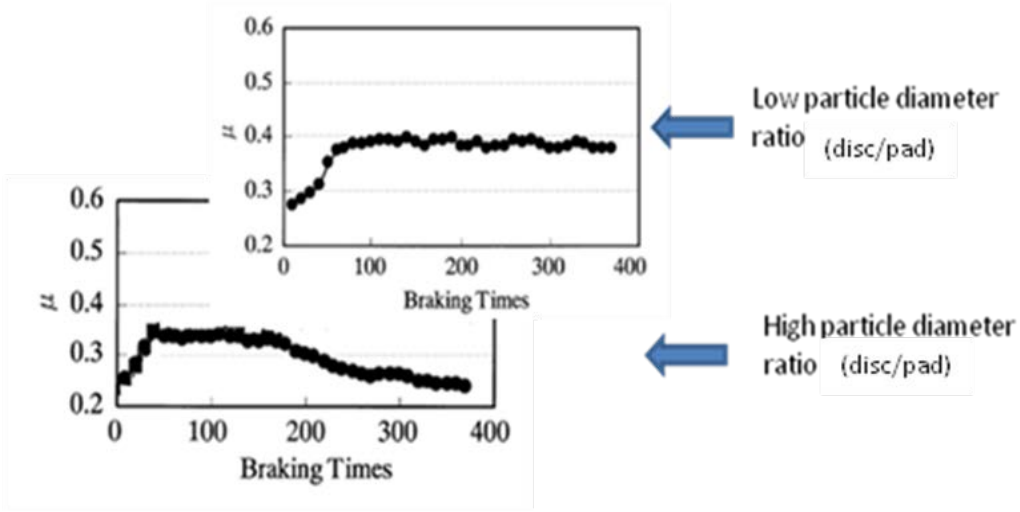

Figure 2-22 The influence of particle diameter ratio on the stability of COF of Al-MMC disc paired with organic pad[73]

2.4.3 C_f/C composite paired by C_f/C composite

The microstructure of transfer layer has close relationship with the change of COF values and the stability of COF in C_f/C composite brake pair. Chen and Ju [93] reported the variation of COF values in continuous friction testing of self-mated C_f/C composite in air. A change of COF occurs with increasing of the sliding distance, the COF values increase sharply from 0.2 to 0.8 and then gradually reduce and stabilise at 0.5; This process is called friction transition. The sharp increase of COF values is corresponded to the microstructure change of transfer layer; deterioration of a thin smooth transfer layer and the generation of a thick powdery debris layer. The powdery layer is then transformed into a thick dense and smooth layer causing the decline and stabilisation

of COF. Yen and Ishihara [95] also reported the microstructure change of transfer layer and the variation of COF values in continuous friction test under different brake load. Three types of COF curves are found, as show in Figure 2-23. At low load, only one friction transition occurs with increasing of sliding distance. At medium load, two friction transitions are observed with increasing sliding distance, as marked in Figure 2-23. At high load, no transition takes place, the COF values decline with sliding distance. The authors found the first friction transition was accompanied by the transition of surface morphology from a dark and lustrous region with a mirror-like polished appearance (indication of formation of dense and smooth transfer layer) to a dull-looking grey region with a machine-finished appearance (indication of formation of powdery debris layer). At the high load condition, lack of the coverage of transfer layer was observed due to severe oxidation of C_f/C friction surface. Observations imply that the formation of dense and smooth transfer layer on the friction surface of C_f/C composite leads to a relatively low but stable COF values, whereas formation of the powdery debris transfer layer leads to a high COF values.

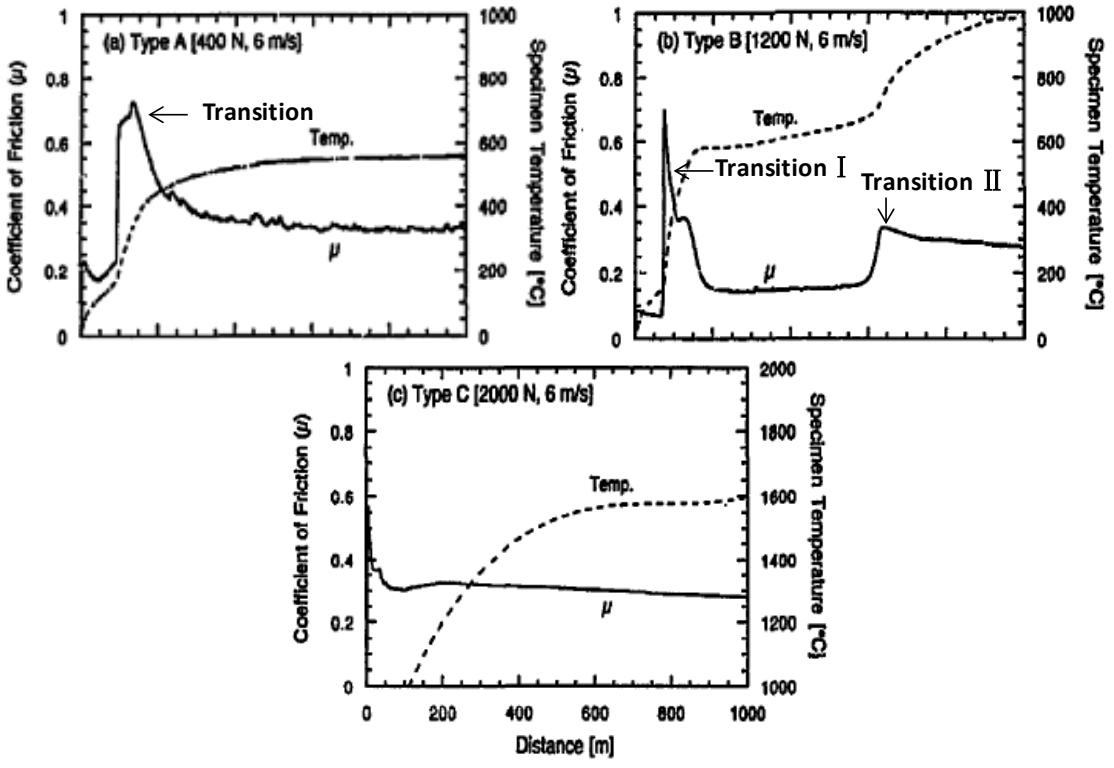

Figure 2-23 Variation of COF values and specimen temperature as functions of sliding distance under different load conditions (X axes have same scale) [95]

The type of carbon matrix, the type of carbon fibre and the interfacial strength between carbon fibre and matrix could influence the formation of transfer layer on the friction surface and therefore COF values of C_f/C composite. Chen et al. [90] reported that PAN fibre reinforced pitch matrix C_f/C composite had more stable COF values compared with pitch fibre reinforced resin-CVI matrix C_f/C composite under same testing condition, due to formation of dense and smooth transfer layer on the friction surface. Chen et al.[92] reported that the enhanced fibre/matrix interfacial strength of C_f/C composite leads to the formation of dense and smooth transfer layer, which results in stable COF values. Lee et al.[91] demonstrated that PAN carbon fibre reinforced pitch matrix C_f/C composite had more stable COF values compared with PAN carbon fibre reinforced pitch-resin matrix C_f/C composite under same testing condition, due to the formation of smooth transfer layer. These observations suggest that the microstructure of C_f/C composite should be carefully engineered for development of transfer layer with a dense and smooth morphology, which is preferred for stabilisation of COF.

2.4.4 C_f/C-SiC composite paired with C_f/C-SiC composites

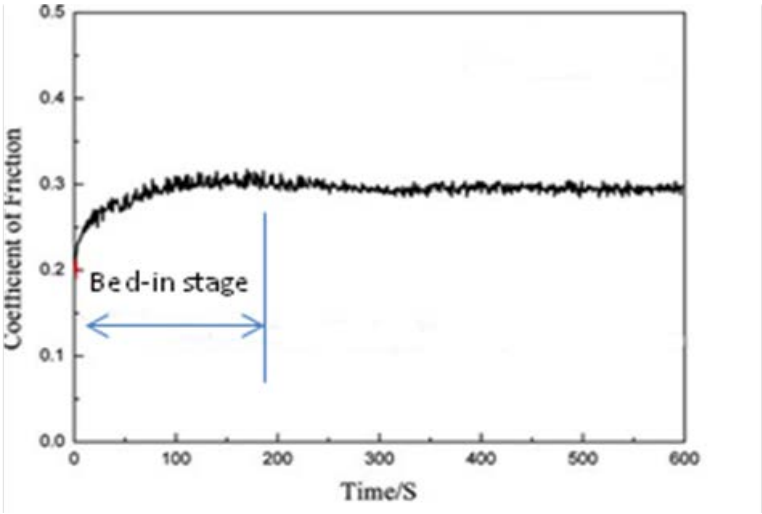

Figure 2-24 The variation of COF values of self-mated C_f/C-SiC composite with time during continuous friction test [107]

The variation of COF values during run-in procedures of self-mated C_f/C-SiC composites is influenced by transfer layer formation. The formation of transfer layer could also influence the stability of COF. Zhou et al. [107] reported the variation of COF values of self-mated C_f/C-SiC composites with time during continuous friction test (Figure 2-24). The COF initiates with a low value and gradually increases and stabilises after bed-in stage. The authors observed a smooth carbon rich transfer layer developed on the friction surface after friction test, and argued that COF values reached to the steady state once the friction surface was coved by the transfer layer. Li et al. [53] studied the friction performance of C_f/C-SiC through repeated braking and found COF values changed with a similar trend as the curve shown in Figure 2-24. They believed that the increment of COF values in the bed-in process was attributed to the transfer layer formation. It seems that the formation of transfer layer could induce the increasing of COF values during run-in stage.

Variation of COF values in single brake was studied in several researches. Fan et al.[20,30,41] observed the change of COF values within the single brake test (Figure 2-25) and explained that the rise of COF values at the early stage of braking attributed to the ploughing effect of surface asperities and the loose wear debris trapped in the interface of the brake pair[20]. As braking proceed, transfer layer developed on the friction surface through wear debris compaction and experienced dynamic growth. The COF values reached a steady state with the dynamic growth of transfer layer. In the later stage of braking, transfer layer gradually deteriorated and transformed loss wear debris with the slowing down of the friction speed. Similar to the early stage, the loose wear debris ploughed the friction surface, leading to the rise of COF values again. It seems that the formation of smooth transfer layer leads to the stabilisation of COF. Once such a transfer layer is destroyed, the COF values become instable.

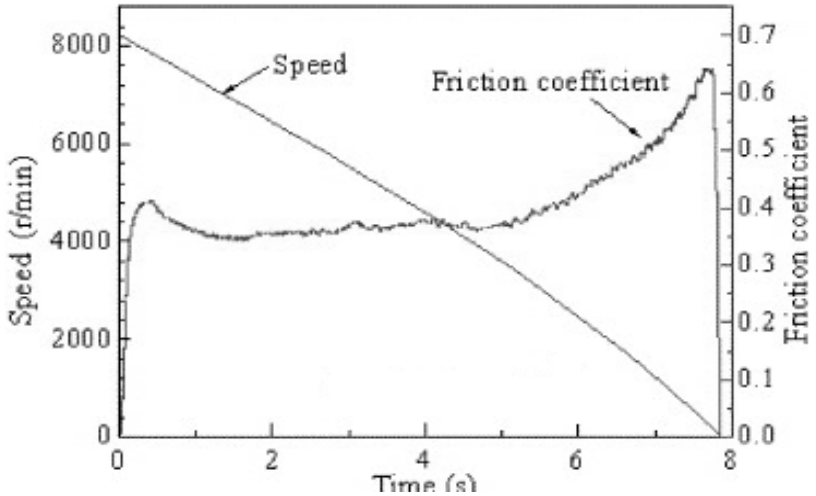

Figure 2-25 Variation of COF values of self-mated C_f/C-SiC during single brake test [20]

2.4.5 C_f/C-SiC composite disc paired with organic pad

For the friction pair of C_f/C-SiC composite disc and organic pad, the influence of transfer layer on the variation of COF values with pad brakes has not been extensively studied. Only Jang et al. [44] reported the influence of transfer layer on the level of COF. They found that increased Si content and reduced C_f/C content in the C_f/C-SiC composite led to the formation of a uniform transfer layer across the friction surface of the disc and a high level of COF (Figure 2-26). They believed that the uniform transfer layer on the disc surface increased the level of COF due to enlarged real contact areas at the friction interface. More research is required to understand the influence of transfer layer on the change of COF values and stability of COF. Due to lack of research information, it is difficult to conclude the influence of transfer layer on the COF.

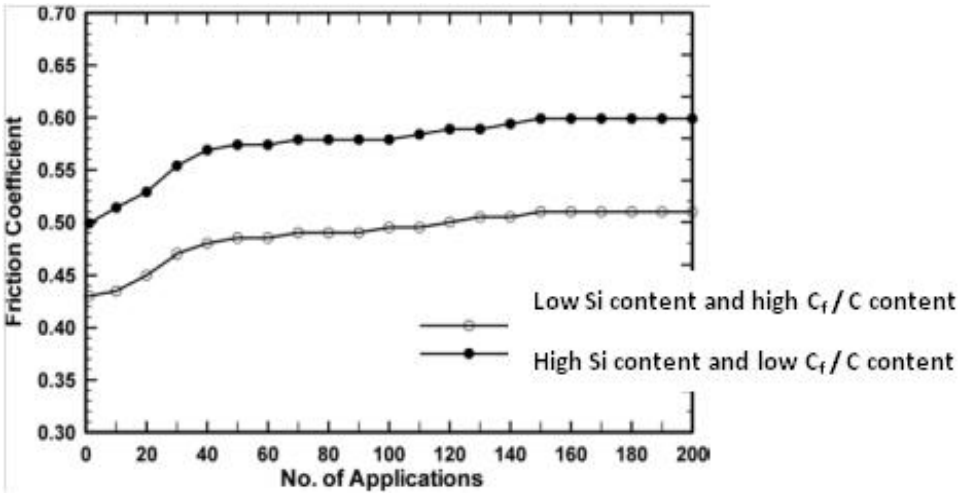

Figure 2-26 Change of COFs during repeated brake testing. C_f/C-SiC having high Si content and low C_f/C content has higher level of friction than the sample having low Si content and high C_f/C content[44]

Summary of literature review

- New generation brake disc material, C_f/C-SiC, was desired for high speed and heavy duty application. It was developed to use in luxury road car, high performance sports cars and aircrafts. This type of material has combination advantages of low density, wear resistance, oxidation resistance, and high temperature resistance.

- From the review of transfer layer development on traditional brake discs and organic pad, it is noted that the transfer layer developed through wear debris compaction in the lowlands on the friction surface, under the brake load. Without accounting any chemical bonds, mechanical effect alone, can make the transfer layer survivable. However, when the mechanical support is lost, transfer layer would no longer survive. Therefore, for friction materials, engineering their microstructure and constituents are important for formation and stability of transfer layer on the friction surface.

- The current review has already demonstrated that deformation, fragmentation and oxidation could occur on the contact surfaces of brake disc and pad during friction

process. The transfer layer is a mechanically compacted layer of mixed wear debris produced through these processes. The microstructure and chemical composition of transfer layer are influenced by the microstructure and constituents of pad and disc, as well as the testing conditions. Therefore, the microstructures of friction pairs need to be properly engineered for optimise the microstructure and chemical composition of transfer layer.

- Based on the reviewing of existing researches, the COF values could be stabilised with the formation of transfer layer. Moreover, researchers have also highlighted that the formation of transfer layer, its microstructure and chemical composition have impact on the variation of COF values in the bed-in process of a friction couple and the level of COF.

- So far, the influence of transfer layer on friction performance of C_f/C-SiC composite disc has still not been fully understood, since there is no fundamental understanding of the development of transfer layer on C_f/C-SiC composite, the chemical composition of transfer layer, the microstructure of transfer layer and the relationship between transfer layer and substrate.

- In this thesis, to understand the influence of transfer layer on the COF of C_f/C-SiC composite disc, a comprehensive study was carried out on the development of transfer layer on the friction surface of C_f/C-SiC composite. Then chemical composition of the transfer layer, the microstructure of the transfer layer and the interface between transfer layer and the substrate were investigated as well.

Chapter 3 Experiment work

3.1Materials

As-manufactured C_f/C-SiC composites were provided by Surface Transforms (Cheshire, England). The composites were manufactured through chemical vapour infiltration (CVI) to generate carbon fibre/carbon (C_f/C) preforms, where almost all spaces inside carbon fibre bundles were fully filled in with pyrolytic carbon, and around each fibre bundle was wrapped a layer of pyrolytic carbon. Such preforms were then infiltrated with silicon melt at a temperature above the melting point of silicon in a protecting atmosphere, normally argon. It is believed that during the infiltration, the contact regions between silicon melt and pyrolytic carbon could be quickly converted into silicon carbide regions through a carbonisation process of silicon[108 109]. The degree of siliconisation should be controlled by the kinetics and the appearance of local deficiency of either of the two chemicals; it is therefore not unusual to see significant amount of residual silicon and pyrolytic carbon existing in the microstructure of composites[110].

Selected organic pad was provided by Federal Mogul (Chapel-en-le-Frith, England). The pad sample was manufactured by hot pressing friction lining material on a steel back plate. The formulation of the friction lining material was not released by supplier, therefore the possible chemical elements in the friction lining material were studied by field emission gun scanning electron microscopy equipped with energy dispersive X-ray (EDS) system. More details of the pad are reported in section 4.2.

3.2 Sample preparation for laboratory scale dynamometer testing

3.2.1 Machining of sample

As shown by drawings in Figure 3-1, the as-manufactured C_f/C-SiC composite blocks were cut into discs in laboratory with a diameter of 50 mm and a thickness of about 12 mm. Two countersink holes with a diameter of 7 mm were drilled on a circular with a diameter of 22 mm on the discs for bolting the discs on the sample jig, which was attached to the rotor shaft, as shown in Figure 3-3.

The friction lining materials, which were bonded on back plates, were machined to a ring shape, having outside diameter 50 mm and inside diameter 40 mm. Four 4 mm holes were drilled on the back plate for bolting on testing jig, which was attached to the stator shaft. The thickness of brake pad was 12 mm. The design of pads is shown in Figure 3-2.

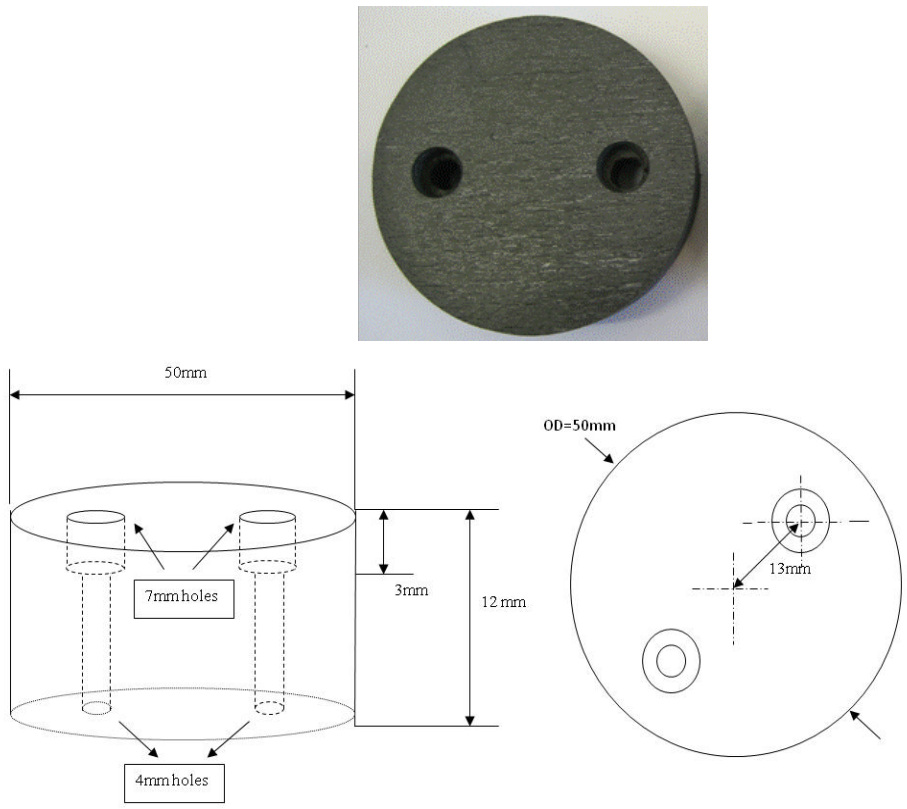

Figure 3-1 Drawing and digital image of C_f/C-SiC discs sample

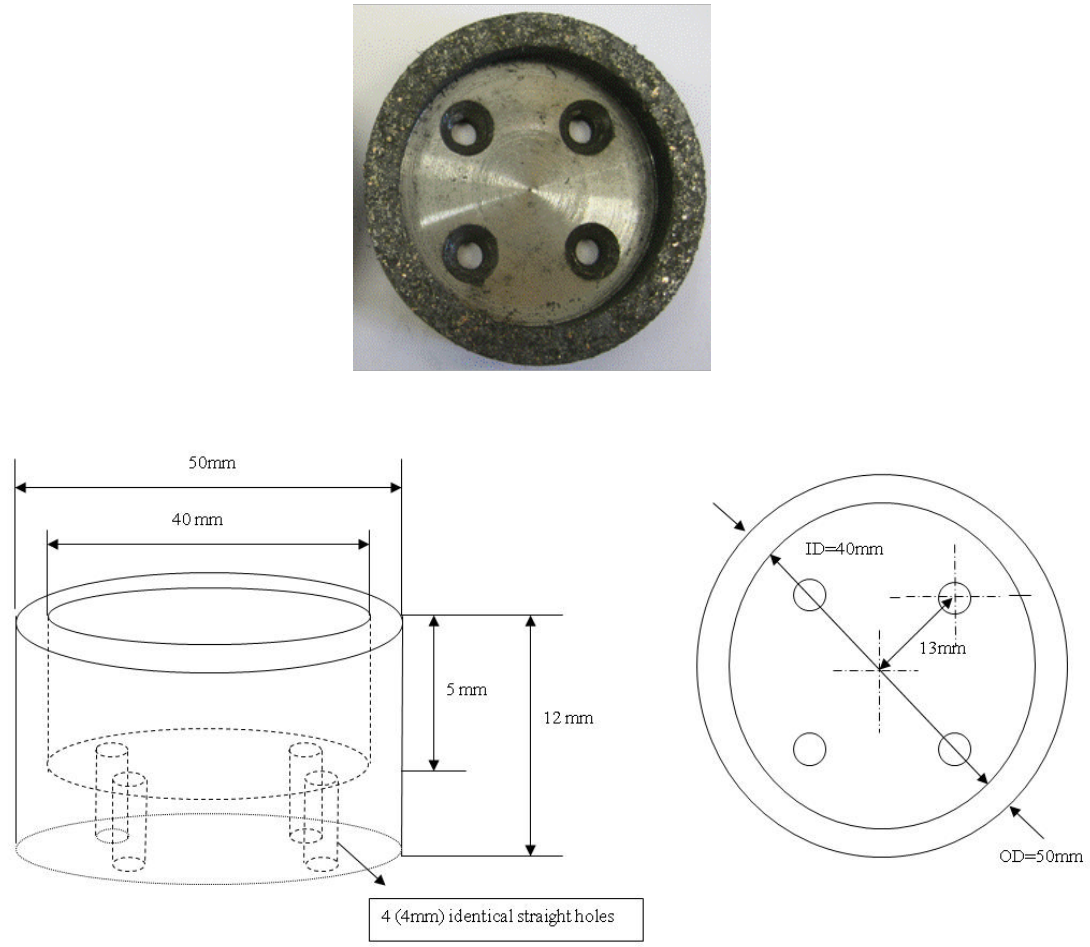

Figure 3-2 Drawing and digital image of pads sample

3.2.2 Surface preparation

Before dynamometer testing, all surfaces of C_f/C-SiC discs were finished following the same procedure: the as-received surfaces of C_f/C-SiC discs were ground on a grinder (Struers Tegrapol-25, Denmark)) with diamond grinding plates starting from a grit size of about 68 µm (220 mesh), then 26 µm (600 mesh), and 15 µm (1200 mesh), with a removing thickness of about 300 - 400 µm per step; the ground surfaces were polished with 3 micron diamond paste on a polisher (Struers Tegrapol-25, Denmark), to ensure any damage left from previous grinding step were completely removed. Surface of pad lining material was also ground by grinding wheel with 3 mm SiC grits. This grinding process was accomplished by pad supplier.

3.2.3 Chemical etching

Before and after the dynamometer testing, dilute HF acid (H_2O: 40% HF =40:1) was used to etch the surface of C_f/C-SiC disc to remove oxidized layer (e.g. SiO_2) formed on SiC, if any. C_f/C-SiC was washed with acetone after 1 hour etching in HF at room temperature, and then washed with deionised water in ultrasonic bath. This scheme was designed and used to ensure the change of surface topography in SiC region can be clearly exposed under optical microscopy, before and after friction test. Chemical reaction, taking place between SiO_2 and HF, are expressed in the following formula;

$$SiO_2+HF \longrightarrow SiF_4\,(g)+H_2O$$

To reveal the crystal size and defects in SiC, C_f/C-SiC samples were etched in molten KOH at temperature of about 500^{o}C for 20 minutes. Si and crystal defects in SiC, like stacking faults and dislocations, can react with molten KOH preferentially.

3.3Laboratory scale dynamometer testing equipment

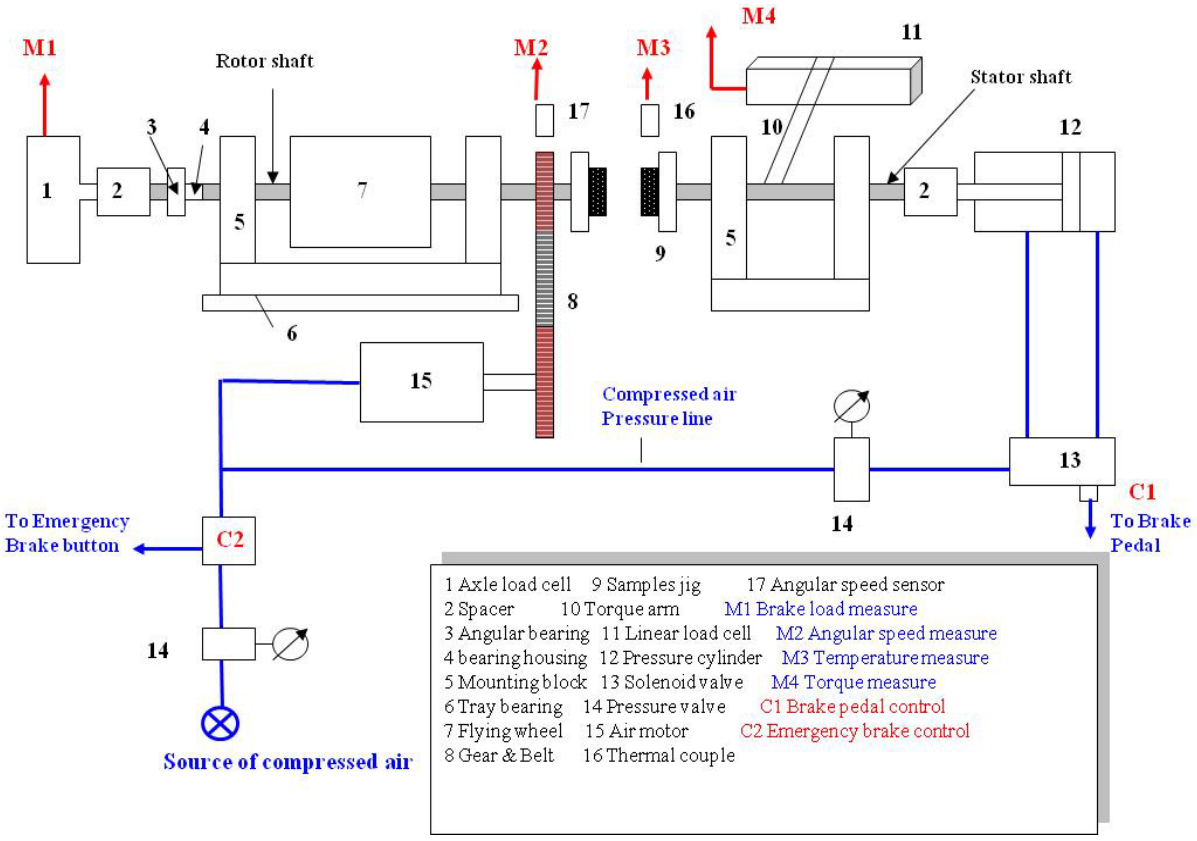

Figure 3-3 Schematic diagram of laboratory scale dynamometer testing equipment

In this research, all friction tests were conducted on a laboratory scale dynamometer. The schematic diagram of assembles of the dynamometer is shown in Figure 3-3. This dynamometer can provide inertia of 0.0007 kg.m^2 and capability of operation with a rotation speed up to 18,000 rpm and braking force up to 800 N. In each braking test, the C_f/C-SiC disc rotated, with its kinetic energy being provided through a spinning flying wheel driven by an air motor. The gas cylinder and solenoid valve were used to control the engagement of the pad with the spinning disc through an operation of the brake pedal. Solenoids valve was triggered to push the piston in gas cylinder moving forward, once the brake pedal was pushed down. This action led to an engagement between spinning disc and pad until the disc was completely stopped by pad. The piston retracted back when brake pedal was released. This action allowed pad to

separate from disc such that the disc can start rotation again. The braking time needed for each stop was about 1 second, and the time interval for the start of next braking after a stop was about 6 seconds. The pressure valves were used to control the disc rotation speed and braking pressure. The signals of rotation speed, normal braking load and braking torque were directly collected by a data logger with a capture frequency of 50 Hz; these signals were then converted into numerical data by designed software. Throughout all the tests in this research, a constant disc rotation speed of 11000±200 rpm was maintained until the first touch by the pad. And a normal braking force of 540± 20 N was chosen to carry out the testing. For each brake application, the coefficients of friction were calculated using following equation:

$$\mu = \frac{T}{W \times R_e}$$

where T is the braking torque, W the normal braking load and Re the effective radius (22.5mm here) of friction contacting area. Under current testing conditions, braking pressure was about 0.9 MPa, and linear velocity of C_f/C-SiC disc ~25m/s; such a test set-up on a small scale dynamometer was inside the test regime for most vehicle-based tests, apart from the size of the braking area was significantly scaled down.

3.4 Laboratory scale dynamometer friction test procedures

3.4.1 Discrete friction testing

The discrete small dynamometer testing was performed in laboratory in order to trace the development of transfer layer step-by-step on contact surface of C_f/C-SiC composites, especially on each key phase. In order to follow the development of friction surface, observing points were set after braking stop at the 1st, 2nd, 3rd, 6th, 9th, 14th, 19th, 29th and 49th, where the disc and pad were taken off from the friction testing rig, and re-fixed as they were in the original set-up, after completing all

examinations. One observation is called hereinafter for all measurements between the closest observing points; these measurements included COF values of all stops, and microstructure details on the friction surface after the last stop inside an observation. Figure 3-4 schematically illustrated the procedures of discrete small sale dynamometer friction test.

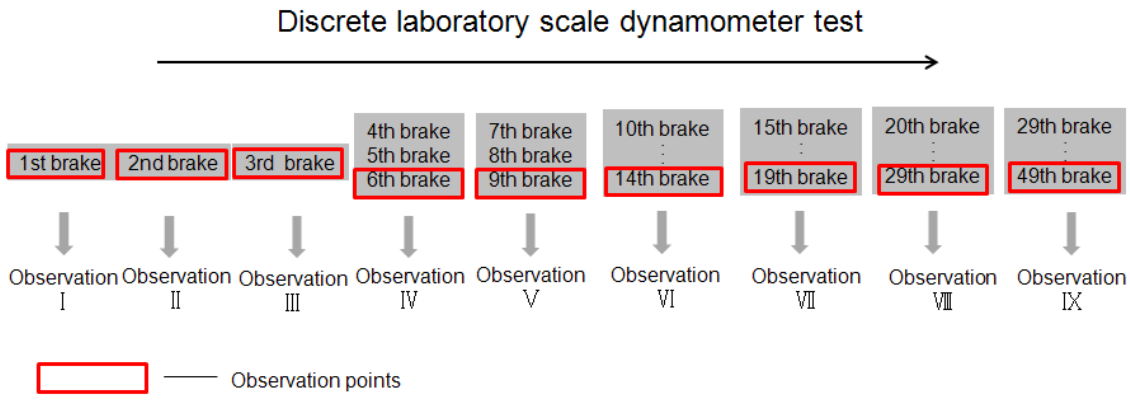

Figure 3-4 Schematic illustration of the discrete small dynamometer testing procedures

3.4.2 Continuous friction testing

Continuous friction testing was conducted without taking components off for any examinations. In this research, a total of 200 accumulated stops were done for continuous friction testing.

3.5 Characterisation

3.5.1 MEF3 optical microscopy

Optical microscopy (OM) (MeF3, Reichert-Jung, Wien, Austria) was used to image the virgin surface after polishing of C_f/C-SiC composites and in-plane friction surface after dynamometer test. Polarised lighting was used to differentiate key phases, e.g. silicon carbide, graphite, silicon, carbon fibre filaments and transferred materials. Differential

interference contrast (DIC) was also applied to exam topography of friction surface after dynamometer test.

3.5.2 Field Emission Scanning Electron Microscopy

Field Emission Gun Scanning Electron Microscopy (FEG-SEM) (Leo S360, Cambridge Instruments, Cambridge, UK), equipped with EDAX energy dispersive X-ray (EDS) system, was used in this research for imaging the friction surface of C_f/C-SiC disc, chemical analysis of transfer layer and mapping the chemical elements in organic pad. For imaging and chemical analysis of thin transfer layer on friction surface of C_f/C-SiC composite disc, the operating electron acceleration voltage was set to 5 kV. For mapping the chemical compositions of organic pad, 20 kV voltage was selected for this operation.

3.5.3 DBFIB electron microscopy and TEM electron microscopy

Cross section of friction surface was examined by transmission electron microscopy (TEM) with the assistance of double-beam focused ion-beam microscopy (DBFIB). Cross section samples were made with DBFIB (FEI Nava 600 nanolab, Oregon, USA) as following: on interested area, a gallium ion beam was used to dig two trenches from both sides of interested site under a HT of 30 kV and currency of 20 nA, after platinum layers were deposited by low energy electron beam (10 kV) first and then ion beam (30 kV), which provides a protection of the original surface from any damage by the high energy ion beam. Before the thickness of the cross-section wall reduced to about 2 micrometres, both sides were milled with low energy beam with a currency of 7 nA to clean and smooth the cross section of the foil. Then the membrane of TEM sample was lifted out and welded on Cu grids. A final thinning process was carried out by using 5 kV and 0.3 nA ion beam to further minimise the depth of any residual damage by the ion beam, if any. The typical thickness made by this procedure was about 200 nm. Cross section TEM foils made for this study included these regions containing following

substrate constituents: silicon; silicon carbide; carbon fibres (C_f) bonded by pyrolytic carbon (pyC) through CVI process.

TEM observation was carried on JEOL 2000F (JEOL, Japan) with EDX probe (Oxford Instrument, UK). Typical imaging condition was under 200 kV and EDX spectra acquisition at 200 kV. Bright field image and EDX analysis were carried out to study the fine-scale morphology and chemical composition of transferred material, as well as the interaction between transfer layer and substrate material. Double tilt sample holder was used to rotate and tilt TEM sample to obtain zone axis diffraction patterns for observation of deformation of friction surface.

3.6 Quantification from optical image

After capturing optical images on as-polished surface of C_f/C-SiC, the software Image J was used to measure the area percentage of key phases displayed on OM images. The measurements procedures are illustrated in the Figure 3-5(a)-(e). For instances, in Figure 3-5 (b) Si phase was distinguished from others by grey scale, and it was highlighted to red region through adjusting threshold (as shown in the insert); after then the software automatically worked out the area percentage of the red region by calculating the number of red pixels. The SiC regions and C_f regions were highlighted in the same way as shown in Figure 3-5(c) and (d). The area percentage of these three regions was listed in Figure 3-5(e).For any claimed measurements, 30 optical images were taken from arbitrarily selected areas, and area percentage of each phase was averaged from the 30 OM images by using equation 3-1

$$A_{(average)}\% = \sum_{i=1}^{n} A_{(i)}\% \Big/ n \quad (n=30) \qquad \text{Equation 3-1}$$

Standard deviation s, is calculated from equation 3-2

$$s = \sqrt{\frac{\sum_{i=1}^{30}\left(A_{(i)}\% - A_{(average)}\%\right)^2}{n-1}} \qquad \text{Equation 3-2}$$

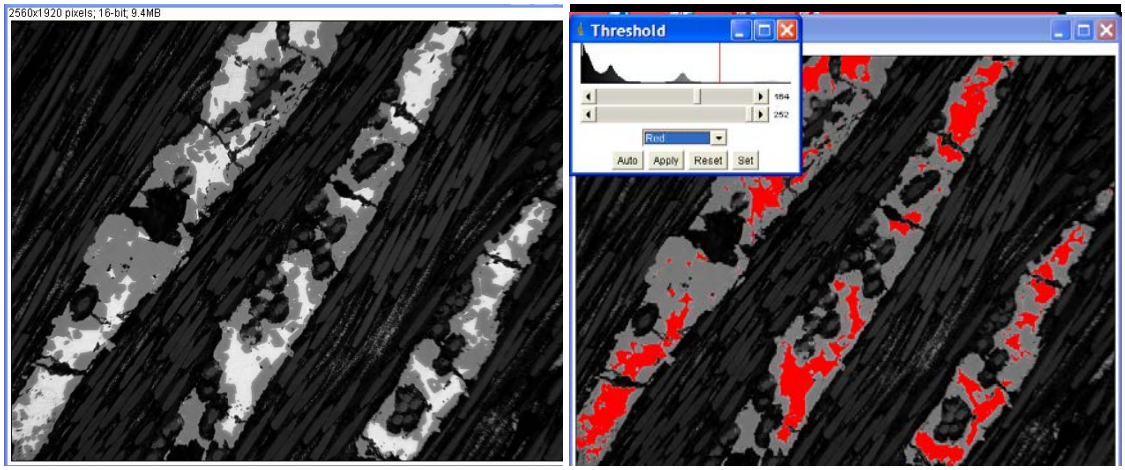

(a) (b)

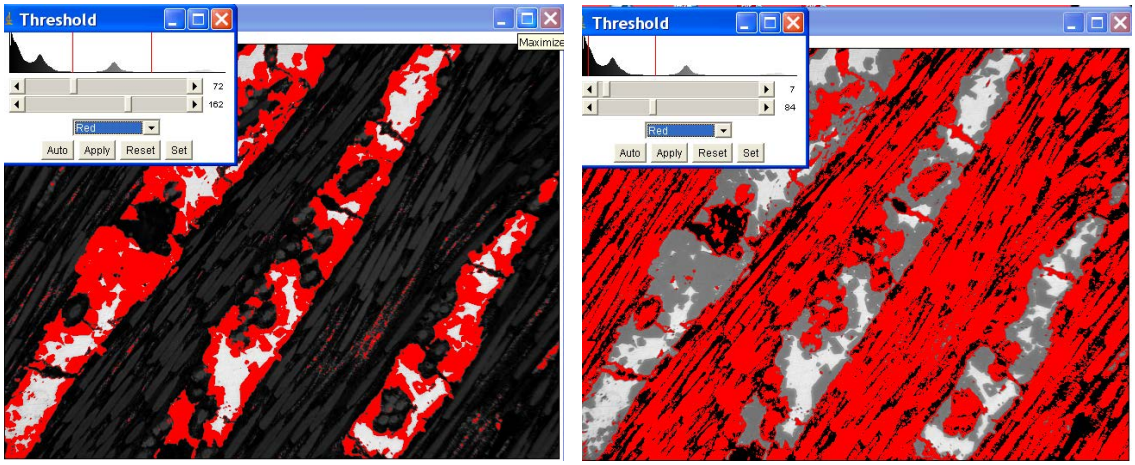

(c) (d)

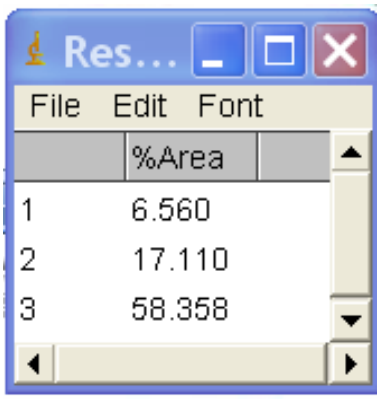

(e)

Figure 3-5 Estimation of area percentage by using Image J software: (a) original optical image (b) highlighted Si region (c) highlighted SiC region (d) highlighted C_f region (e) list of results

Chapter 4 Results

4.1Microstructure of virgin C_f/C-SiC brake disc material

4.1.1 Architecture of C_f/C preform

In this research, the C_f/C preform, used for silicon infiltration, had 3D structure. The layout of the 3D structure is schematically illustrated in Figure 4-1. The 3D preform was made from alternate layers of 0° unidirectional long carbon fibre layer, chopped carbon fibre mat having no preferential carbon fibre orientation, and 90° unidirectional long carbon fibre layer. Vertical long carbon fibres bundles were needled through these layers to hold the fibre lamina together. There were three types of fibre layout on the friction surface: (a) surface was composed of longitudinally orientated in-plane long carbon fibre bundles, carbon matrix (CVI C), and needled carbon fibre bundles with fibre ends exposed on surface (Figure 4-1), called **UDC type** of surface microstructure hereinafter (UDC stands for unidirectional carbon fibre); (b) surface was composed of chopped carbon fibre bundles without preferential orientation direction, carbon matrix, and needled carbon fibre bundles with fibre ends exposed on surface (Figure 4-1), called **CC type** of surface microstructure hereinafter (CC stand for chopped carbon fibre); (c) surface was composed of both UDC and CC type of fibre layouts. In this study, most of friction surface had the third type of fibre layout.

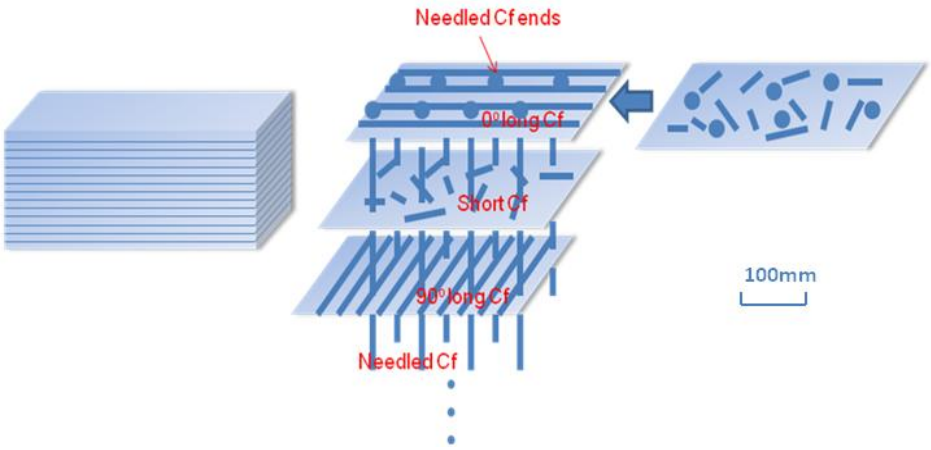

Bulk prefrom UDC type of surface microstructure CC type of surface microstructure

Figure 4-1 Schematic diagram of 3D C_f/C preform with UDC and CC type of surface microstructure

4.1.2 Microstructure of as-manufactured C_f/C-SiC

4.1.2.1 Microstructure of cross-section

Figure 4-2 (a) is the optical image from polished cross section of C_f/C-SiC composites. Cross-section structure of 0° unidirectional long C_f/C layer is shown on the left hand side of image; in-plane structure of 90° unidirectional long C_f/C layer is shown on the right hand side. In the middle of the image, the random orientated short carbon fibre layer shows between these two layers. The thickness of each layer is about 500 µm. The three layers were needled together through a long carbon fibre bundle. The space between the nearest needled C_f is about 150µm. Intensive Si and/or SiC were found inside short carbon fibre layer and around needled carbon fibre, as marked in Figure 4-2 (a). Only a small amount of ceramic constituent was observed in longitudinally orientated C_f/C layer, since the dense carbon fibre bundles only provided limited space for Si infiltration taking place.

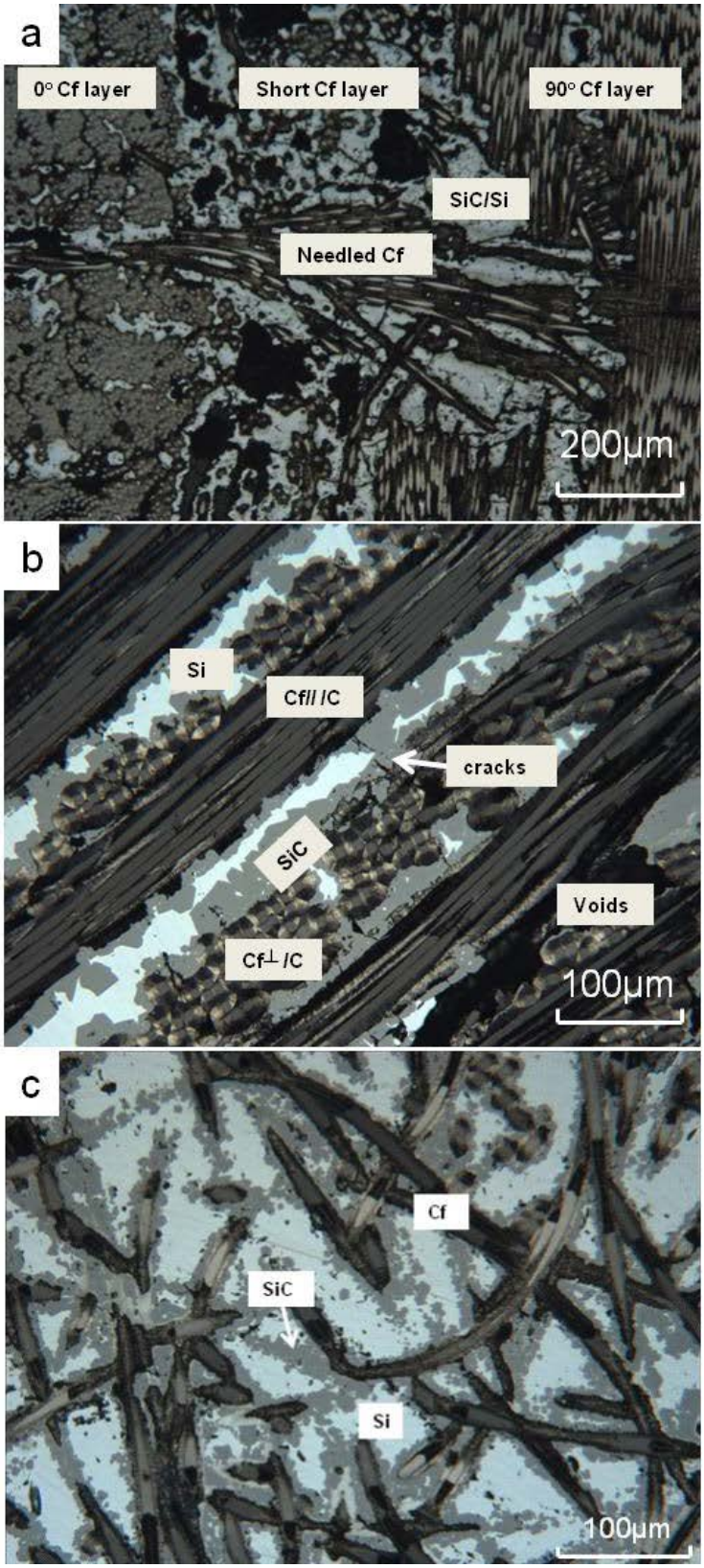

Figure 4-2 Optical image of as-polished C_f/C-SiC composites (a) cross-section of C_f/C-SiC, (b) C_f/C-SiC with UDC type of surface microstructure, (c) C_f/C-SiC with CC type of surface microstructure

4.1.2.2 Microstructure of the in-plane surface

As mentioned before, the different layout of C_f/C preform produced two kinds of surface microstructure. Figure 4-2 (b) and (c) show two types (UDC and CC type) of typical microstructure of as-polished virgin in-plane surface of C_f/C-SiC composite. They can be distinguished by the length and orientation of the carbon fibres.

In surface region with UDC microstructure, shown in Figure 4-2 (b), two types of oriented carbon fibres can be identified: in-plane long fibres (C_f//) with fibre parallel to the in-plane surface, and needled fibres ($C_f\perp$) with fibre directions nearly perpendicular to the friction surface. Each fibre filament was surrounded by a layer of carbon. These carbon regions showed double refraction (bright and dark contrast) under polarized lighting conditions, which indicated that the carbon matrix could be graphitised region with fairly uniform structure. Silicon carbide and silicon regions existed among the fibre bundles, which showed grey and white contrast respectively. In microstructural aspect, voids with a size scaled up to hundreds micrometres and cracks/crevices existed on the as-finished surface as marked in Figure 4-2(b) , as well as small porosity within a scale of a few microns inside SiC.

In surface region with CC microstructure, shown in Figure 4-2 (c), two types of carbon fibres were identified on the polished surface, in-plane short carbon fibres with length in a range of few hundred microns and no preferential orientation, and needled fibres ($C_f\perp$) with fibre directions nearly perpendicular to the friction surface. Carbon fibre filaments were surrounded by a layer of carbon. A layer of SiC with thickness of tens microns existed between residuals Si and carbon. In addition, there were some isolated SiC islands lying in the residual silicon. Apart from SiC and C_f/C regions, other surface areas were occupied by un-reacted residual silicon.

It was clear that the amount of each phase was different for UDC type and CC type of surface microstructures. 30 optical images were taken under the same imaging condition, and then image J was used to measure the area percentage of key phases for all images. The averaged area percentage and standard deviation of each key phase were listed in Table 4-1. Apart from the microstructure variations, it can be concluded that, the C_f/C-SiC composites were composed of a structure with a clearly arranged hierarchy of multi phases, C_f, C, SiC and Si, along with voids/porosity and cracks.

Table 4-1 Averaged area percentage of each key region on surface consisting of UDC and CC architecture

Fibre architectures	**Si**	**SiC**	**C_f/C**
UDC	3.2±2.2%	14.8±3.8%	62.2±6.3%
CC	10.5±3.8%	42.2± 6.6%	18.5±3.2%

The SiC phase in C_f/C-SiC composite had a polycrystalline structure. Figure 4-3 shows the SiC crystals on the interface of Si/SiC after removal of Si by KOH chemical etching; the SiC crystals in this observed region had grain size ranging from 2 to 20 micrometres. The kinks observed on SiC crystals were produced by defect-selective etching of KOH. These kinks indicated the existence of crystal defects in SiC, i.e. stacking faults. The crystal defects were originated from the manufacture process.

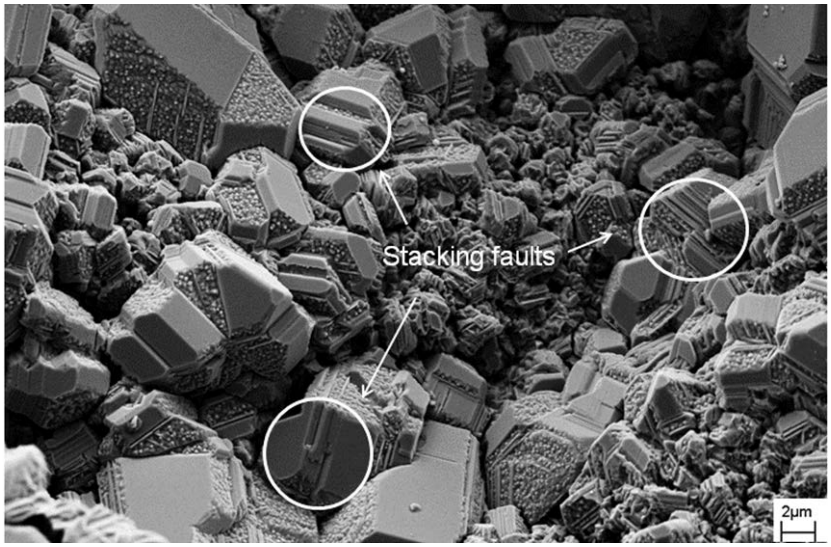

Figure 4-3 SiC crystal on interface of SiC/Si after removal of Si by chemical etching

Further TEM cross-section examination was taken to exam the crystallography and microstructure of SiC before friction testing. Figure 4-4(a) shows the cross sections image of SiC (A single Si crystal is presented in the upper part of image). This TEM image confirmed that the stacking fault exist in the SiC crystals. The diffraction pattern from SiC region with a zone axis of [111] is shown in Figure 4-4(b). The diffraction pattern indicates the SiC has f.c.c cubic structure (β-SiC).

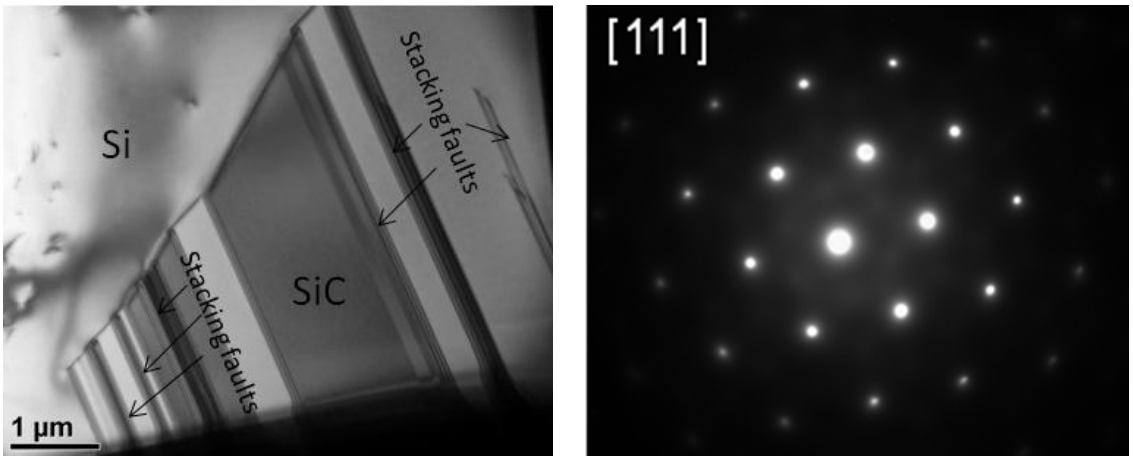

(a) (b)

Figure 4-4 (a) TEM image shows the stacking faults in as-manufactured SiC (a single Si crystal is presented in the upper part of image), (b) diffraction pattern taken from as-manufactured SiC

4.2 Microstructure and chemical composition of organic pad lining material

The microstructure of the organic pad was investigated by FEGSEM (Figure 4-5(a)). The EDX maps of possible chemical elements are shown in Figure 4-5(b). The organic pad consists of Al, Ca, C, Cr, Cu, Fe, Mg, O, P, Si, S, Sn, Ti and Zn. Among these elements, Fe exists as fibre with a length of several hundred microns, and C exists in a form of particle with size of several hundred microns. There are two types of Cu, one is associated with Zn having a particle size of several hundred microns, another is pure Cu having particle size of tens microns. Ca is associated with Mg, Si and O having a particle size of several hundred microns. There are two types of Al, one is associated with O, and another is associated with Si and O. Both of them have particle size of several hundred microns. P is associated with O having particles size of tens microns. Cr is associated with O particles having size of tens microns. Ti is associated with O having particles size of tens microns. S is associated Sn having particles size of tens microns.

According to EDX mapping analysis, the possible major chemical constituents in the organic pad include iron (Fe), brass (Cu/Zn), copper (Cu), carbon (C), aluminium oxide (e.g. Al_2O_3), calcium magnesium silicates (e.g.$CaMgSi_2O_6$), aluminium silicates (e.g.$Al_2(SiO_3)_3$), calcium sulphides (e.g. CaS), tin disulphides (e.g. SnS_2), phosphate oxides (e.g. P_2O_5), titanium oxides (e.g. TiO_2), and chromium oxides (e.g. Cr_2O_3).

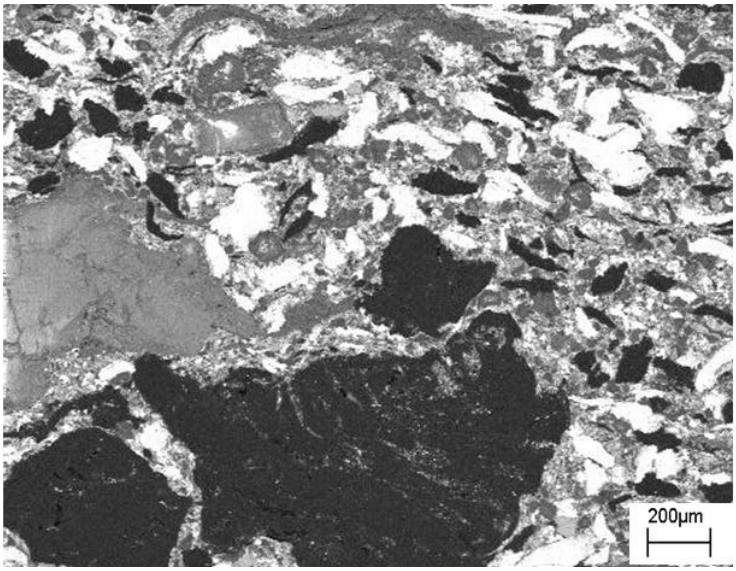

(a)

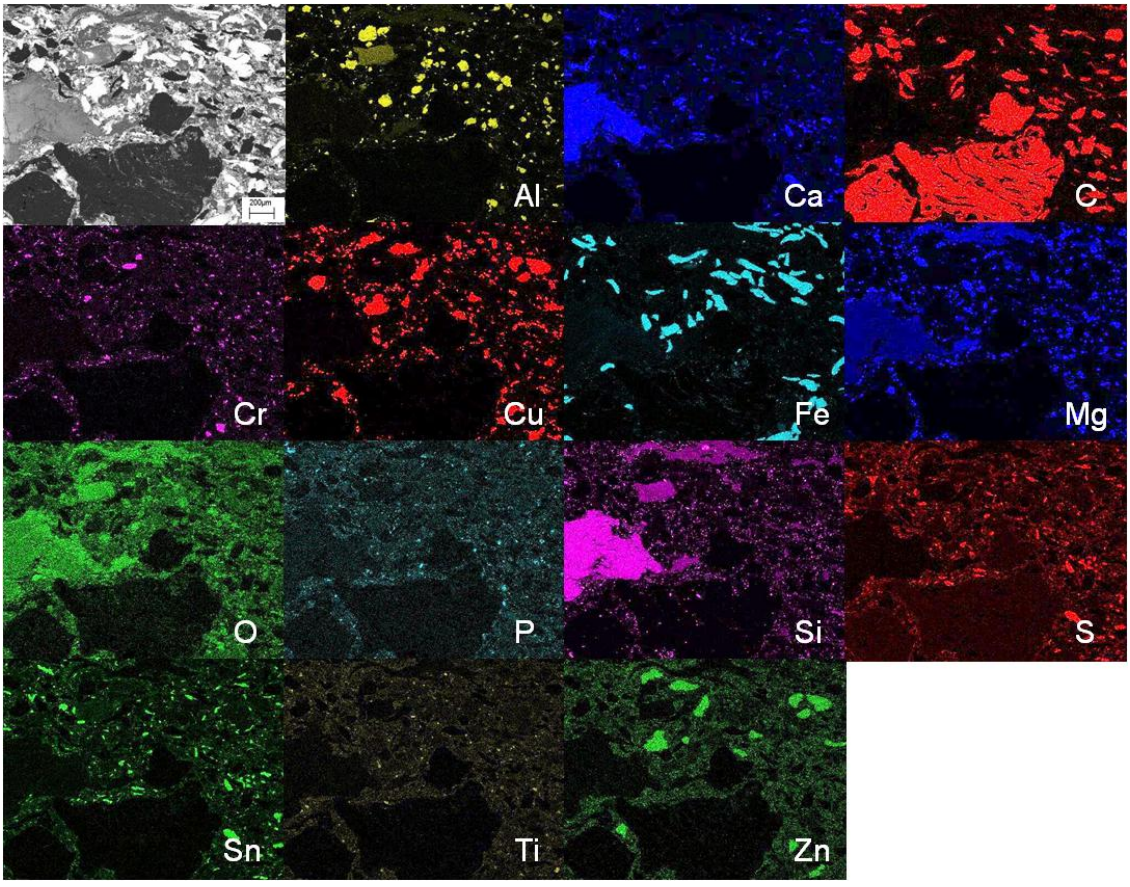

(b)

Figure 4-5 (a) SEM image of as-polished surface of organic pad and (b) maps of possible chemical elements on the surface acquired via EDX probe

4.3 Discrete dynamometer testing of C_f/C-SiC against organic pad

4.3.1 Friction performance measurement

The measurements of COF of C_f/C-SiC composites, when organic lining was used for the pad, are plotted in Figure 4-6 against the accumulated braking stop numbers. For each stop, the averaged value, with its standard deviation, was a result of four repeated tests using the same disc and pad lining under the same testing conditions. The results were also grouped into observations as shown in Figure 4-6, and measurements inside each observation were linked with a line to show the trend of variation of COF with braking stops. Inside each observation, the measurements of COF showed an ascending trend with the increase of the accumulated braking stops (see observations IV–IX), apart from observation I–III where only one braking stop was included. In any observations consisting of multi braking stops, the first stop gave the lowest COF, comparing to the others following it; the COF values of the first stops in all observations were mostly at a similar level. Among these first brakings, the very first one in observation I had the lowest COF, and the one in observation IX gave the highest value, whilst the average values and standard deviations for both first brakings were inside the ranges of error bars of other first brakings. From observation IV to IX, after same number of braking stops, the COF values in the later observation were generally higher than that in previous one. It was also noticed that from observation VII, the second braking clearly boosted the level of COF, and then a gradual improvement was followed for each further braking. Among all observations, none of these showed that the measurements of COF had reached a plateau, an indicator that was usually used to mark the end of bedding process, even in the last observation where most stops were applied.

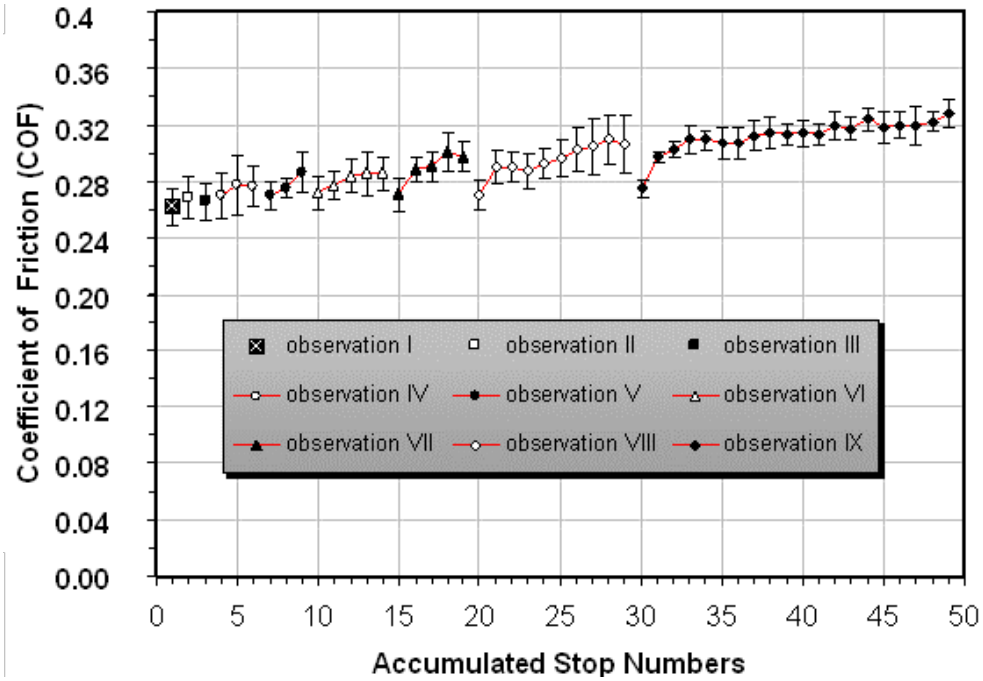

Figure 4-6 COF measurements from discrete laboratory scale dynamometer testing

4.3.2 The generation of friction surface on C_f/C-SiC disc

4.3.2.1 Overview of friction surface

The optical image, Figure 4-7, shows the overview of friction surface after dynamometer friction test. The Si region, which had white contrast and was typically surrounded by SiC on virgin surface (as shown in Figure 4-2(b)), was no longer to be differentiated on the friction surface. Instead, dark grey layers deposited on SiC region in patches with variable sizes. It looks these patches were fairly dense under the OM imaging condition. The exposed SiC still remained similar surface morphology as that on the as-polished, but among them, there were deposites. The carbon fibre regions were exposed as they were on as-polished surface, but friction tracks appeared along friction direction. The pyrolytic carbon matrix inside carbon fibre bundle (C_f/C) behaved in a similar way as carbon fibre. No sizable transferred materials patches were observed above the C_f/C regions. More details on the transferred materials development process on each key region will be studied step by step in the following sections.

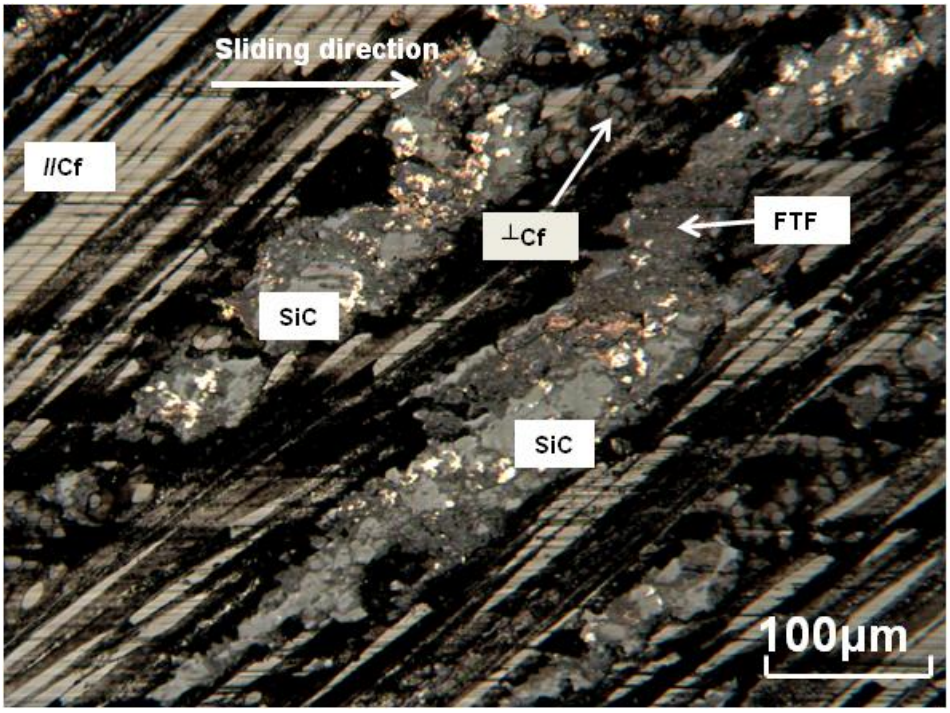

Figure 4-7 Optical image of overall friction surface of C_f/C-SiC after discrete dynamometer testing with 49 accumulated stops

4.3.2.2 Friction surface on Si region

Development of friction surface

A series of OM images in Figure 4-8 show the development of friction surface in a silicon region. All images were taken from same region. With the increase of accumulated numbers of braking stop, a transfer layer has been built up continuously on the top of this region. Under the current imaging condition, the friction surface after two stops showed three types of contrast: type A in brownish (or light grey in black and white printing), type B in bright white, and type C a mixture of dark grey and white or dark grey only, as marked in Figure 4-8 (b); it was evident that type A layer prevailed on the friction surface, whilst type B and C existed in isolated patches. By increasing one more braking stop, more type B and type C patches appeared, with a significant shrinkage of type A area, as arrowed in Figure 4-8 (c). Up to 19 stops, type A contrast was observed in scattered small areas only, but type B and C predominated

the friction surface (Figure 4-8 (d)). By further increasing the number of braking stop to 49, the friction surface showed predominant type B and C contrasts (Figure 4-8 (e)). As transferred materials with different contrasts were observed on the friction surface of Si phase by OM method, secondary electron microscopy and EDX were used to analysis their morphology and chemical composition. SEM images and corresponding EDX spectra from areas with different contrasts are summarized in Figure 4-9. The friction surface with type A contrast was copper-rich, comparing to other areas; type B was iron rich, and type C contained both copper and iron in a significant amount, as indicated by the intensity of the L lines of Fe and Cu in the EDX spectra. Inside the type A and type C, there existed a significant amount of magnesium and oxygen, while in type B, both oxygen and magnesium were in a very low level, if any. It is yet impossible to confirm whether the existence of oxygen is related to the appearance of other elements, e.g. copper/magnesium, at the level of SEM characterization. The morphology of the friction surface can be differentiated among these three types from the secondary- electron images: both the type A and C look a bit of crumbling with visible granulated materials in the layer, though the size of the crumbles in the type A was much smaller than in the type C; the type C had a rougher surface, comparing to the type A, with the existence of craters, voids and cracks. In contrast to the type A and C, the type B layer had a smoother surface with much fewer visible particles and voids.

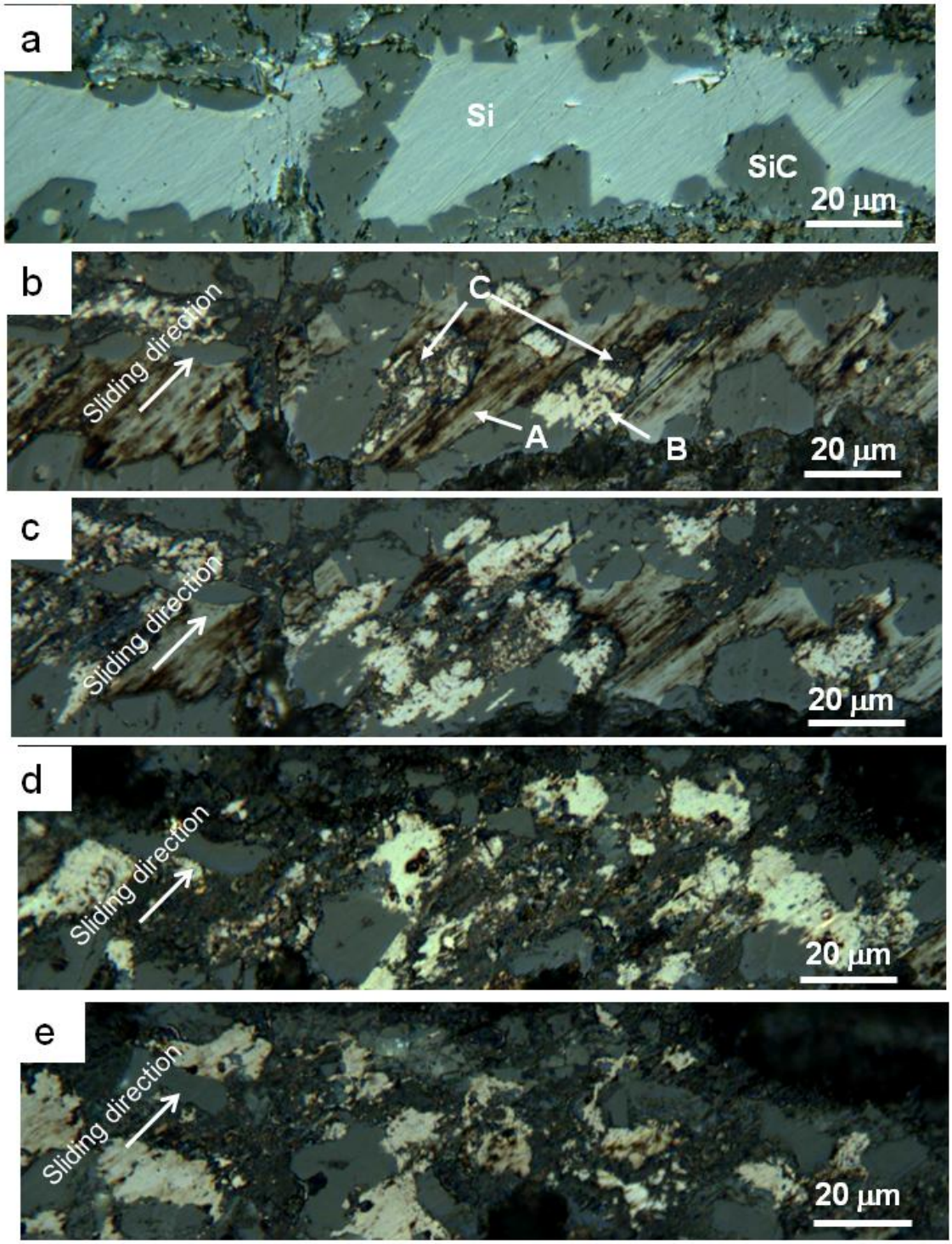

Figure 4-8 Registered OM images to illustrate the development of friction surface in silicon regions of the composite: (a) as-finished surface in silicon regions before braking test; (b), (c), (d) and (e) the surface after the 2nd, 3rd, 19th and 49th braking stop, respectively. The arrowed areas are categorized as type A, type B and type C friction surface that consists of friction transferred layer on top and displays a contrast of brownish, white, and dark grey or a mixture of dark grey and white, respectively.

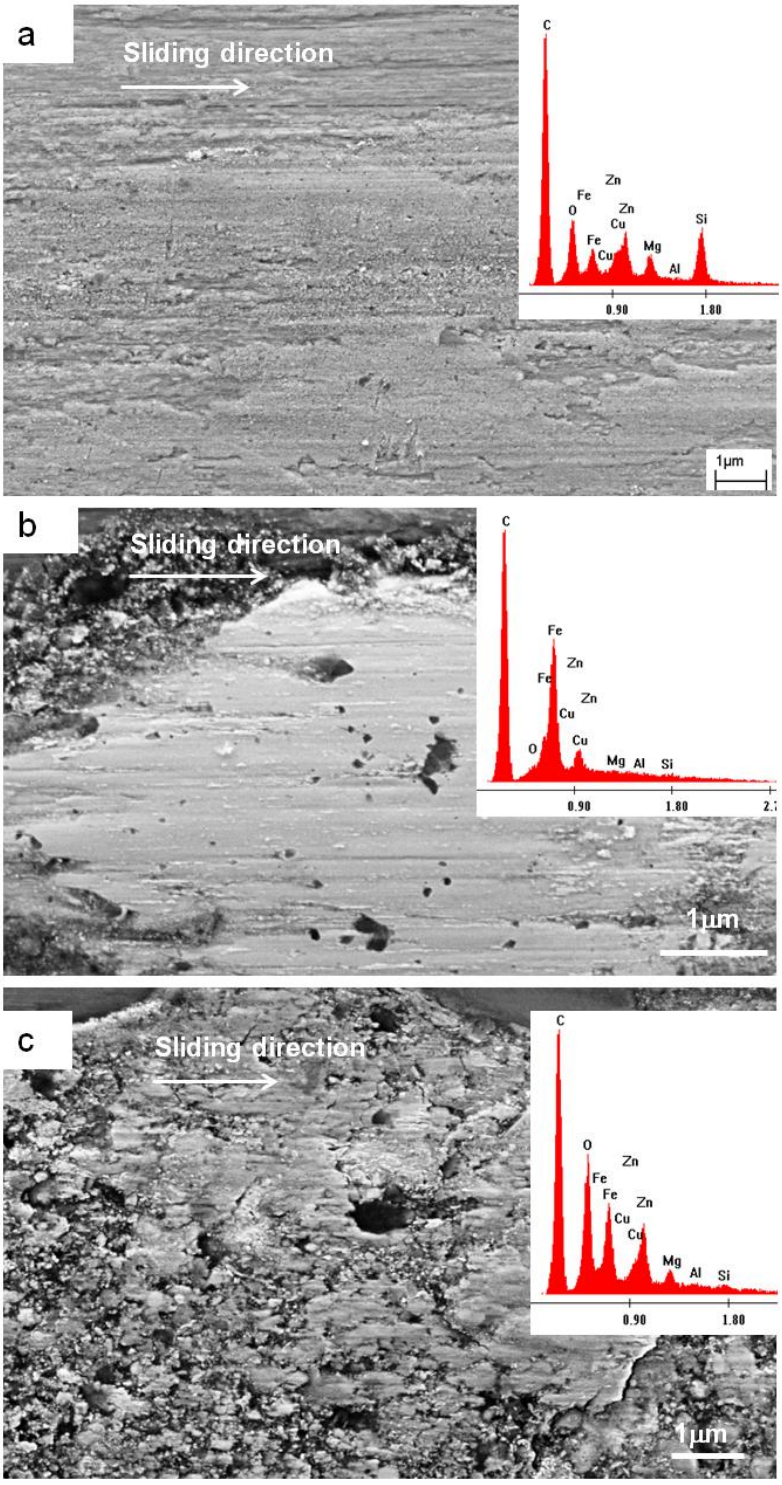

Figure 4-9 Secondary-electron images of silicon regions where three types of friction surface appeared in OM imaged (see Figure 4-8) when the composite disc was subjected to two braking stops. (a) region with brownish contrast (type A); (b) regions with white contrast (type B); (c) region with a mixture of grey and white colour (type C). Inset in each image is the EDX spectrum obtained from this region under an accelerating voltage of 5kV.

Microstructure of transfer layer

The cross section TEM image of transfer layer developed on friction surface of Si reveals a complex morphology. On the investigated area, the thickness of transfer layer was about 5 μm, as shown in the low magnification TEM image Figure 4-10(a). The framework of the transferred layer was composed of three types of constituents having different chemical composition and morphology, including: very fine particles with size about tens nanometres; fine particles with size about a few hundred nanometres; and binding phase which bonded two types of particles together, as shown in high magnification image Figure 4-10(b). The details of each constituent were shown in separated TEM images with higher magnification, from Figure 4-11 to Figure 4-13.

When only binding phase was analysed, small beam size was chosen. When large beam size was chosen, X-rays from both nano-sized particles and binding phase were included in the analysed area, as marked on Figure 4-11(a). The EDX spectrum taken from the binding phase only, by using smaller beam size (as marked in Figure 4-11(a)), was shown in Figure 4-11(b), it contained Si and O. As shown in Figure 4-11(c), apart from Si and O, Fe and a small amount of Cu, Zn and S appeared which should be the chemical constituents of nano-sized particles.

In Figure 4-11 (a), the insert diffraction pattern on the lower-right, taken from the binding phase, shows a diffused ring. This type of diffraction pattern suggests that the binding phase had an amorphous structure. Diffraction pattern on upper-left corner was taken from nano-sized particles embedded area. The diffraction spots appeared around the diffused ring were contributed from nano-sized particles. The d-spacing values were calculated from this diffraction pattern, and listed in Table 4-2. It was found that the calculated values could match with the d-spacing of $FeSiO_3$[111] and $Fe_{0.91}Si_{0.09}$[112] crystal planes (Table 4-2) in database[111, 112]. Combined EDX results and DP

analysis together, the author believes that binder phase was amorphous SiO_x and the nano-particles contained $FeSiO_3$ and/or $Fe_{0.91}Si_{0.09}$, which could be the alloyed product of SiO_x and FeO_x, and Fe and Si, produced during friction.

Figure 4-12 (a) shows TEM image taken from nano-particle enriched area. The insert different pattern was composed of sharp diffraction rings and spots. Calculated d-spacing values from diffraction rings are listed in Table 4-3. These d-spacing values could be matched with d-spacing values of $Cu_{2.7}Fe_{6.3}Si$ [111], $Ca_{0.15}Mg_{1.85}(Si_2O_6)$ [111], MgO [112] and CuO [112] as compared in Table 4-3. EDX spectrum in Figure 4-12 (b) indicates these nano-crystals contain O, Fe, Cu, Zn, Al, Mg, Si, S and Ca.

It can be deduced that there are three major resources of nano-crystals: fine wear debris originating from minerals constituents in organic pad, such as $Ca_{0.15}Mg_{1.85}(Si_2O_6)$ and MgO; oxidation products of metal constituents in pad friction lining, such as CuO; alloyed products of metals and Si, such as $Cu_{2.7}Fe_{6.3}Si$ and $Fe_{0.91}Si_{0.09}$; and the alloyed products of metal oxides and silicon oxides, such as $FeSiO_3$.

Sub-micron sized particles with dark contrasts were bound together by amorphous binder phases. Figure 4-13 (a) shows the typical microstructure of sub-micron particles. Dislocations appeared in both particle A and B. As shown in EDX spectrum, Figure 4-13 (b), these particles were dominated by Fe, with considerable amount of Si and a small amount of Cu. It was also noticed there was no oxygen involved in these crystals. The quantified results of Si, Fe and Cu are listed in Table 4-4; the atomic ratios of Cu/Si and Fe/Si are 0.4 and 1.3, respectively. This sub-micron sized particles could be an alloyed product of Fe, Cu and Si.

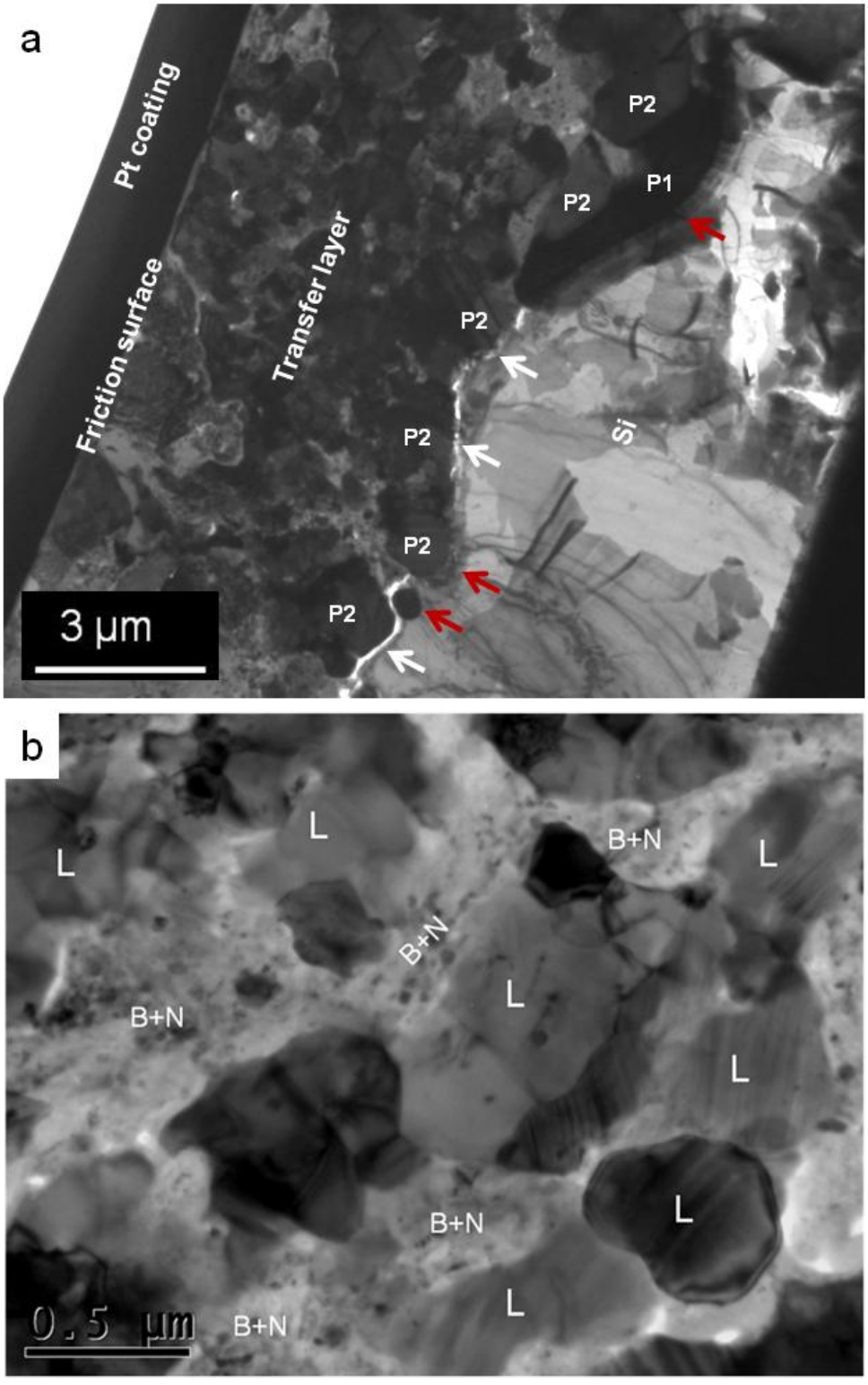

Figure 4-10 (a) Low magnification cross section TEM image of transfer layer developed on fiction surface of Si (Note; P1and P2 particles have different chemical composition, P1 contain Cu and Si; P2 contains Fe, Cu and Si (b) high magnification cross section TEM image of transfer layer (B+N) stands for binding phase and nano-particles, L stands for submicron scale large particles)

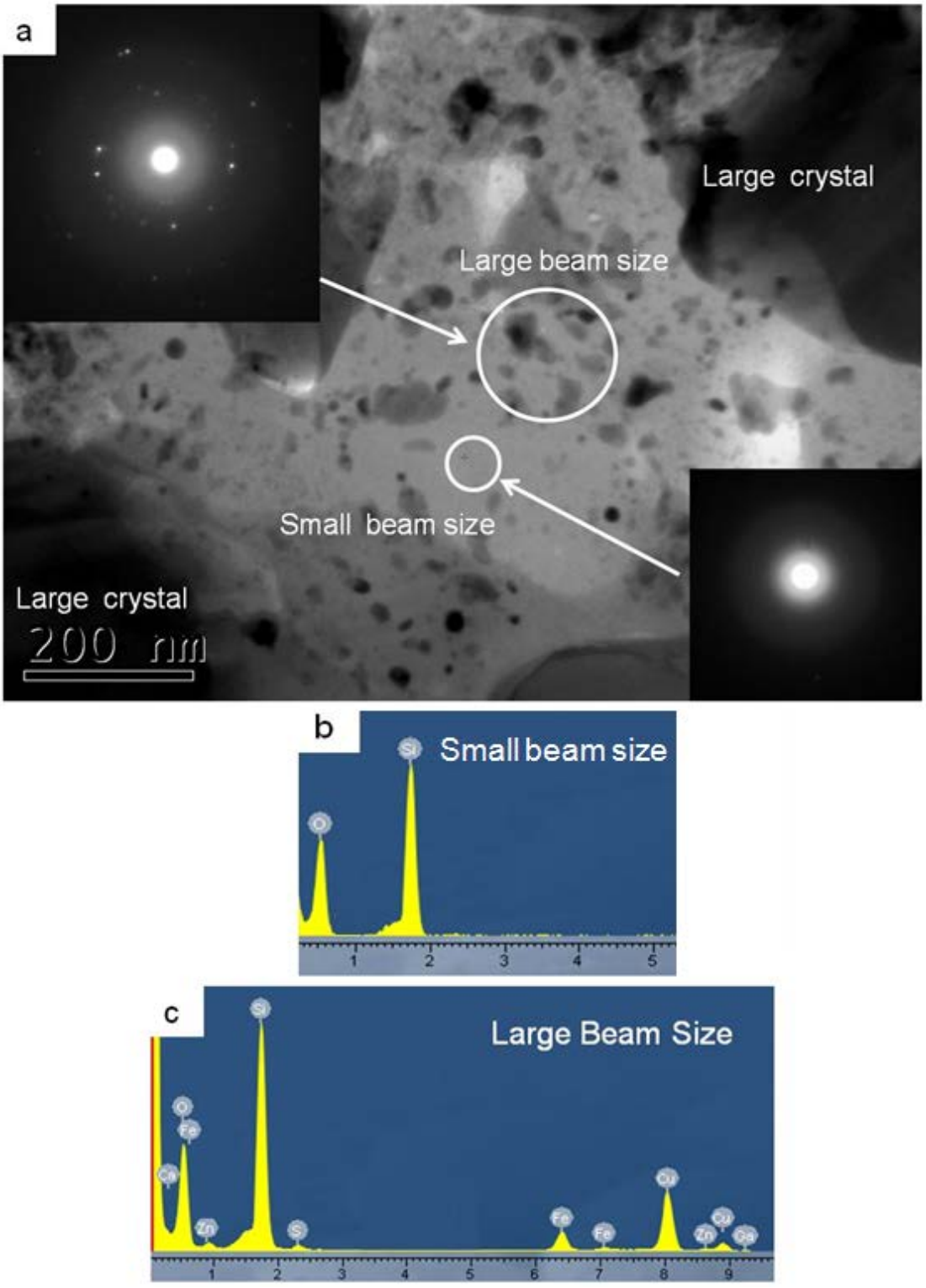

Figure 4-11 (a) TEM cross section image showing nano-sized particles distributed in binding phase; the insert diffraction patterns taken from binding phase (lower-right) and nano-particles included binder phase (upper-left) (b)EDX taken from binder phase (c) EDX taken from region including nano-particles and binding phase

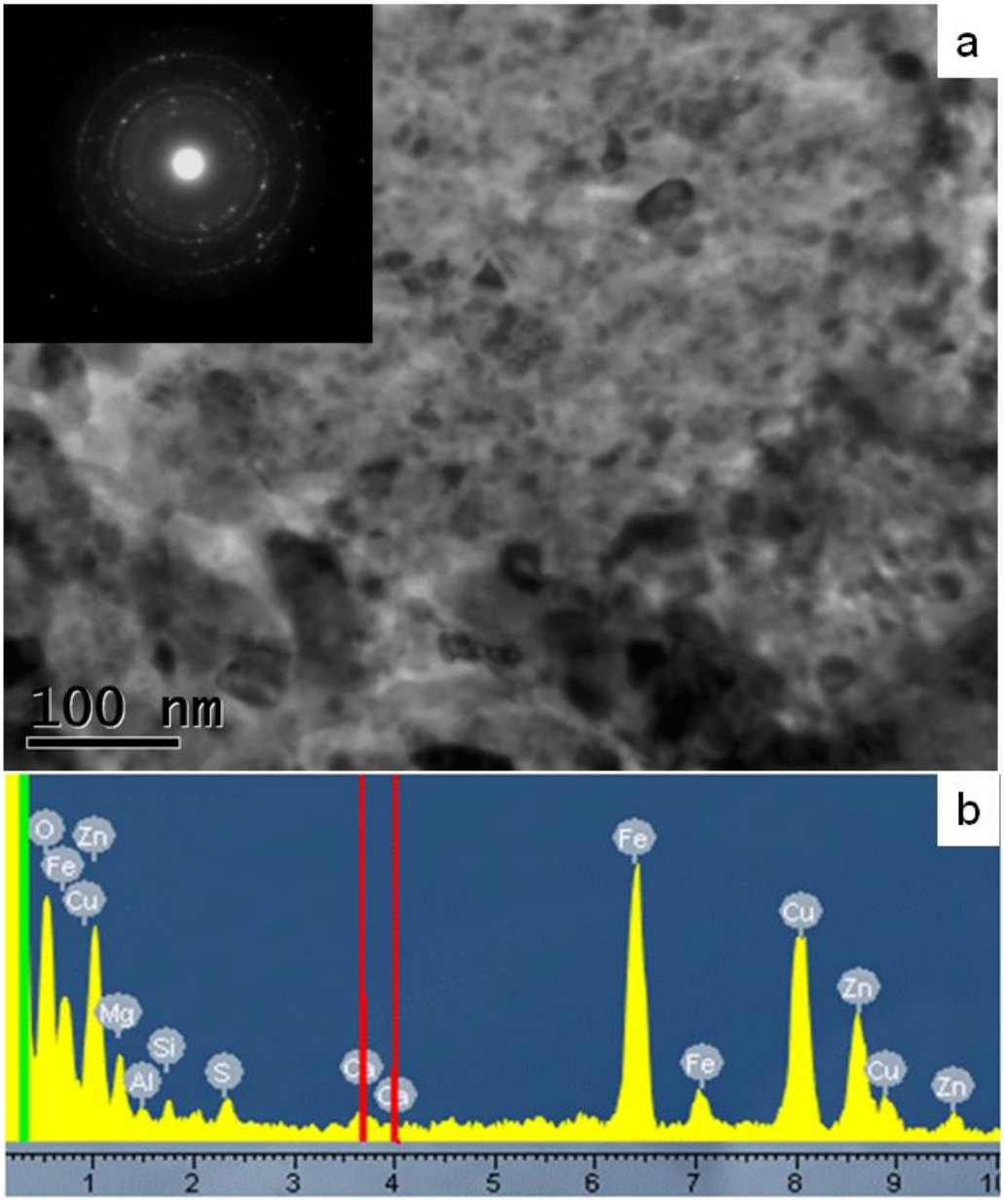

Figure 4-12 (a) High magnification TEM cross-section image of accumulated nano-particles in transfer layer and its diffraction pattern (b) EDX of nano-particles

Table 4-2 d spacing values measured from diffraction pattern in Figure 4-11 (a) and d spacing of $FeSiO_3$ and $Fe_{0.91}Si_{0.09}$

d (Angstrom)	**$FeSiO_3$ PDF No: 01-075-1214**[111]		**$Fe_{0.91}Si_{0.09}$ AMCSD No: 0008189**[112]	
	d	hkl	d	hkl
2.028	2.015	-241	2.012	100
1.159	1.159	-624	1.16	211
1.036	1.037	314, -843	---	---
	1.035	-932, 372		

Table 4-3 d spacing values calculated from diffraction pattern in Figure 4-12 (a) and d spacing values of $Cu_{2.7}Fe_{6.3}Si$, $Ca_{0.15}Mg_{1.85}(Si_2O_6)$, MgO and CuO

d Angstrom	**$Cu_{2.7}Fe_{6.3}Si$ PDF No: 00-047-1434** [111]		**$Ca_{0.15}Mg_{1.85}(Si_2O_6)$ PDF No: 01-074-3637**[111]		**MgO AMCSD No: 0000501**[112]		**CuO AMCSD No: 001789** [112]	
	d	hkl	d	hkl	d	hkl	d	hkl
3.25	---	---	3.257	021	---	---	----	---
2.434	2.441	111	---	---	2.431	111	2.458	111
2.117	2.117	200	---	---	2.106	200	2.129	200
1.872	---	---	1.873	211	---	---	---	---
1.623	---	---	1.629	042,250	---	---	---	---
1.498	1.492	220	1.495	-621	1.489	220	1.506	220
1.391	---	---	1.395	540, 061	---	---	---	---
1.217	1.221	222	1.218	-153	---	---	---	----

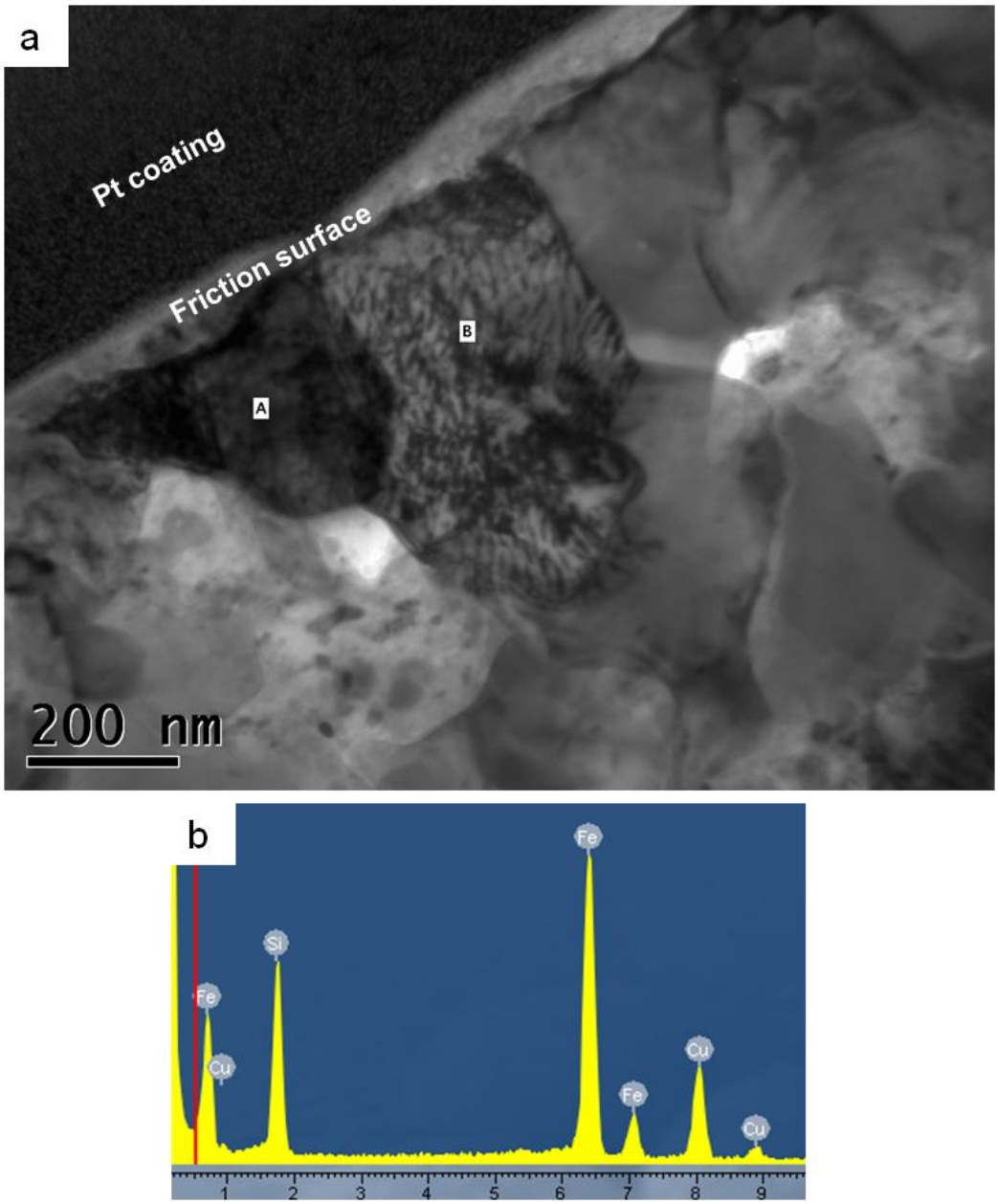

Figure 4-13 (a) High magnification TEM cross section image of micro-sized particle (b) EDX spectrum of particle A

Table 4-4 Quantified result of spectrum in Figure 4-13(b)

Elements	Atomic%
Cu	15.6
Fe	47.85
Si	36.55

Interface between transfer layer and substrate

The interfacial bonding between transfer layer and Si substrate was not continuous. The discrete gaps appeared at positions with white arrows and the bonded interfaces were marked by red arrows (Figure 4-10(a)). EDX analysis indicated that there were two types of particles linked with Si substrate, labelled as P1 and P2, as shown in Figure 4-14 (a) and (b), respectively. P1 particle contained Cu and Si; the atomic percentage of Cu and Si are 78.32% and 21.68% as shown in Table 4-5(a). Whereas, P2 particle contains Si, Fe and a small amount of Cu; the atomic percentage of Fe, Cu and Si are 24.02%, 12.4% and 63.58% as shown in Table 4-5(b). The P1 particles could be alloyed produce of Cu and Si, and P2 particles could be the alloyed produce of Fe, Cu and Si; fusion of P1/Si and P2/Si took place at interface.

To reveal further details across the bonded interface, the chemical compositions were probed across the P1/Si interface at positions A, B, C and D. Visually, position B is closer to the interface between P1 and silicon. The detected compositions at the three positions are plotted in Figure 4-15(c). At position A, the atomic ration of Cu/Si was 4.1, but with no detectable oxygen; at B, the Cu/Si ratio was reduced to 1.2 and O/Si ratio approached to 1.7; at C, the Cu/Si was further reduced to 0.2 and O/Si to 0.8; at position D, inside Si substrate, there is no detectable oxygen apart from silicon.

Table 4-5 Quantified results of EDX spectrum (a) P1 particle (b) P2 particle

Elements	Atomic%
Cu	78.32
Si	21.68

(a)

Elements	Atomic%
Fe	24.02
Cu	12.4
Si	63.58

(b)

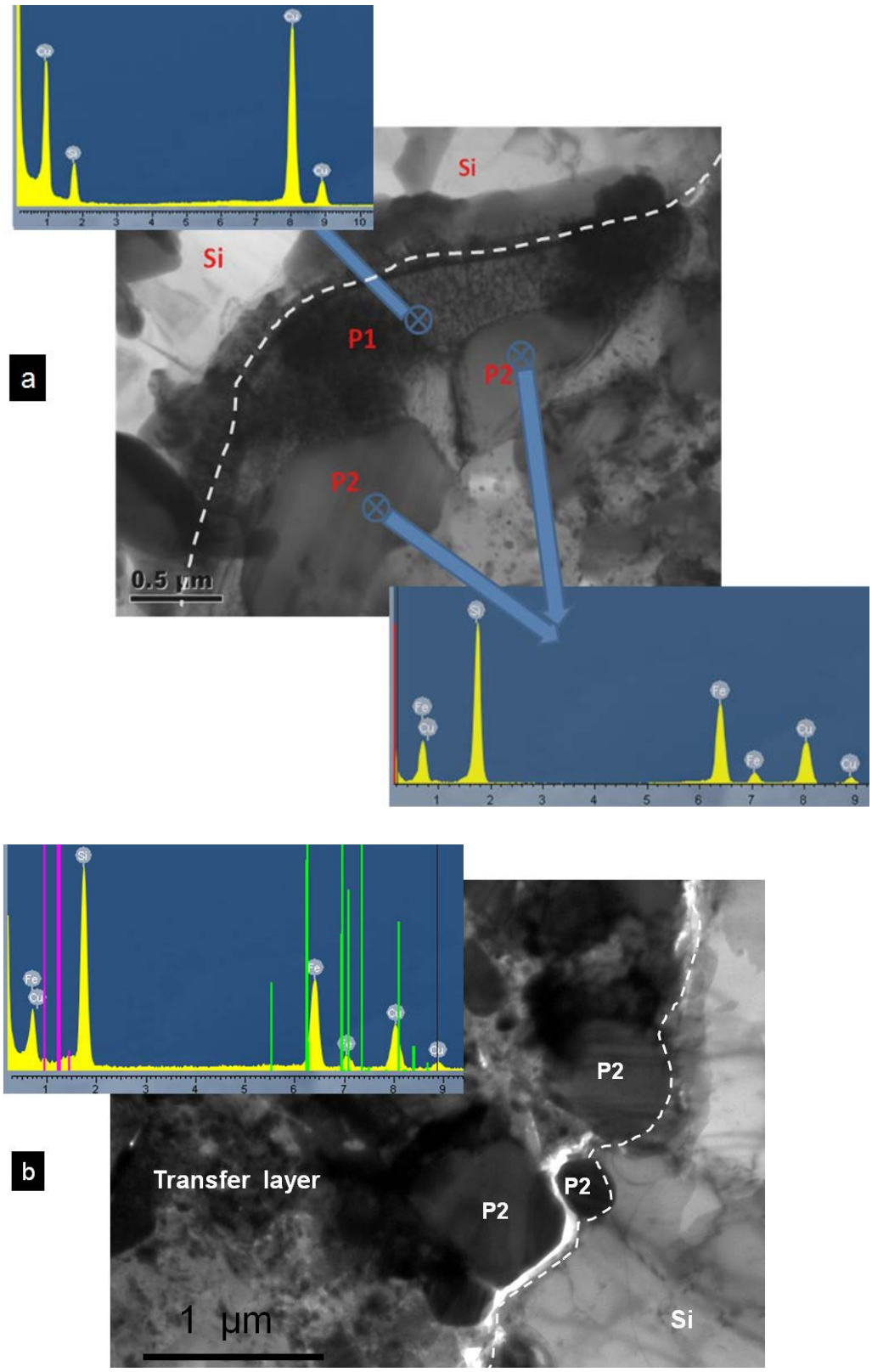

Figure 4-14 (a) High magnification cross section TEM image of P1/Si interface and EDX spectrum of P1, P2 particle (b) High magnification cross section TEM image of P2/Si interface and EDX spectrum of P2 particle

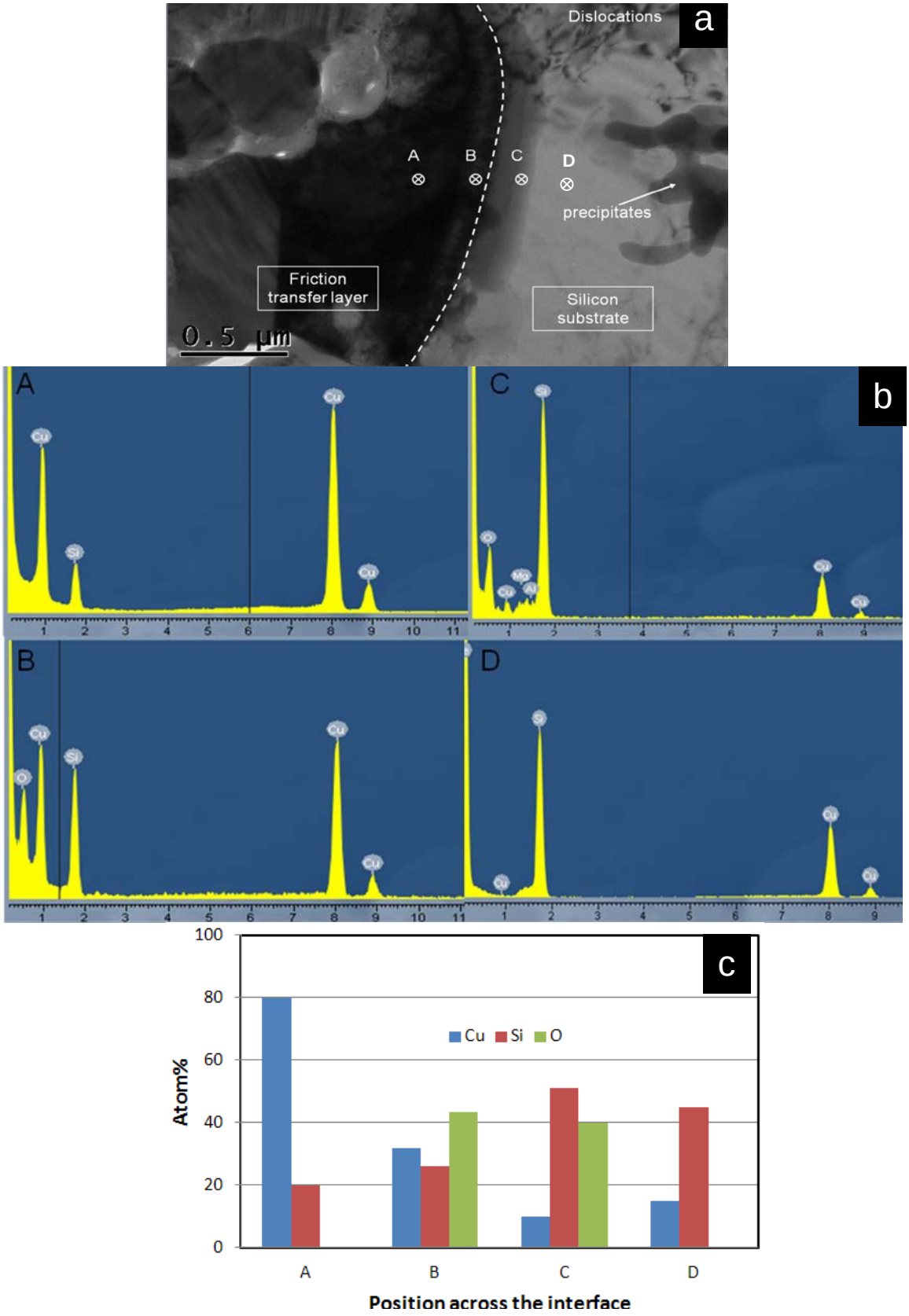

Figure 4-15 (a) High magnification cross section TEM image of P1/Si interface (b)EDX spectrum of position A, B, C and D (c) quantified results of EDX spectrum A,B and C

Substrate

Optical image in Figure 4-16 was taken from friction surface of Si after removing off transfer layer through light polishing with 0.4 micron silica. Precipitates were noticed in the Si substrate; some of these precipitates appeared curved shape and their length varied from 1µm to 30 µm. These precipitates were not found in Si before the friction test. Figure 4-17 (a) shows several precipitates, having typical length of 2-5 microns, clustered together. Figure 4-17 (b) and (c) show the EDX spectra, taken from precipitates and their nearby Si. Similar amount of Cu and Fe were detected from both precipitates and the nearby Si surface. It was noticed that precipitates had higher oxygen content compared with nearby Si.

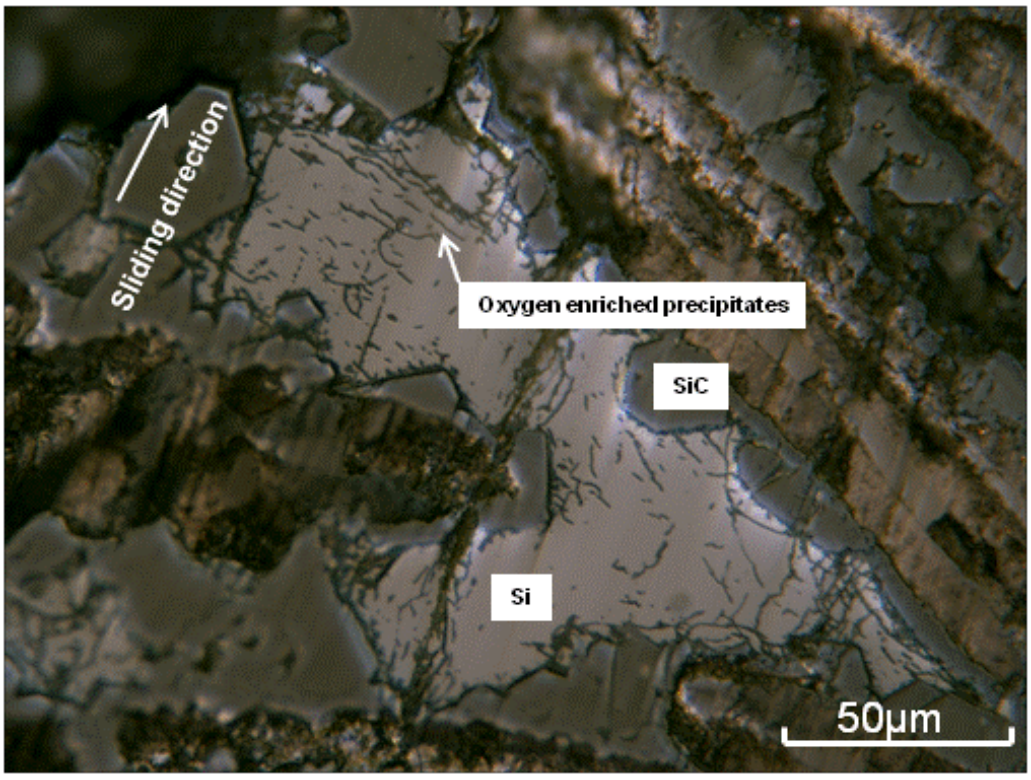

Figure 4-16 Precipitates in Si substrate under optical microscopy after removal of transfer layer

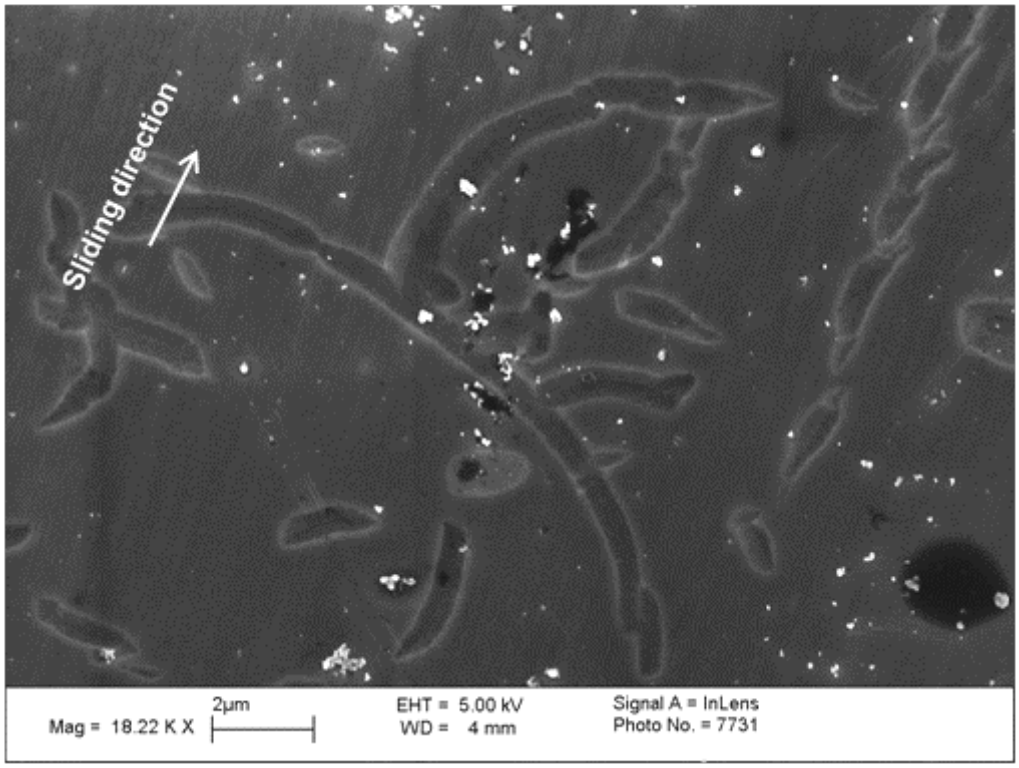

(a)

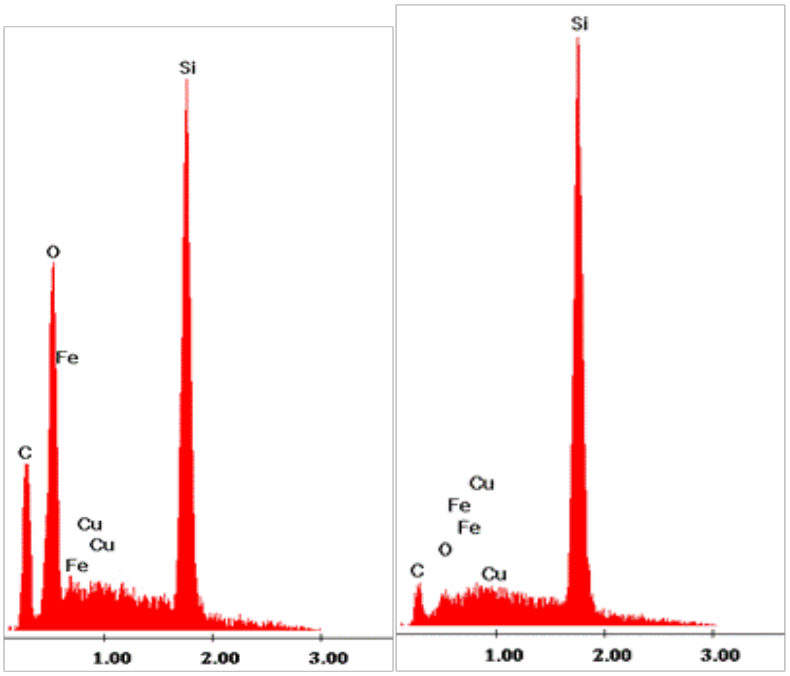

(b) (c)

Figure 4-17 (a) SEM image of precipitates on Si substrate; (b)EDX spectrum taken from precipitates; (c) EDX spectrum taken from Si substrate

TEM cross section analysis on Si substrate showed a cluster of dark contrasting precipitates appeared inside Si (Figure 4-18 (a)). Examined with EDX, these darker phases had high oxygen content, apart from Cu and Si. It is very likely that these regions with darker contrasts in silicon should be the same phase as the precipitates observed on an exposed silicon surface under optical microscopy (Figure 4-16), where EDX also showed the chemical included Si and O.

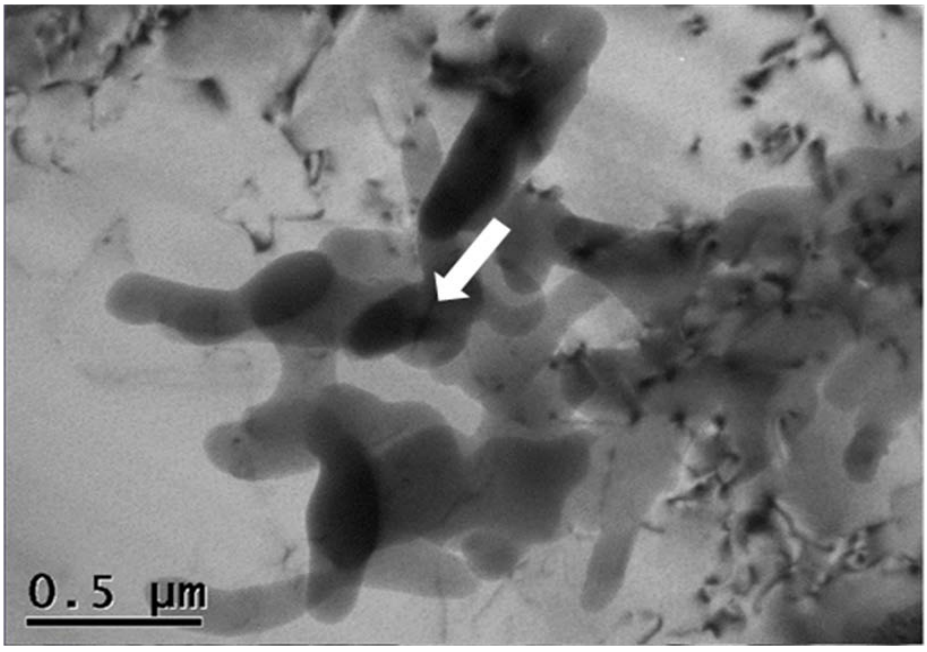

(a)

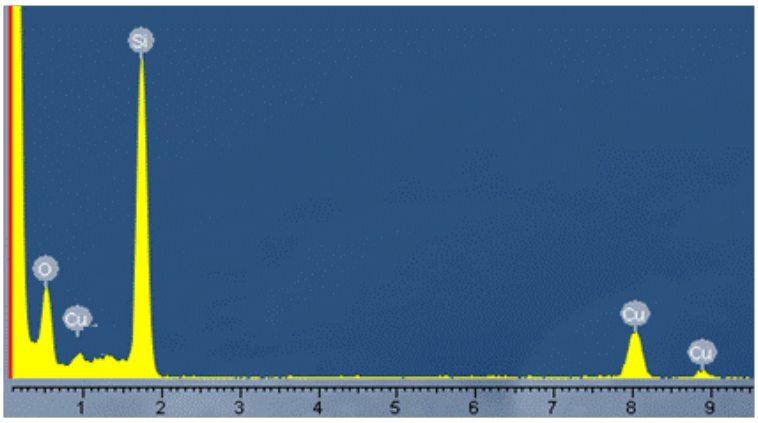

(b)

Figure 4-18 (a) TEM cross section image of in Si substrate containing precipitates (b) EDX spectrum of precipitates

4.3.2.3 Friction surface on SiC region

Development of friction surface

The development process of friction surface in a silicon carbide region is shown in Figure 4-19. All images were taken from same region. Under an imaging condition of differential interference contrast (DIC), a number of small voids/craters were highlighted on the polished surface of this region (Figure 4-19 (a)). Right after the first braking stop, some of these voids/craters were filled with transferred materials showing dark contrast, as shown in the arrowed sites, and a few in bright contrast; they were marked as type B and C (refer to type B and C contrasts in Figure 4-8) respectively in Figure 4-19 (b). After 6 braking stops, these type B patches grew up to a larger extend, and small parts of the type B converted into type C alike, as shown in Figure 4-19 (c). Subjected further braking stops, these large white patches, along with the small white spots appeared in the middle area in Figure 4-19 (c), were partly or completely covered with type C contrast layers, as seen in the surface images in Figure 4-19 (d), (e) and (f) after 14, 19 and 49 stops, respectively. Note, no type A contrast area (refer to type A contrast in Figure 4-8) was observed on the friction surface of SiC. It was noticed that after the first stop, the friction surface near the boundary of the silicon carbide region showed type C contrast and a crumbling appearance. When braking stop number increased, such kind of friction surface developed continuously toward the central area of the region. After 49 stops, most of the friction surface in the SiC region shows type C contrast, as shown in Figure 4-19 (f). It was also noticed that before type C appeared on the friction surface, extensive cracking has occurred on the SiC surface; some surface area tended to chip off due to lateral cracking. Up to the braking numbers of current test, only the core of this region seems to be in good integrity without clear change of image contrast. It was worth noting that the development of a circulated region D in the upper part of this area. Images from (a) to (f) show a lateral cracking has been developed underneath the surface in region D between the 1st and 6th stop, and then the partially-detached surface was crushed into many pieces with transferred materials filling in the cracks between the 6th and 14th stop; up to the 19th stop, the whole area was converted into a region completely

filled with transferred materials, with a typical type C contrast; to the 49th stop, the area filled with transfer material has expanded further (see Figure 4-19 (f)).

Figure 4-20 is SEM image corresponding to the OM image Figure 4-19(f), the morphology and chemical composition of transferred material having type B and C contrast were studied by secondary electron microscopy and EDX. The transferred materials showing type C contrast were composed of iron, copper, magnesium and oxygen; the region showing type B contrast was dominated with iron, as shown by the EDX spectrum at position a and c respectively in Figure 4-20. In the middle area, there was no evidence to show that any transferred material has been deposited on the surface of silicon carbide, as the EDX spectrum shows no more than carbon and silicon lines in position b. Under a higher magnification on the damaged region with type C contrast (Figure 4-21), the transferred materials were exposed, and clearly they all filled inside surface cracks; the surface region looks like granulated silicon carbides, with a size ranging from sub-micron to a few microns, that were held together by the transferred materials on the surface. This kind of feature is likely to indicate that the surface crack on SiC region may be initiated.

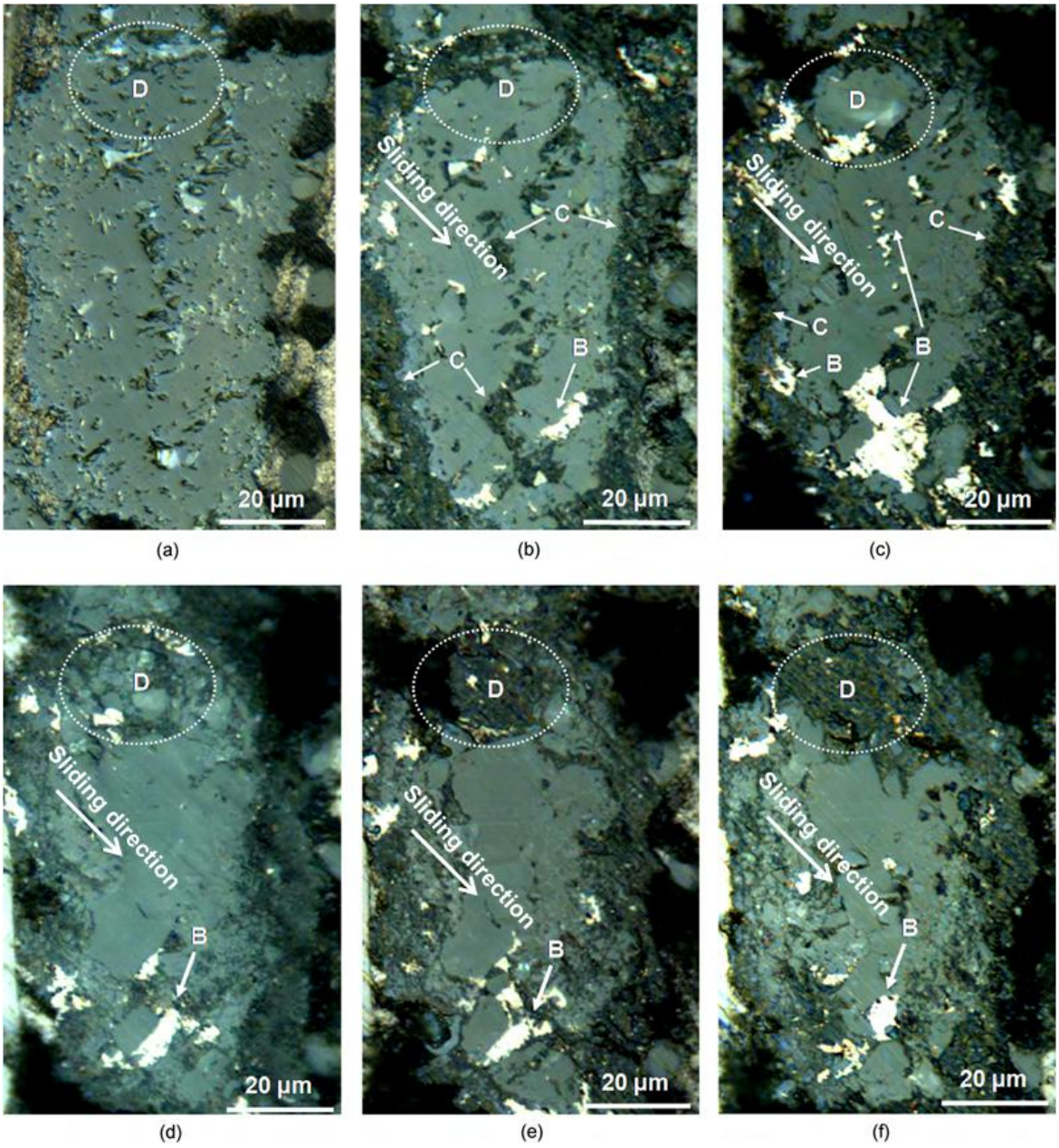

Figure 4-19 Registered OM images on the friction surface of a silicon carbide region: (a) as-finished surface before braking; (b), (c), (d), (e) and (f) the friction surface after the 1st, 6th, 14th, 19th and 49th braking stop, respectively. The arrows indicate places where transferred materials were deposited; B and C represent the type of friction surface showing similar contrast as type B and type C friction surface appeared in Figure 4-8; D is an area highlighted to notice the journey of the mechanical damage followed by a deposit of transferred materials on SiC surface.

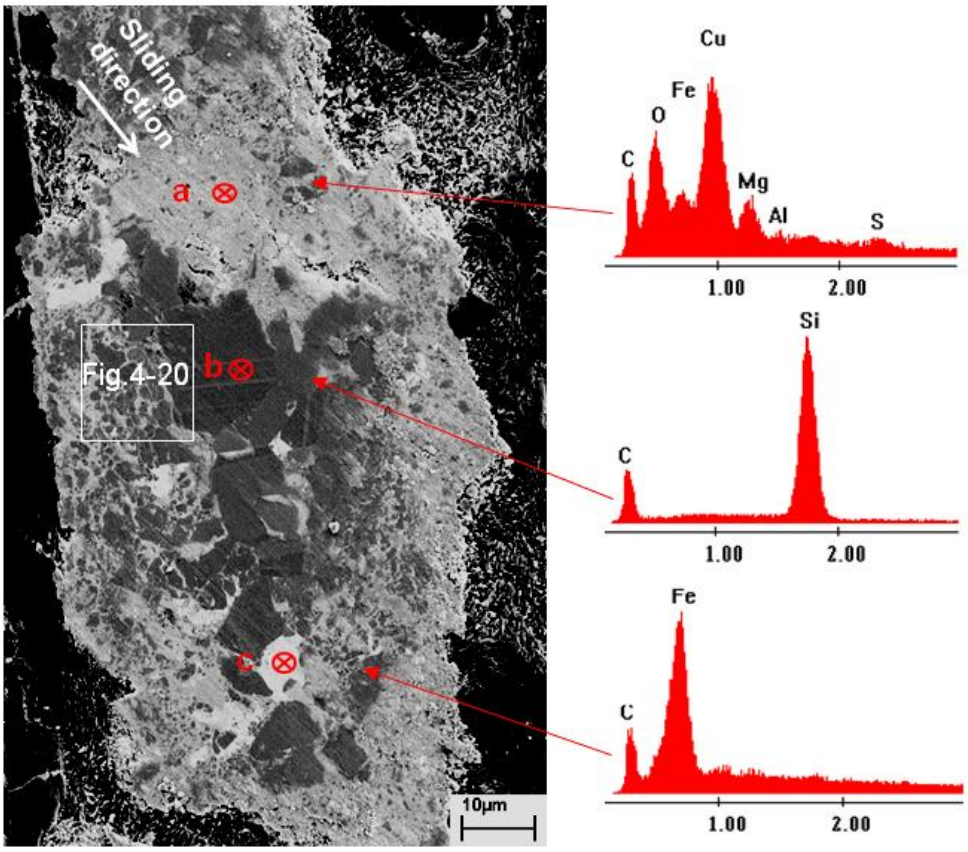

Figure 4-20 Secondary electron images of the friction surface in silicon carbide region after 49 braking stops. A region corresponding to Figure 4-19(f), imaged by OM, and EDX spectra in position a, b and c.

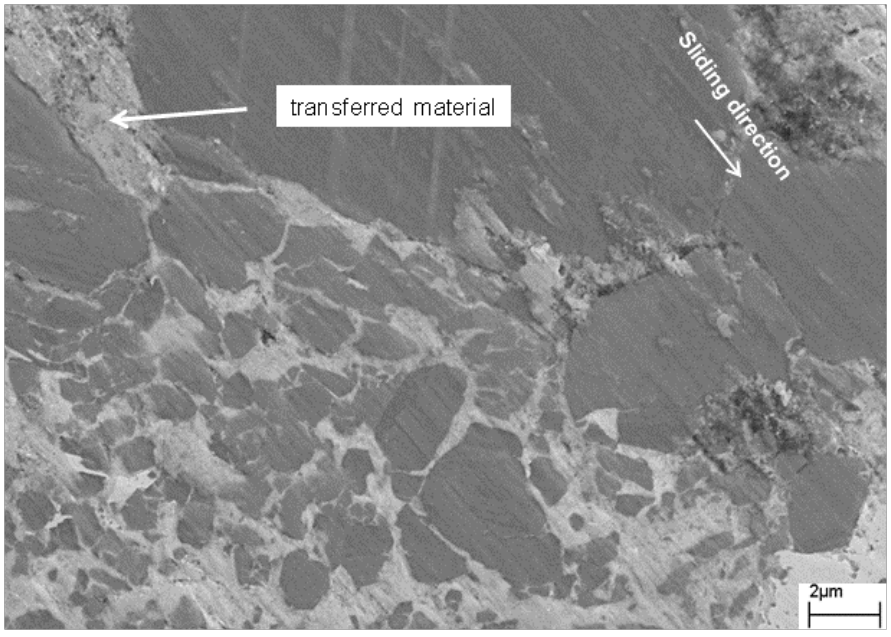

Figure 4-21 Higher magnification image of a damaged SiC region

Third body material

To investigate the transferred material developed on friction surface of SiC, after friction test, cross section TEM sample was lift out from the position which is marked by dashed line in Figure 4-22(a). The TEM image (Figure 4-22 (b)) shows that along the friction surface, the regions circled in dashed lines contain transferred materials. The grain size of SiC was around several few microns in this investigated region. Extensive crystal defects appeared inside the crystallites, including dislocation lines and stacking faults. Fracturing cracks were also noticed: one large crack went through the region underneath the surface, propagating along a transgranular path (Figure 4-22 (b)). High magnification cross section micrograph in Figure 4-22 (c) shows that the transferred materials, enveloped by the dashed white line and the friction surface, root inside a crater surrounded by SiC crystallites. This crater is likely to be created through dislodging of SiC. This result may indicate that no strong chemical bonding existed between transferred material and SiC. It seems that the transferred material was only mechanically clamped inside the crater. EDX spectrum in Figure 4-22 (d) shows the transferred material contains O, Si, Cu, Zn, Al, Mg, S, P and Ca.

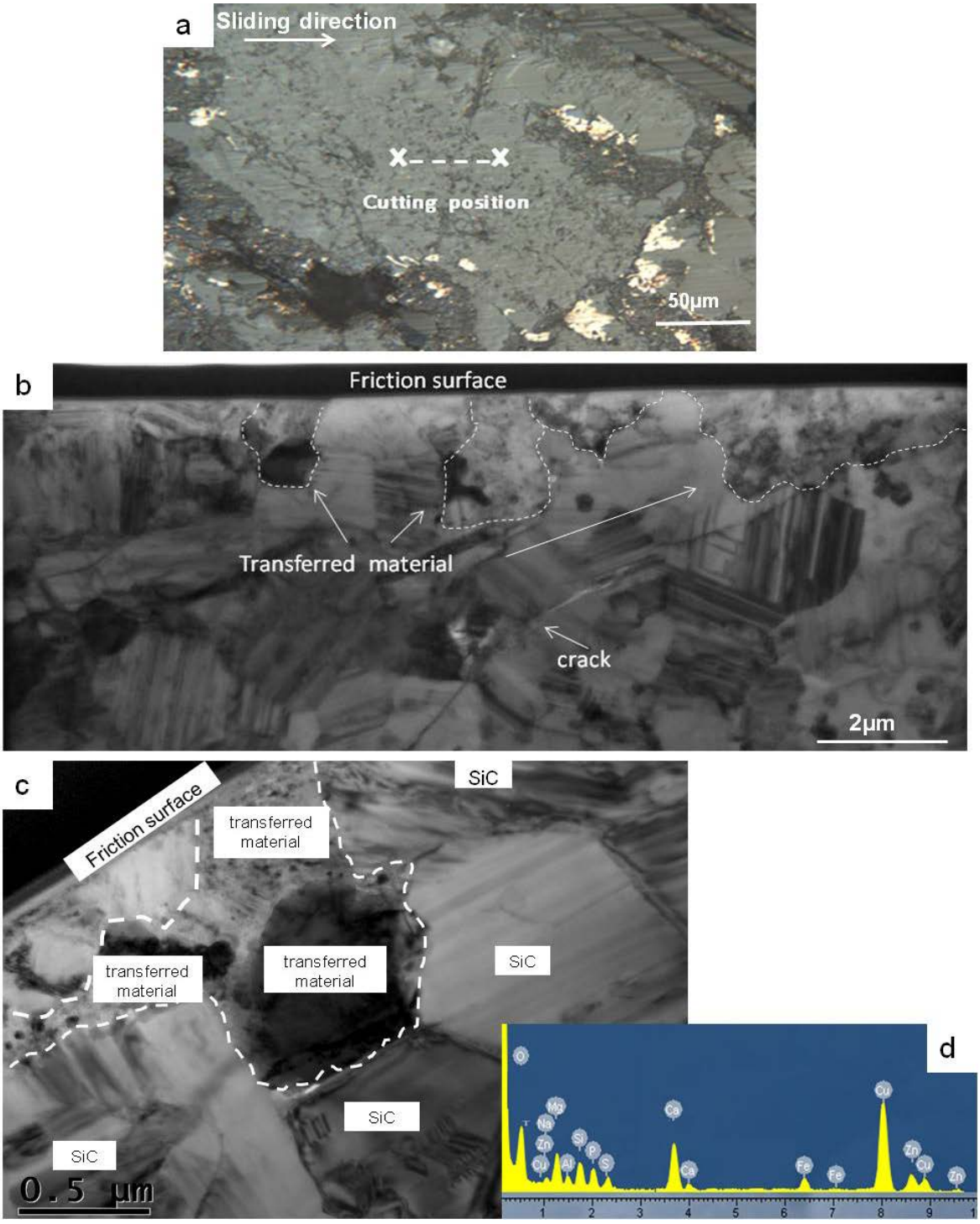

Figure 4-22 (a) Optical image taking from in-plane friction surface of SiC shows the transferred material deposited on SiC after friction test. TEM sample was lift out from the position marked by dashed line; (b) cross section TEM image of friction surface of silicon carbide showing transgranular crack and transferred material (c)high magnification image showing the transferred material rooting inside a crater surrounded by silicon SiC crystallites ;(d) EDX spectrum of transferred material in (c). The dashed lines in (b) and (c) are presented to indicate the possible boundaries between transferred material and the silicon carbide matrix.

Substrate

Except for the fracture damage in SiC substrate, the extensive plastic deformation of SiC friction surface was observed after friction testing. The optical image, shown in Figure 4-23, was taken under DIC image condition. Although the SiC region consisted of polycrystal SiC particles, all SiC grains existed at the same level of height after polishing with 3 micron diamond grits. Figure 4-24 shows the typical friction surface of C_f/C-SiC after laboratory scale dynamometer test followed by HF wash; a number of kinks were developed on SiC surface (the middle region in SiC was Si covered by a transfer layer, which was unable to be removed by HF). With the formation of kinks, the as-polished flat surface was transformed into a bumpy surface by the friction.

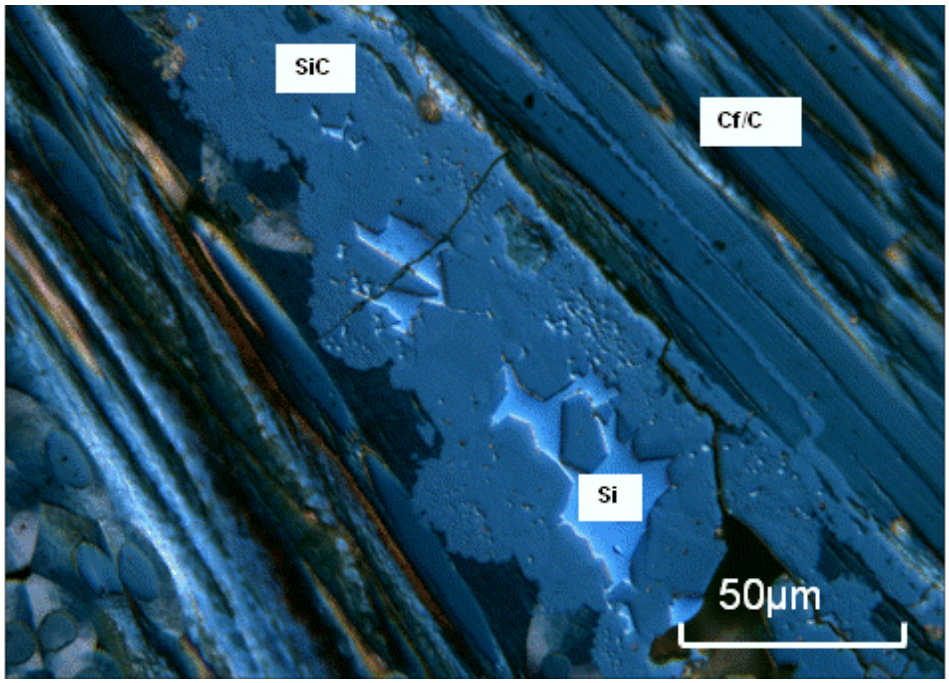

Figure 4-23 OM image of as-polished surface of C_f/C-SiC

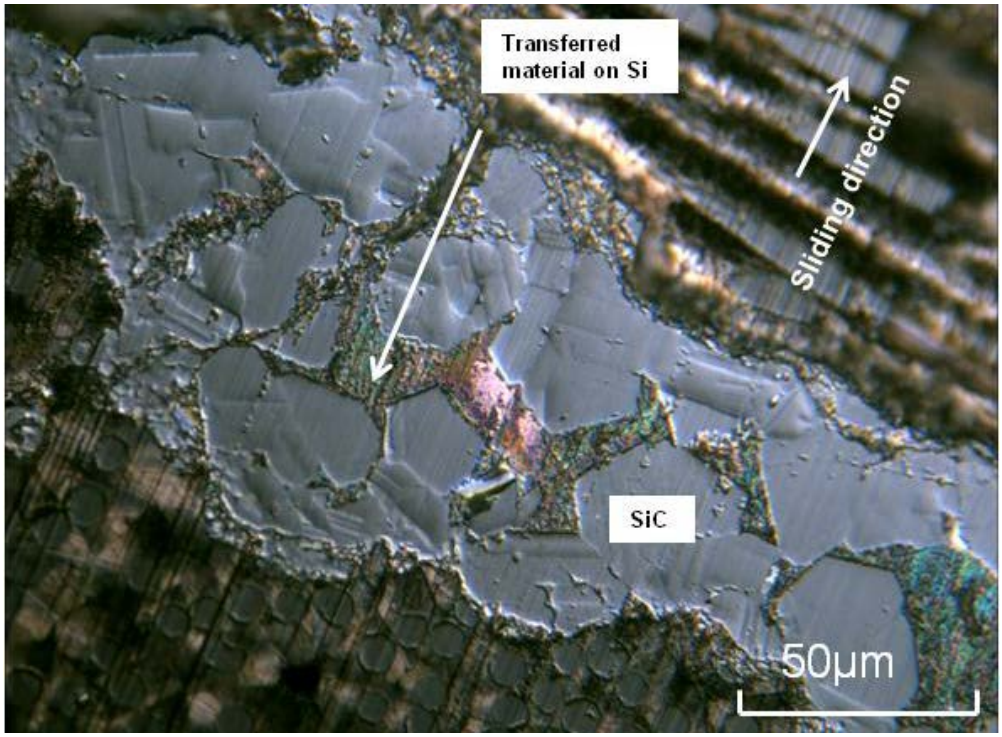

Figure 4-24 OM image of friction surface of C_f/C-SiC after laboratory scale dynamometer test followed by HF wash (Si region was covered by transfer layer)

After friction testing, a cross section TEM sample was prepared from the deformed SiC friction surface. Figure 4-25 shows SEM image of in-plane friction surface of deformed SiC and its corresponding cross section TEM image. Cross section TEM image shows a Si underlayer is located underneath SiC crystals. Although the kinks observed on the in-plane friction surface was not able to see in the cross-section TEM sample, it was noticed that the terrace steps appeared along the interface of Si/SiC, as circled in the dashed box (Figure 4-25). The kinks formed on the friction surface might be damaged during TEM sample preparing process. According to the features on the in-plane surface, the SiC is divided into four regions, and SiC_1, SiC_2, SiC_3 and SiC_4 were used hereinafter to define the SiC at position1, 2, 3 and 4, as labelled in Figure 4-25. To study the crystal orientation of SiC at these positions, the diffraction patterns were taken from the cross-section of SiC_1, SiC_2, SiC_3 and SiC_4 by using TEM. The diffraction patterns revealed that the SiC crystals have f.c.c structure (see diffraction patterns in Table 4-6).

Table 4-6 summarizes the zone axis (<011>, $< \bar{1}12 >$ and $< \bar{1}23 >$) diffraction patterns taken from the positions marked in Figure 4-25. Position A, B, C located in SiC_1, SiC_3, SiC_4, respectively, whereas position D included both SiC_3 and SiC_4. When acquiring diffraction patterns from SiC at the different positions under same zone axis, the rotation and tilting angles of double tilt sample holder were remain unchanged. $< \bar{1}12 >$ and $< \bar{1}23 >$ zone axis diffraction patterns taken from position A, B and C are same. <011> zone axis diffraction patterns of position A and B are same, but they are different from the one taken from position C; a 140^o angle exists between the $(11\bar{1})$ reflections of their diffraction patterns, as marked. The diffraction pattern of position D consists of two superimposed <011> zone axis diffraction patterns, which is originated from <011> zone axis diffraction patterns of position B and C. This result suggests that SiC_1 and SiC_3 have same crystal orientation, and SiC_4 is twin of SiC_1 and SiC_3. The parent and twin crystal diffractions are related by a mirror reflection across the {111} twining plane.

Figure 4-26 (a) shows the <011> zone axis diffraction pattern taken from SiC_2. The two superimposed <011> zone axis diffraction patterns indicates that twins could exist in SiC_2. As indexed in Figure 4-26 (a), the parent and twin crystal diffractions are related by a mirror reflection across the {111} twining plane. Figure 4-26 (b) shows the microtwins (with dark contrast) exist in SiC_2. Figure 4-26 (c) schematically illustrated the spatial relationships of beam direction, TEM sample plane and twinning plane. The beam direction is perpendicular to the TEM sample plane and parallel to the twining plane {111}.

Based on the diffraction analysis, it can be concluded that SiC_1 and SiC_3 have same crystal orientation; SiC_4 is the twin of SiC_1 and SiC_3; micro-twins exist in SiC_2. The twins and microtwins are likely produced by the friction process.

Dislocations were obviously originated on the friction surface, and then glided to a depth of >1 μm inside the crystallites. The density of dislocation seems to be very high. They are likely to be produced by friction process.

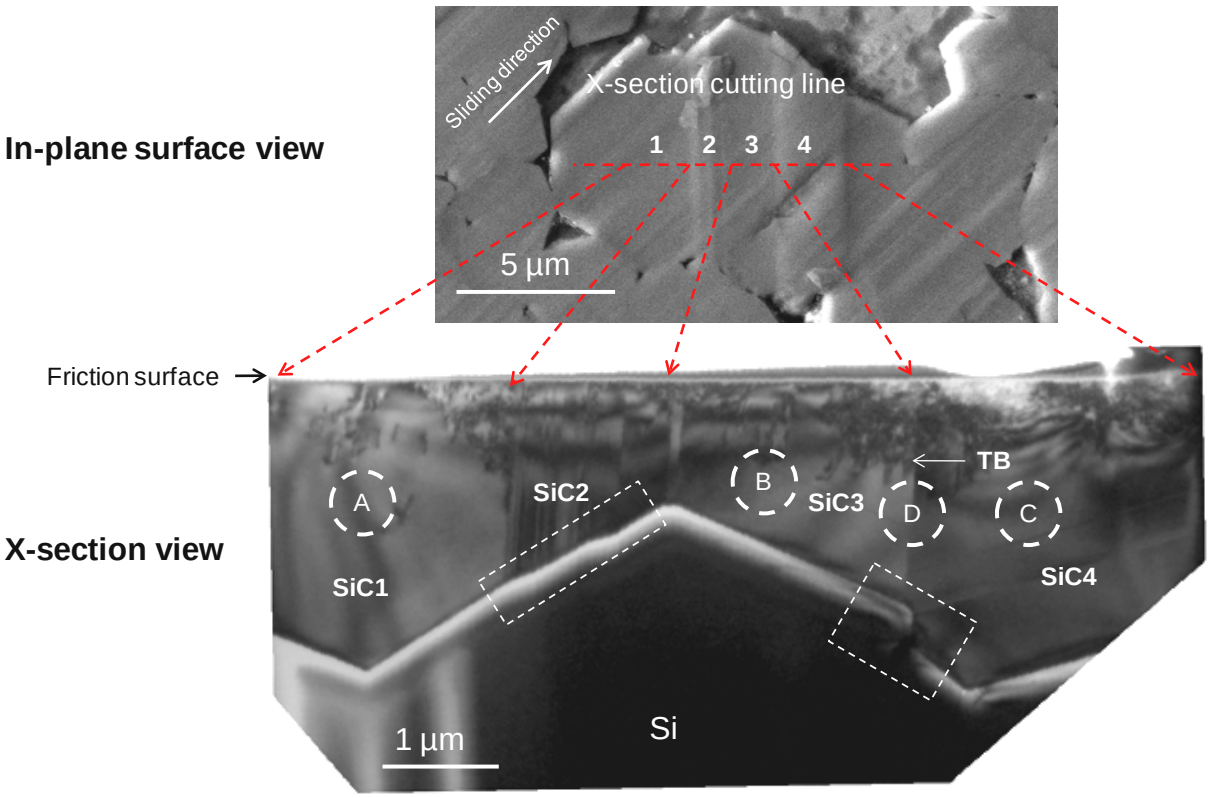

Figure 4-25 SEM image of kinks on friction surface of SiC and its corresponding cross-section TEM image

Table 4-6 Zone axis diffraction patterns took from cross section of SiC_1, SiC_3 and SiC_4. Zone axes are [011] [-112] and [-123]

Position	<011> Zone axis	$< \bar{1}12 >$ zone axis	$< \bar{1}23 >$ zone axis
A (SiC_1)	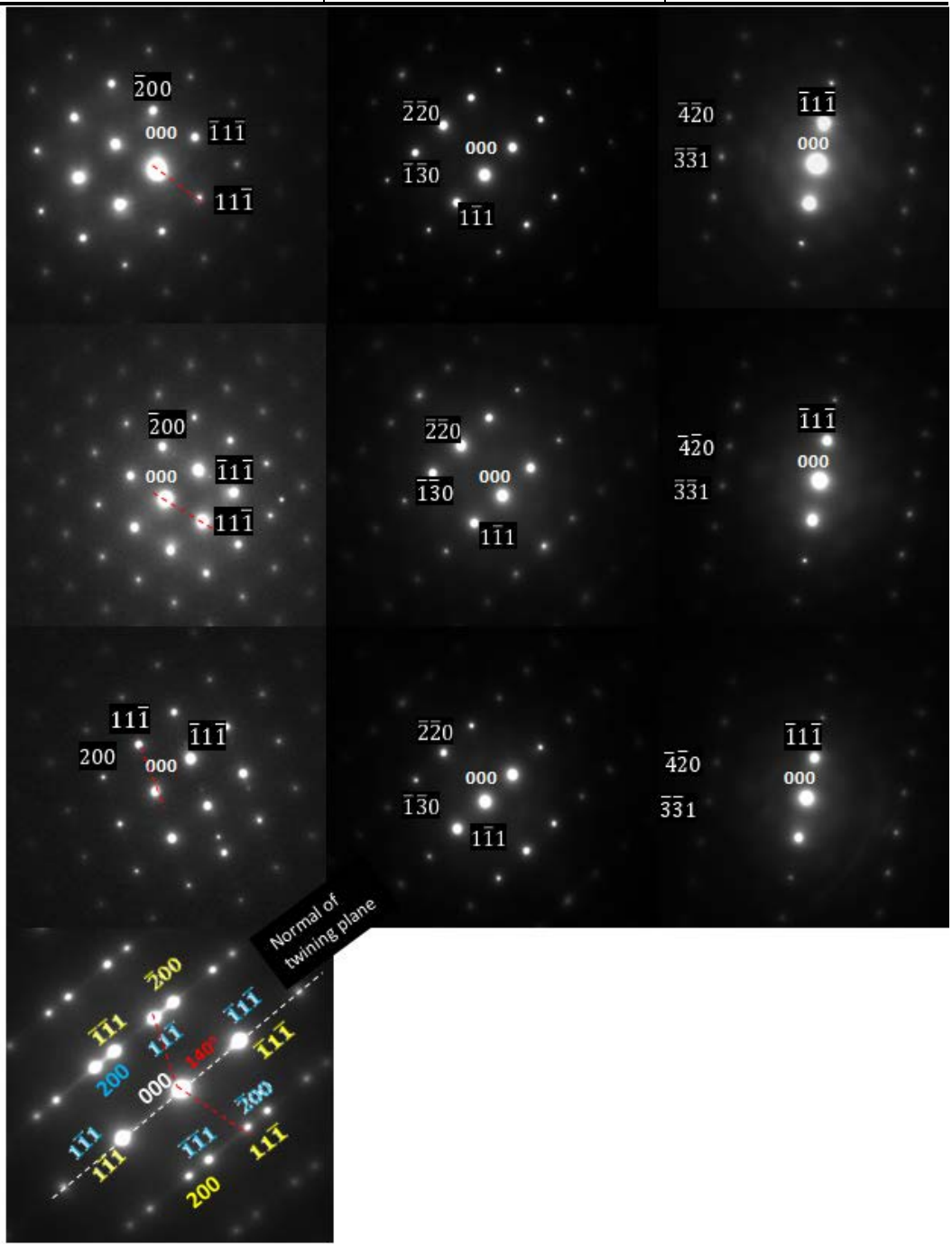		
B (SiC_3)			
C (SiC_4)			
D (SiC_3 + SiC_4)			

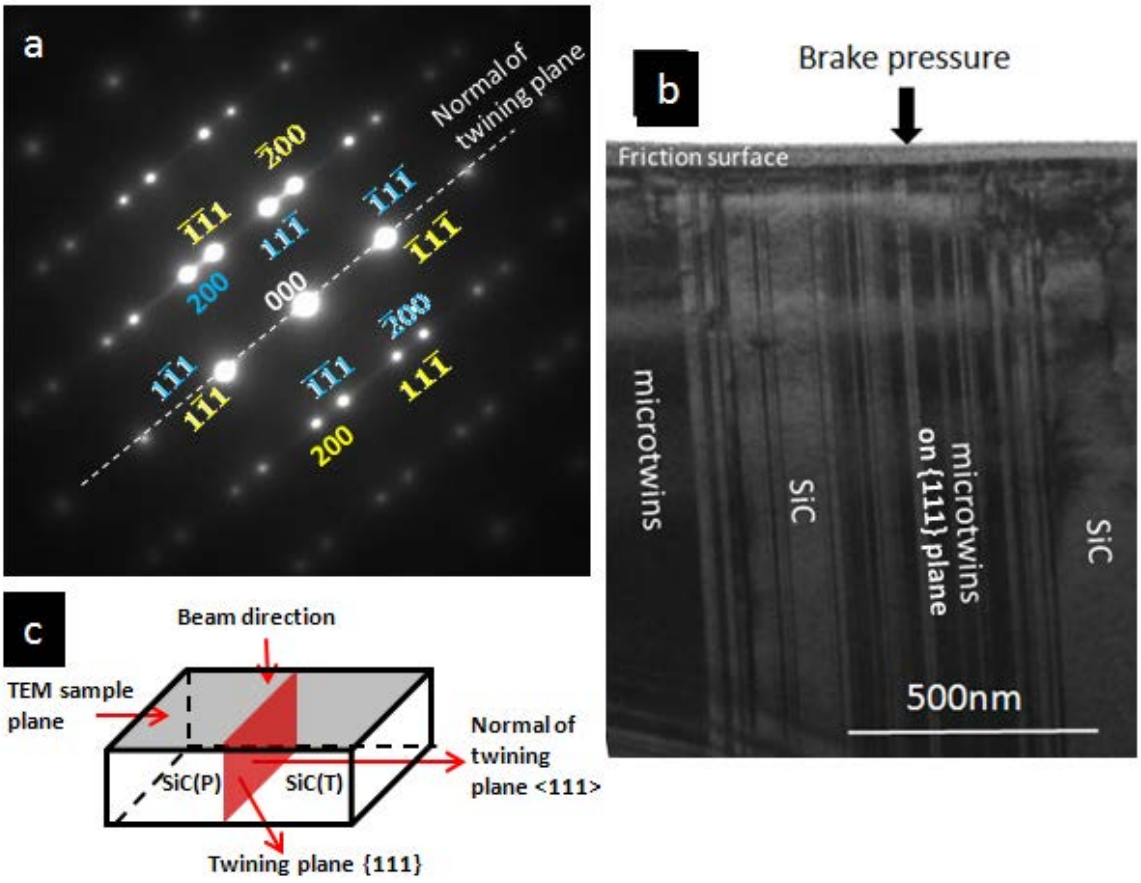

Figure 4-26 (a) diffraction pattern from SiC_2 (b) High magnification cross section TEM image of micro-twins in SiC_2 (c) spatial relationship between beam direction, TEM sample plane and twinning plane.

4.3.2.4 Friction surface on C_f/C region

Development of friction surface on vertical C_f/C region

After first braking stop, the carbon matrix was subjected to significant mechanical damage, and simultaneously the damage areas were filled with transferred materials; same situation occurred on the interfaces between vertical carbon fibres and carbon matrix, as shown in Figure 4-27(b). However, the vertical carbon fibres themselves were still in good condition. After 49 brakings, majority of the region, including carbon fibre and carbon matrix, has been damaged, and left with transferred materials, as shown in Figure 4-27 (c). There was no clear type B and C contrast (refer to type B and C contrasts in Figure 4-8) that could be differentiated under the imaging condition.

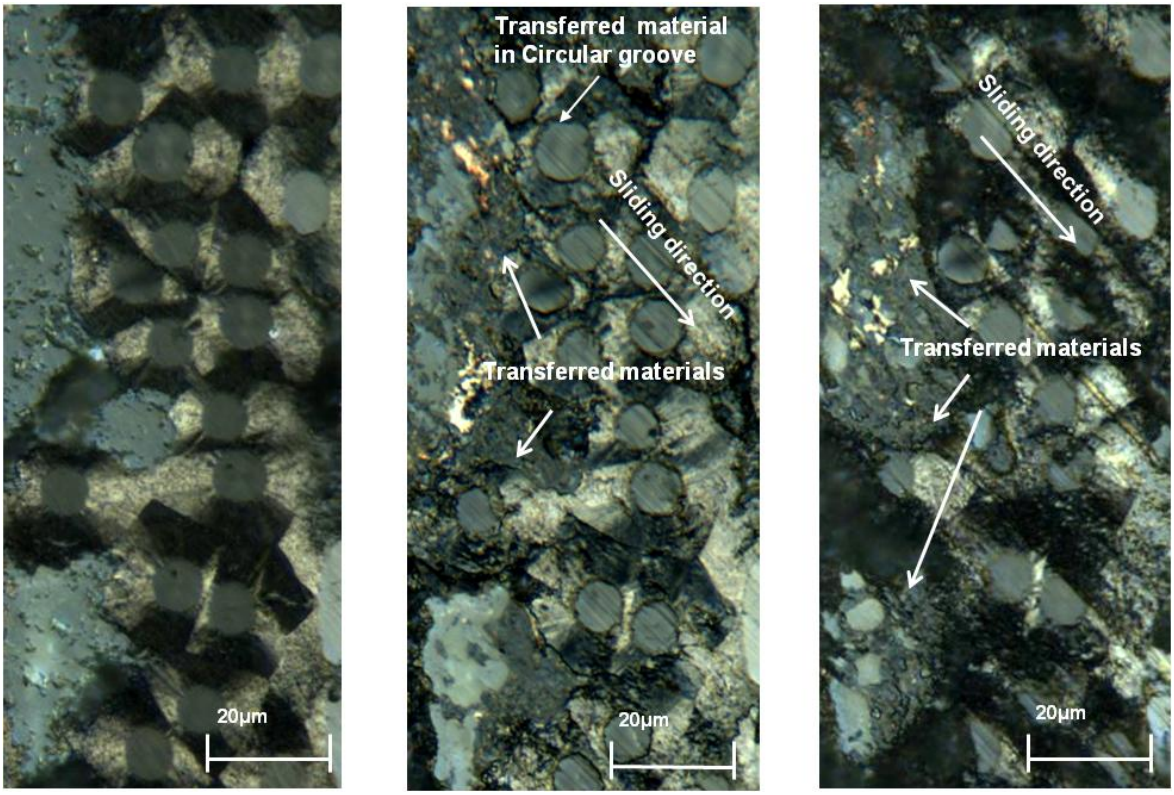

(a) (b) (c)

Figure 4-27 Registered OM images of the friction surface in a vertical C_f/C region of the composite:(a) as-finished surface before braking; (b) and (c) the surface after the 2nd, and 49th braking stop, respectively. The arrows indicate a position where circular groove was generated along the interface between vertical C_f and carbon matrix after two braking stops.

Figure 4-28 is the SEM image and EDX spectrum from friction surface of vertical C_f/C region, after 49th dynamometer testing. It indicates that the voids formed by surface cracking (position a) were filled with wear debris with chemical constituents that are typical for transferred material with type C contrast observed on the friction surfaces of silicon and silicon carbide. On the cross-sectional surface of carbon fibres, the smooth and flat part has no transferred materials deposited, as confirmed by the EDX spectrum at position b, so does the exposed carbon matrix surface (position c). It was also noticed that some transferred materials also filled in the damaged interface between carbon matrix and carbon fibre.

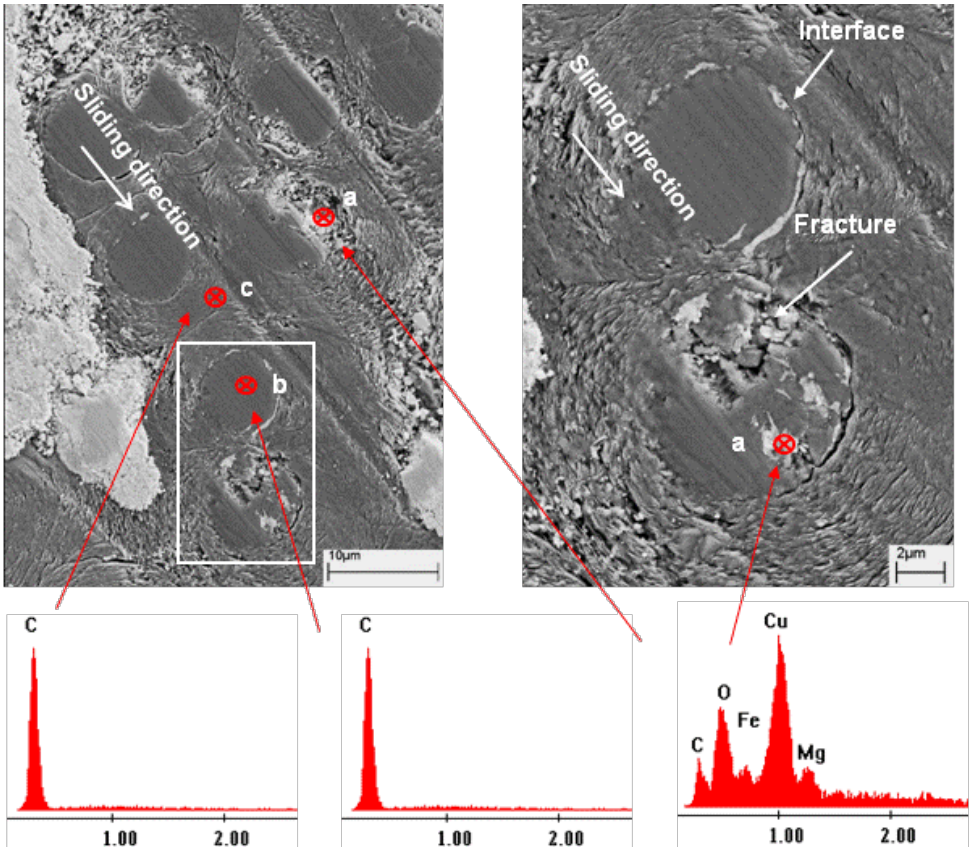

Figure 4-28 The secondary-electron image of the friction surface in vertical C_f/C region after 49 braking stops; wear debris accumulated in voids created by fracturing and dislodging, and split interfaces. Spectra from positions b and c indicate no transferred materials being deposited on the surface of carbon matrix and the cross section surface of carbon fibre; spectrum from position a indicates that deposited debris in voids/gaps contain Cu, Fe, Mg and O.

Development of friction surface on in-plane C_f/C

Like the vertical carbon fibres, all in-plane fibres were surrounded with carbon matrix (Figure 4-29). After initial braking, fracture occurred in both carbon fibres and carbon matrix, as marked in Figure 4-29 (b); some fractured parts have been dislodged and stripped away, and the left positions were filled with transferred materials. When more brakings were applied, the more carbon fibres and matrix were dislodged through fracturing, the more were transferred materials deposited on the friction surface, as shown in Figure 4-29 (c-e). It is noted that all the transferred materials in in-plane C_f/C region look fairly crumbling, lack of enough cohesion.

Figure 4-30 is the morphology and chemical analysis on friction surface of in-plane C_f/C region, correspond to OM image in Figure 4-29(e). The transferred materials stayed in the low areas created by the fracturing and then dislodging of carbon materials (position a), having the same chemical composition as that with the type C contrast (refer to type C contrast in Figure 4-8) in silicon and silicon carbide regions. These transferred materials had crumble format. On the exposed surface of carbon fibres (position b) and matrix (position c), there was no transferred material deposited, as shown in the EDX spectrum of Figure 4-30. Same as the vertical C_f/C region, the interface of C_f and carbon matrix was filled with transferred materials, as indicated with white arrow in SEM image of Figure 4-31. The transferred materials in interfaces seem pretty dense.

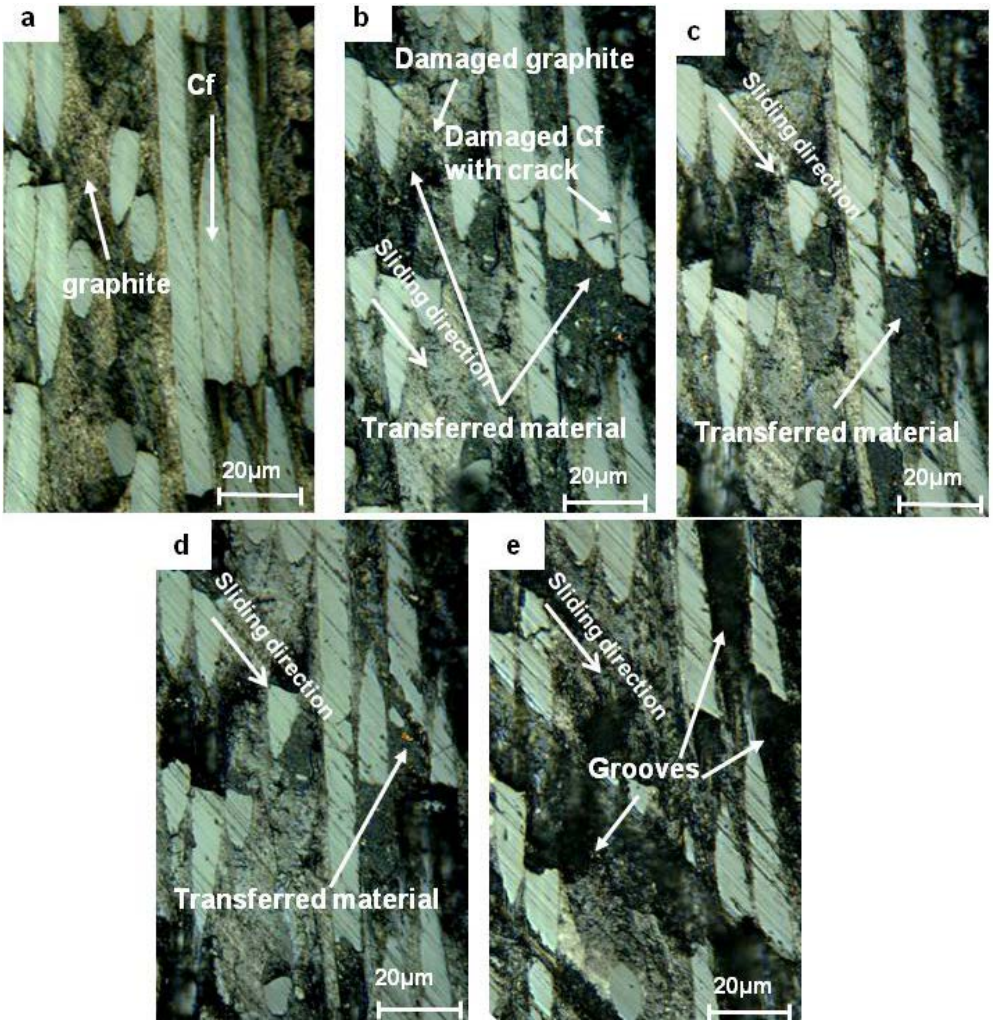

Figure 4-29 OM images of friction surface in in-plane C_f/C region:(a)as finished surface before braking, (b) after 1 stop, (c) after 2 stops, (d) after 3 stops, (e) after 49 stops.

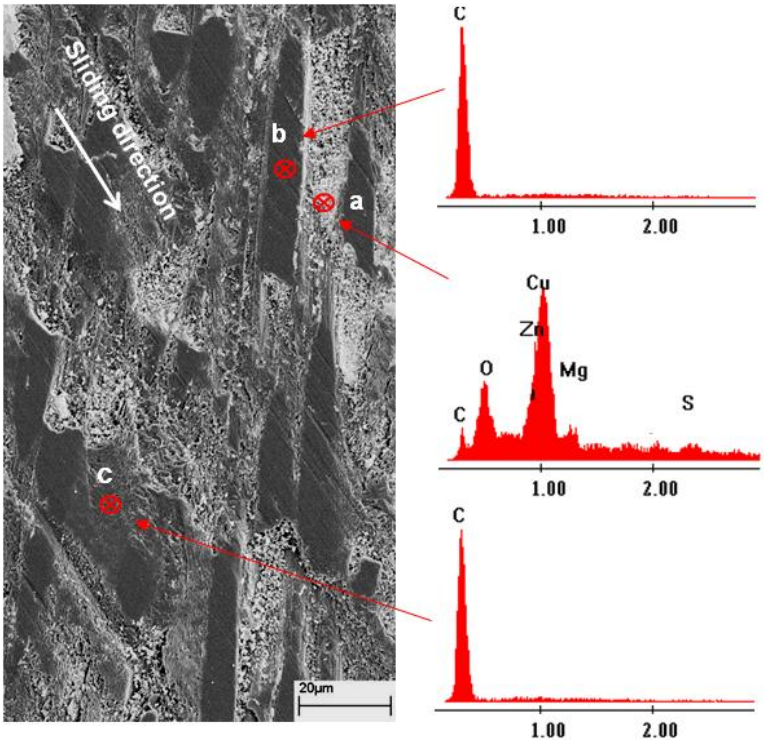

Figure 4-30 SEM image and EDX spectra for the friction surface after 49 braking stops; no transferred materials were identified on the surface of carbon fibre and most of the carbon matrix.

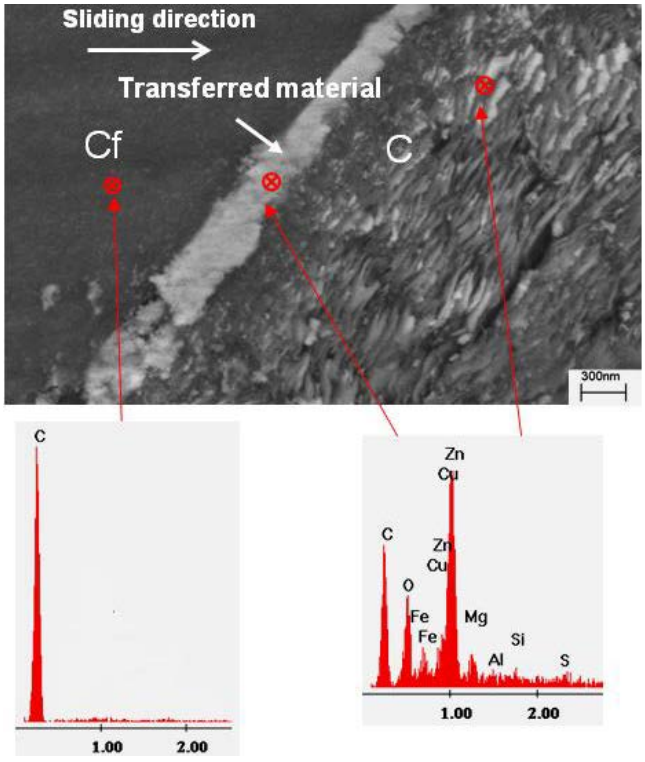

Figure 4-31 SEM image and EDX spectra for the interface of in-plane C_f/C after 49th dynamometer testing.

Third body material and transfer film

Cross section TEM image of transferred material developed in interface of carbon fibre and CVI carbon matrix is shown in Figure 4-32(a). CVI carbon matrix located between two carbon fibres and the surface of carbon matrix was 0.2 μm lower than the friction surface of carbon fibre. Visually, the transferred materials deposited on the top of CVI carbon as filler, which may suggest that there was no strong bonding existing between transferred material and CVI carbon. EDX spectrum, Figure 4-32 (b), shows the composition of transferred materials include iron, copper, aluminium, sulphur, carbon, oxygen as the main chemical elements, which were typical ones in a formulation of the organic friction lining material. The thickness of transferred material was about 0.1 μm.

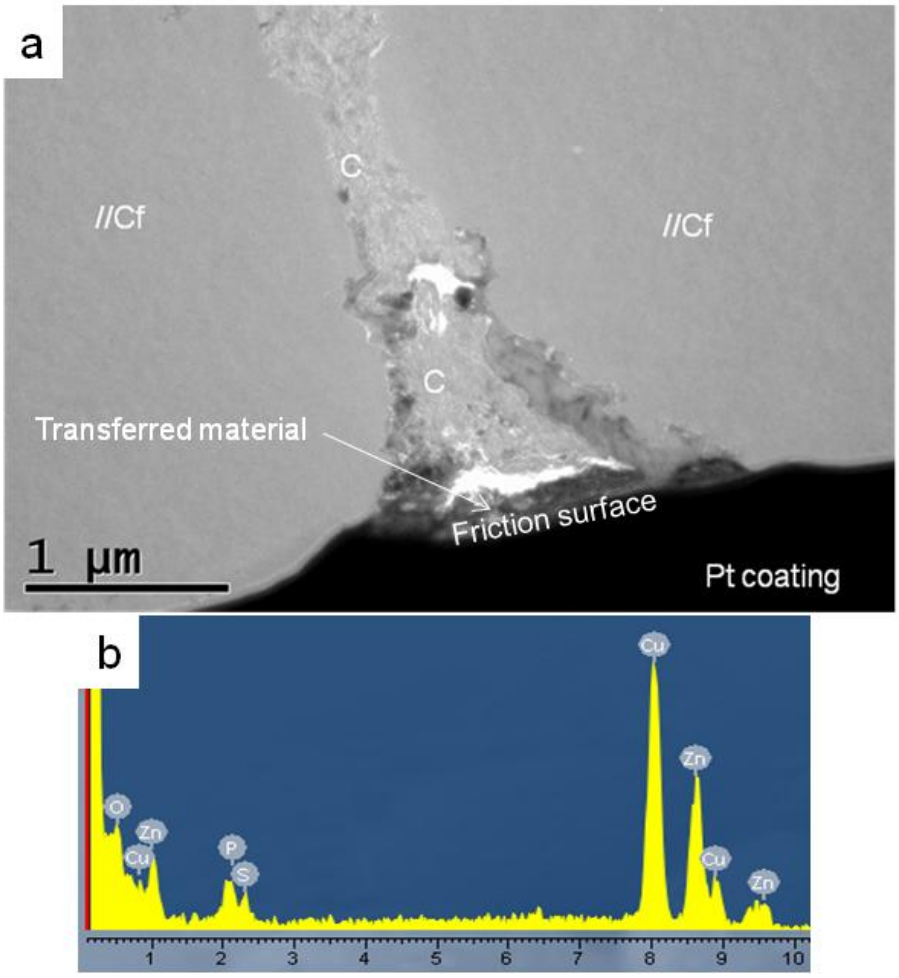

Figure 4-32(a) Cross section TEM image of C_f/C after laboratory scale dynamometer friction test; (b) EDX spectrum of transferred material remained on the top of CVI carbon matrix

No transferred materials were found on top of the carbon fibres. However, TEM image and diffraction pattern from the top of carbon fibre indicates that a very thin layer of amorphous carbon generated on the friction surface of C_f, as see in Figure 4-33. Figure 4-33(b) is diffraction pattern taken from the C_f below the friction surface; the (0002) diffraction ring is sharp. While the diffraction pattern, taken from the top of C_f, shows the sharp (0002) diffraction ring merged with transmission beam (Figure 4-33 (c)). Diffusion of diffraction ring is a sign of amorphisation. The author believes this layer should be similar to that observed on the friction surface of carbon fibre reinforced carbon composites (CCC)[88]. It was noticed that a small amount of debris occasionally penetrated into the surface of the carbon fibre, but with a depth inside ~200 nm, as shown in Figure 4-34; their crystallinity was approved by the diffraction patter which appeared in the inset.

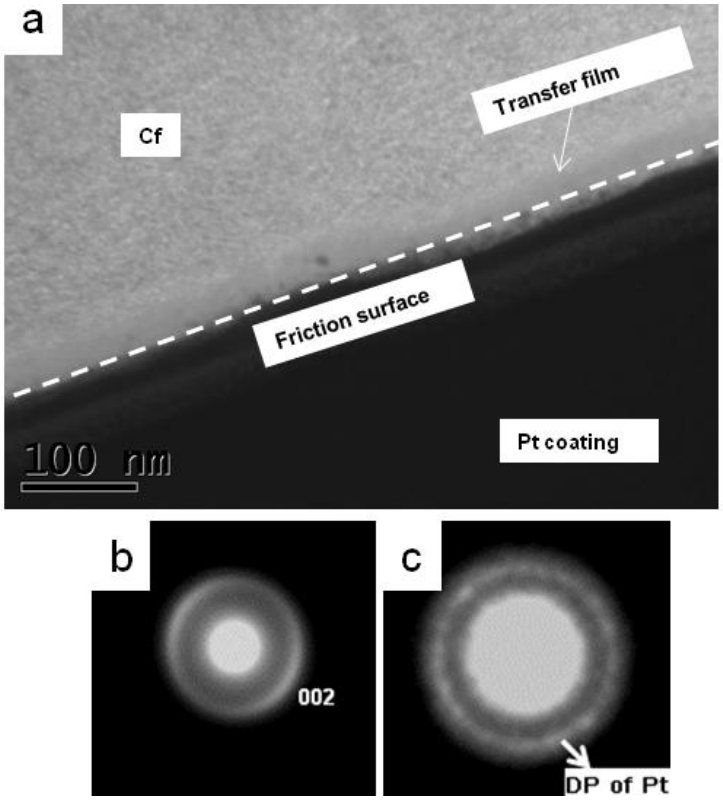

Figure 4-33 (a) Cross-section TEM image of C_f/C showing an amorphous film generated on friction surface of C_f; (b) diffraction pattern of C_f below the friction surface; (c) diffraction pattern taken from the top of carbon fibre, diffused (0002) diffraction ring indicates the amorphisation of carbon fibre (Note: the Pt coating was included into the selected area. Therefore, except for DP of amorphous carbon, DP of Pt coating appears as well)

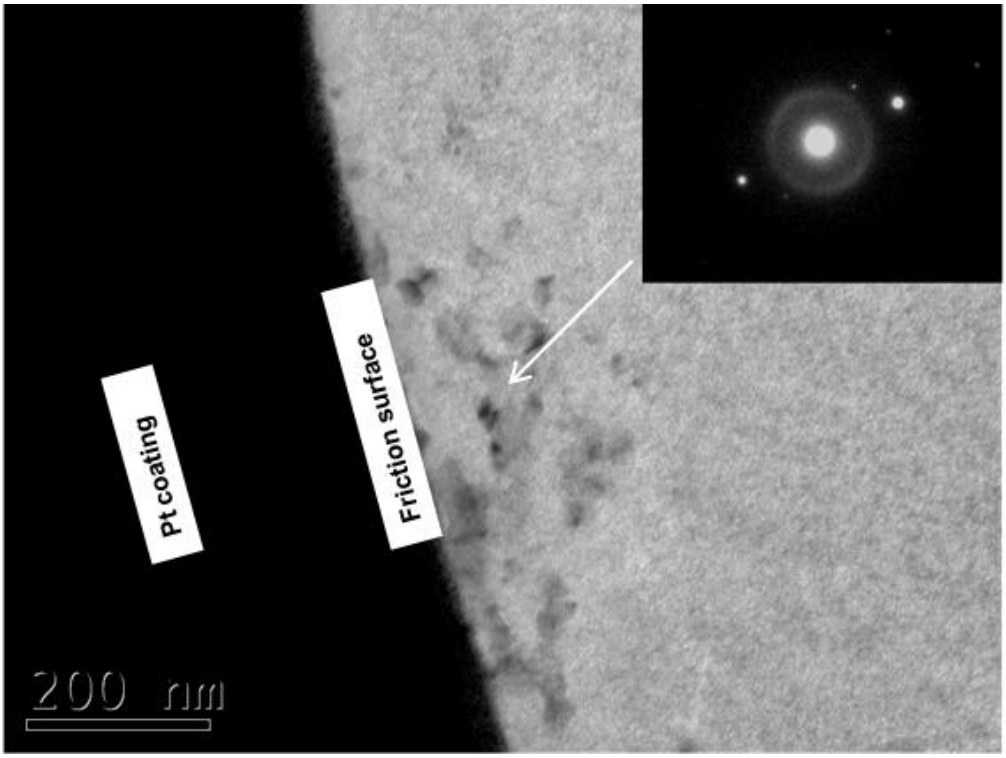

Figure 4-34 Cross-section TEM image of C_f/C showing small amount of debris occasionally penetrated into the surface of the C_f. Diffraction spots in the insert diffraction pattern indicates the crystallinity of debris

Substrate

Particular attention was put on the interfaces of carbon fibre and CVI carbon matrix, which are highlighted with white dash lines (Figure 4-35). Along the interfaces of C_f/CVI carbon matrix, there existed a string of fine silicon carbide particles, with a size range from tens to hundreds nanometers. These silicon carbide particles were mostly separated by the similar transferred materials as shown on top of CVI carbon. The transferred materials did penetrate deeply along the interface region; the observed maximum penetration was up to ~2 μm. Underneath the C_f/C region, micro-cracks were initiated along the interface between carbon fibre and carbon matrix, as shown in Figure 4-36, whilst no crack was noticed inside either fibre or matrix.

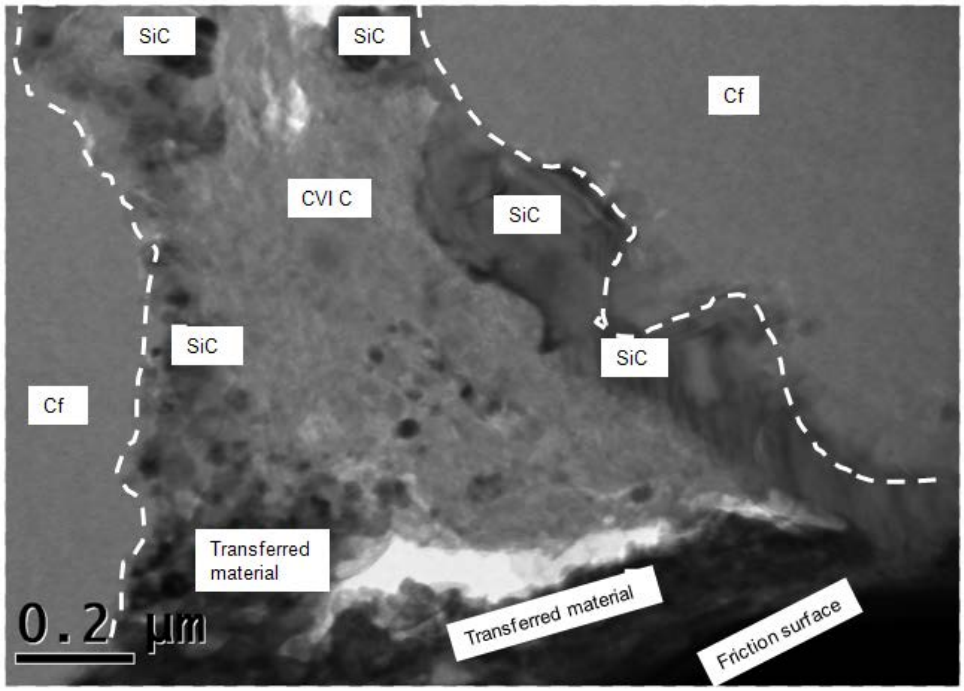

Figure 4-35 Cross section TEM image of C_f/C interface after laboratory scale dynamometer test showing a string of fine particles existing on their interface; these particles were separated by the similar transferred materials as shown on top layer

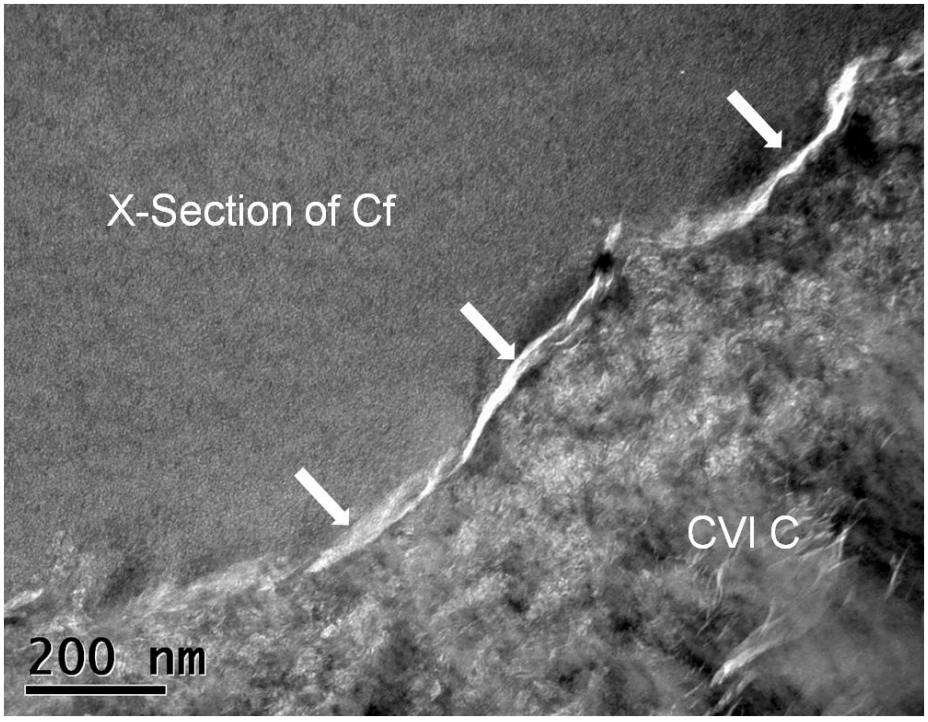

Figure 4-36 Cross-section TEM image of C_f/C interface underneath friction surface; micro-cracks were initiated along the interface between carbon fibre and matrix

4.3.2.5 Third body material developed in voids and cracks

Figure 4-37 (a) shows typical large voids on the as-polished surface. After one braking stop, the void was completely filled with transferred materials (Figure 4-37 (b)); they look fairly dense. After further braking, some of the filled materials were pulled out (Figure 4-37 (c)). As the braking was kept going, it seems such regions had undergone a process of filling in and partially dislodging. As seen in Figure 4-37(d), the same void was fully filled with transfer materials again. Figure 4-38 shows that cracks in silicon carbide regions on the as-prepared surface were also filled by transferred materials fairly swiftly during braking. A similar dynamic process of filling-in and partially-dislodging was observed as that appeared in other large voids.

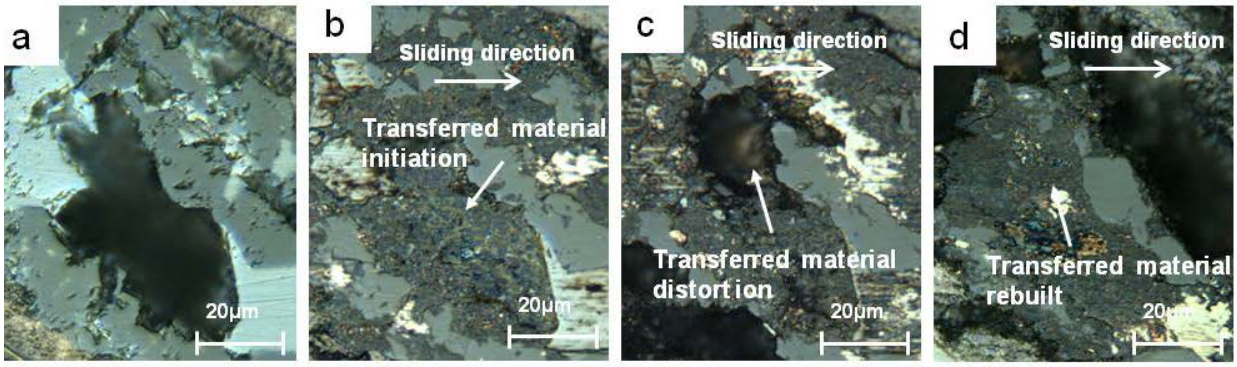

Figure 4-37 Optical microscopy images the friction surface in voids: (a) as-finished before braking, (b) after 1 stop, (c) after 3 stops, (d) after 49 stops.

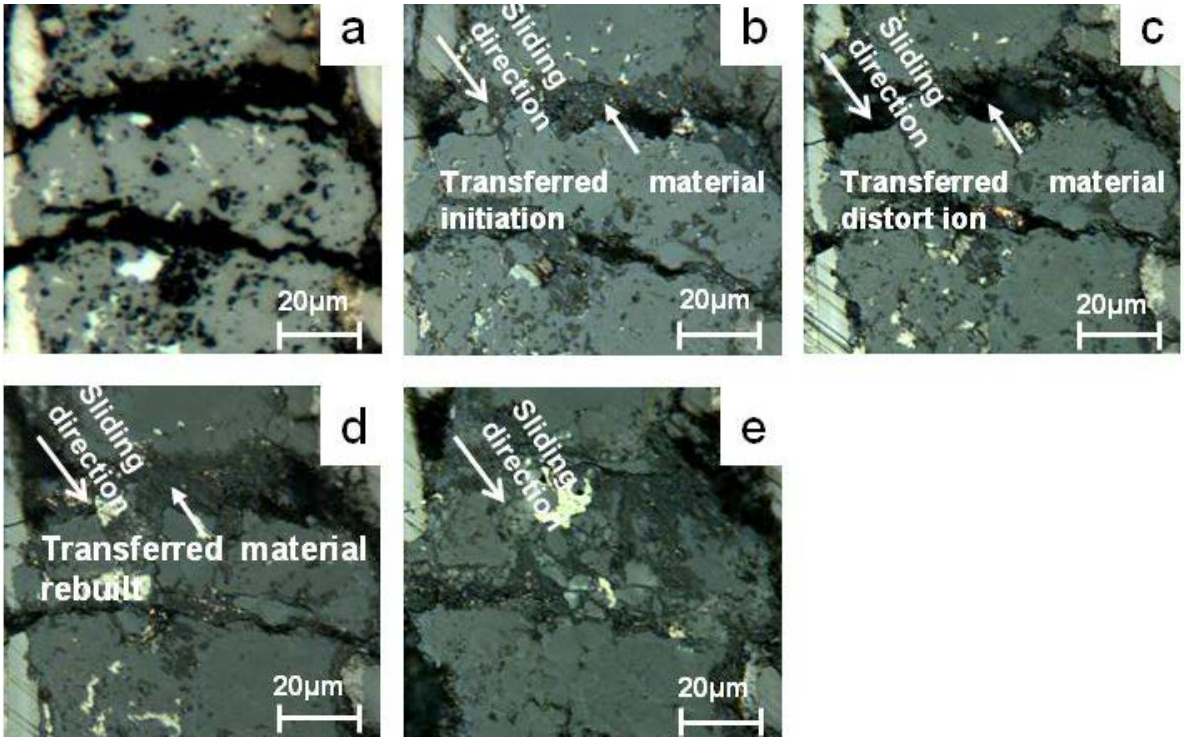

Figure 4-38 Optical microscopy image of friction surface on cracks: (a) as-finished surface before braking, (b) after 1 stop, (c) after 3 stops, (d) after 9 stops, (e) after 49 stops.

4.4 Friction surface of C_f/C-SiC after continuous dynamometer testing

The friction surface of C_f/C-SiC composite, generated after a friction test with continuous 200 stops, was studied. Figure 4-39 shows the overall optical image taken from friction surface; most of the visible transfer layers were developed between SiC crystals as marked. According to the optical image of as-polished C_f/C-SiC composites (Figure 4-2), the regions existed between SiC crystals were Si before friction. Same as the friction surface generated after friction test with 49 discrete brake stops, no transfer layers were developed on the friction surface of SiC and C_f/C by increasing the number of brake stops up to 200. A number of grooves, which were parallel to the longitudinal direction of carbon fibres, appeared on the friction surface of C_f/C.

High magnification optical image, Figure 4-40, shows the typical friction surface of SiC generated after friction test with 200 brake stops followed by HF wash; the friction surface was bumpy due to the formation of kinks. As shown in Figure 4-41, high magnification SEM images and EDX spectrum confirmed that the transfer layers were not developed on top of in-plane carbon fibres and vertical carbon fibres, although the transferred materials deposited in the interface between carbon fibre and CVI carbon and the grooves parallel to carbon fibres, as marked. These grooves are likely to be created by fracturing and then dislodging of carbon fibres.

These results indicate that the development of transfer layer on C_f/C and SiC region was not promoted by increasing the number of braking stops up to 200 under the current testing conditions. It is believed that lack of strong interface bonding and/or substrates dislodging restricted the development of transfer layer on C_f/C and SiC regions.

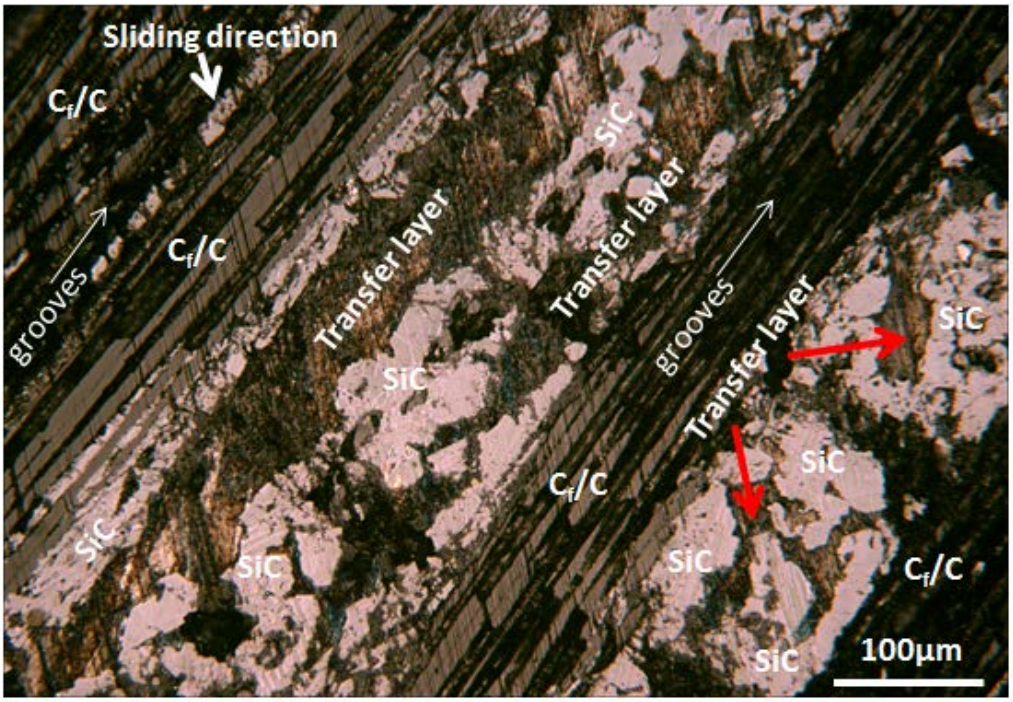

Figure 4-39 Overall image taken from friction surface of C_f/C-SiC disc generated after friction test with 200 continuous brake stops

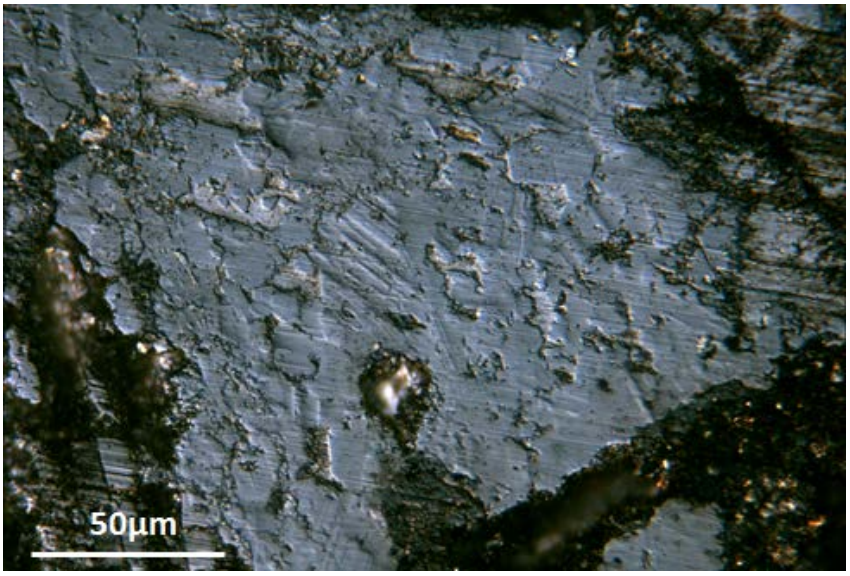

Figure 4-40 OM image of friction surface of SiC generated after friction test with 200 continuous brake stops followed by HF wash

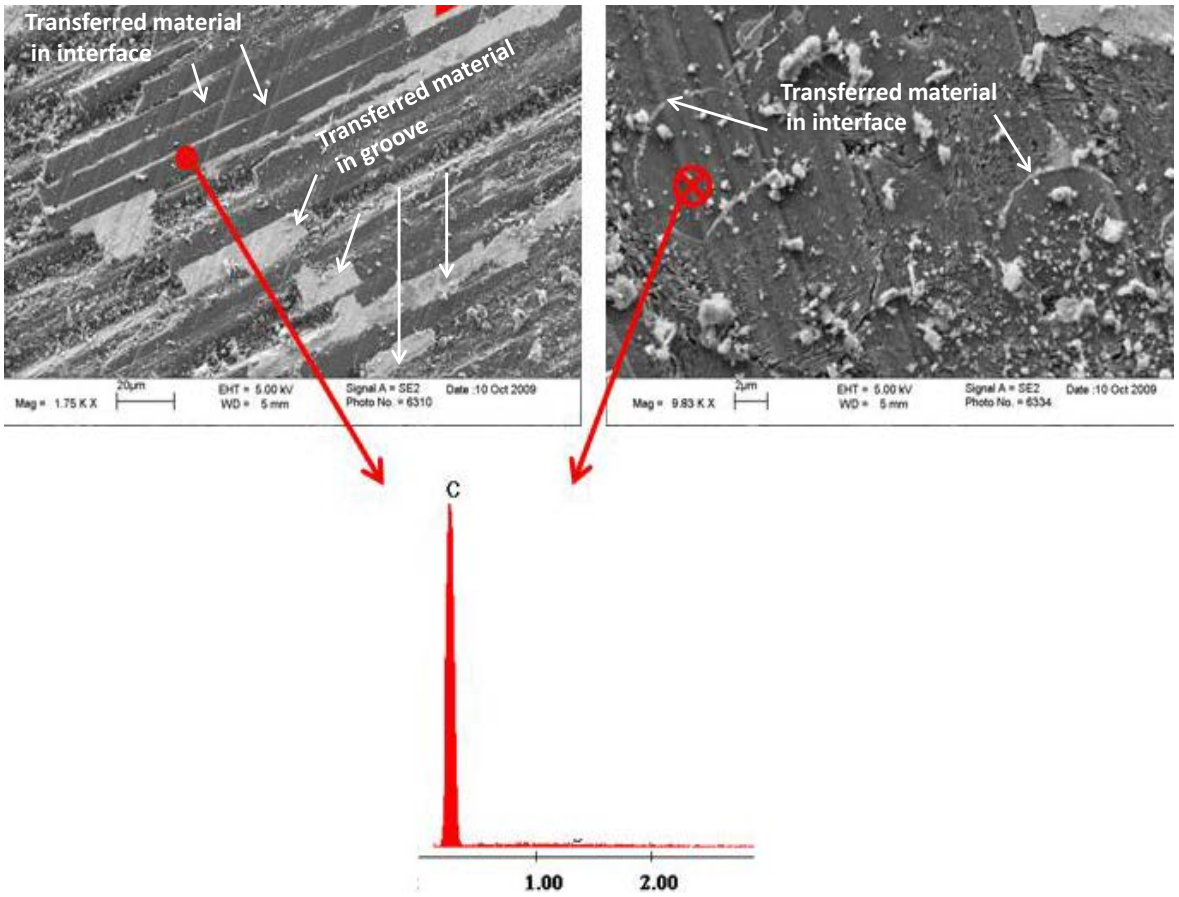

Figure 4-41 High magnification SEM image of fiction surface of $C_{f//}$ /C and $C_{f\perp}$/C generated after friction test with 200 continuous stops; EDX spectrum taken from friction surface of carbon fibers

Summary of results

1. The transfer layer was composed of materials that were transferred from pad and disc; its development during friction was strongly dependant on the adhesion between the transferred materials and the constituents in the composite, as well as the steadiness of the composite surface. Three types of friction surface were identified on the composite's surface: the transfer layer developed on all Si region and some silicon carbide regions had a steady relationship with the matrix and good longevity; the transferred material developed on all C_f/C regions and most of silicon carbide regions had an unstable relationship with the matrix and poor durability; the transferred material developed in large voids and cracks/crevices had a steady relationship with the matrix but short lifetime. The development of transfer layer on the friction surface of C_f/C and SiC was not promoted by increasing the number of braking stops up to 200. Transfer layer developed on Si leads to steady COF vales quickly, but the transfer layer developed on SiC surface, C_f/C surface and cracks/voids lead to a longer braking time to approach a stable level.

2. Cross-section TEM analysis revealed:

(1) The Si region was covered by a transfer layer with a thickness of about 5 μm. The transfer layer was composed of three types of constituents, including: (a) very fine particles with sizes of about tens nanometer. These particles included CuO, MgO, $Ca_{0.15}Mg_{1.85}(Si_2O_6)$, $FeSiO_3$, $Fe_{0.91}Si_{0.09}$, $Cu_{2.7}Fe_{6.3}Si$; (b) fine particles with size of about few hundred nanometers. These particles are likely metal silicides, which are generated by alloying of silicon and metals in transferred material, such as alloyed product of Cu and Si, and Cu, Fe and Si; and (c) amorphous binding phase which bonded all particles together and was likely to be amorphous SiO_x developed by oxidation of Si in the C_f/C-SiC composite.

(2)The bonding between transfer layer and silicon substrate was developed on the interface.

(3) Inside silicon substrate, the damage of Si was not widely observed, but the precipitates with high oxygen content were developed.

3. Cross-section TEM analysis on the friction surface of SiC revealed that:

(1) Most of the contact surface of SiC had no transferred materials. The transferred material was observed in craters which were produced by fracture-induced chipping-off of SiC. No interface bonding was detected between transferred material and SiC.

(2) Deformation twining was observed on the friction surface of SiC after braking

4. Cross-section TEM analysis of the friction surface of C_f/C revealed that:

(1) No transfer layer bonded on the surface of carbon fibres, although a thin amorphous film with a thickness of ~50 nm, produced by friction induced amorphisation of carbon fibre, was developed on top of carbon fibre. Wear debris penetrated into deeper position along the interfaces between carbon fibres and carbon matrix. A maximum penetration depth of ~2 μm was observed.

(2) Microcracks could be developed along the interface between carbon fibres and carbon matrix. This mechanical damage could eventually cause the chipping-off of carbon fibres along the carbon fibre-carbon matrix interface, especially for the in-plane C_f/C regions, where the entire longitudinal fibre/matrix interface exposed on friction surface.

Chapter 5 Discussion

5.1 Development of friction surface on C_f/C-SiC brake disc

Registered microscopic images on friction surfaces have revealed that transfer layer, or third body materials, were introduced onto the surface of the C_f/C-SiC composites by the braking operations, when an organic pad was used to against the ceramic disc. These third body materials were observed on the friction surface right after the initial braking, regardless the constituents and the microstructure features on the surface of the composite, as shown in Figure 4-8 (b), Figure 4-19 (b), Figure 4-27(b),Figure 4-29(b), Figure 4-37(b), Figure 4-38(b). However, their embedding configuration and existing morphology vary greatly on the surface.

On the top of the silicon, the deposition of the transferred materials could be on anywhere on the as-finished surface spreading across the whole region. For silicon carbide, the transferred materials tended to embed in wherever that was topographically lower, e.g. micro-cracks, pits, voids and porosity; these microstructural feature were likely generated by the Hertizan contacting damage of abrasives during surface machining and friction braking, or borne inside the composites themselves. In the C_f/C region, the depositing tendency of the transferred materials was very similar to that observed on silicon carbide. Certain embedding places were nevertheless believed to be created immediately after the friction contact through a possible process of fracturing first, and then dislodging of the materials; these sites can be distinguished by comparing the friction surfaces after 1 to 3 braking stops (Figure 4-27 (b) and Figure 4-29 (b-d)) with the as-finished ones (Figure 4-27(a), Figure 4-29(a)). For pre-existing large voids and cracks/gaps, despite their existing locations, they were all

filled with transferred materials immediately after the initial braking. The author believes that the structural features of the voids/cracks/gaps on the surface could provide these regions a function just like a cheese grater does, and the cavities might have collected most of the filled materials that were chipped off from the pad, as seen in Figure 4-37 and Figure 4-38. Note, judging from the appearances of the compacts in Figure 4-37 and Figure 4-38, their density, cohesion and their longevity may vary a lot with the nature of the cavities/gaps, i.e. their depths, in-plane dimensions, shapes and materials surrounding them.

After the preliminary deposition of the transferred materials and any further development in the following up braking, the morphology of the friction surface had subjected to a fairly dissimilar route in different regions; details on the development have been described in chapter 4.

Based on the observations, three types of friction surface can be generalized, and they were categorized as following:

(a) *type I*, the transferred materials had a relatively stable relationship with the matrix, and any cumulative development should involve an interaction with the previously deposited materials and were able to maintain their longevity in a friction transfer layer;

(b) *type II*, the transferred materials had unstable relationship with the matrix, and the longevity of the transferred material was likely dependant on the durability of the interface between the transferred materials and the matrix, as well as the sturdiness of the near-surface region of the matrix;

(c) *type III*, the transferred materials had a relatively stable relationship with the matrix, but the longevity of the transferred materials were likely determined by the cohesion of the compact.

The registered images have revealed that transfer layer were able to successfully deposit on silicon regions and the friction surface consisting of the developed layer

should belong to the type I; friction surfaces with those transferred materials on the silicon carbide and on the C_f/C regions can be categorized into the type II; the trapped materials in large voids/gaps existing on the surface should fit in the type III. Under the current dynamometer testing condition, no visible fracture damage of the silicon substrate has yet been seen up to the last braking of the discrete friction test. Instead, it was noticed that the transferred materials were deposited on the surface as long as the pad had a direct contact with the surface of the composite; transferred materials introduced by the following up brakings were fused with the previous ones to generate friction transferred layer over the substrate (Figure 4-8). In addition, the transfer layer was found to be strongly bonded with Si (Figure 4-15). In silicon carbide and carbon fibre/carbon regions, the development of transferred layer showed a tendency to be influenced by the unsteadiness of the substrate. Surfaces in both regions subjected to braking damage from the early brakings, as shown in Figure 4-19, Figure 4-27 and Figure 4-29; such damage could obviously lead to an unstable surface region. In addition, after friction test with 49 braking stops, no evidence was provided that the transferred materials had a strong adhesion with silicon carbide and carbon. Furthermore, under the current testing condition, the development of transfer layer on C_f/C and SiC region was not promoted by increasing the number of stops up to 200 (Figure 4-39), which also suggests the lack of strong bonding between transfer layer and substrates, C_f/C and SiC. Therefore, it is believed that if the transferred materials had had a better adhesion with the substrates and/or the substrates had higher fracture resistance, the surface of substrate could have suffered less contact damage.

5.2 Factors that govern the formation and sustainability of transfer layer on C_f/C-SiC disc

It has been clearly shown that it was generally difficult to develop an extensive transfer layer on the friction surface of the C_f/C-SiC under the braking pressure. Why friction transfer layer is difficult to be developed on C_f/C-SiC composite? The post-mortem

TEM analysing of transfer layer developed on SiC, Si and C_f/C might have exposed two underpinning mechanisms that can influence the development and sustainability of transfer layer on the surface of C_f/C-SiC discs: (a) bonding between the transfer layer and the constituents in the C_f/C-SiC composites; (b) mechanical damage in the near surface of the C_f/C-SiC composites. The lack of strong bonding leads to no transfer layer remained on the surface after braking; the existence of mechanical damage, even in a micro-scale in the near surface region of the disc, could lead to a loss of the surface integration and an unsustainable friction surface even if a strong bonding was developed between the transferred materials and the composite surface. These two aspects are discussed in this session based on the experimental evidences and existing knowledge.

5.2.1 Bonding between transfer layer and C_f/C-SiC composite

For the friction surface of C_f/C-SiC disc generated under current testing conditions, it was found that the interface bonding existing between transfer layer and Si (Figure 4-14 and Figure 4-15). However, no interface bondings were observed between the transferred material and SiC (Figure 4-22) and C_f/C (Figure 4-35). Two possible mechanisms could be borrowed to understand the possibility of developing a bond between transfer layer and the surface of the composite: fusion and brazing joining.

Fusion joining involves melting of materials. On the ceramic composite surface, Si can fuse with Cu and Fe in transferred material when temperature is high enough, e.g. 802^{o}C for Si-Cu and 1200^{o}C for Si-Fe[113]. In addition, Si can be oxidized into SiO_2 when oxygen is involved and temperature is high enough. SiO_2 can fuse with other oxides or compounds pre-existing in the transferred materials or oxidising variants of some constituents, such as Al_2O_3, FeO_x and CuO_x, if temperature is high enough. For example, eutectoid temperatures of typical binary systems, i.e. CuO-SiO_2, FeO-SiO_2, likely appearing on interface, are 1050 and 1173^{o}C respectively [114]. As shown in Figure 4-15,

the copper silicide and copper silicate were developed on the interface between copper and silicon. Also, iron silicide and iron silicate were found in the transfer layer developed on Si, as proved by diffraction patterns (Table 4-2). These observations indicate that the temperature of more than 1000^{o}C was generated on the friction surface, under the current dynamometer testing condition.

SiC and C have no melting but subliming as temperature high enough. Therefore, no direct fusion joining exists between SiC or C and other transferred materials from the pad. When oxygen is involved and temperature is high enough, SiC can be oxidised into SiO or SiO_2[115]. Fusion between transferred materials and SiC could occur via its oxidation. For example, SiO_2 can fuse with FeO_x and CuO_x in transferred material. However, under current small dynamometer testing condition, the silicates were not identified on the interface between SiC region and transferred materials after testing with the selected organic pad. It seems that the SiC wasn't oxidised enough for occurrence of fusion between silicon oxides and metal oxides.

During friction, significant amount of metallic materials were stripped off from organic pad. If there is no fusion bonding, ceramic constituents and metals can be jointed together on the basis of adhesion bonding. In materials joining sector, this is called brazing joining. To predict the adhesive joining, the following relationship is well established between melt and solid surface:

$$\gamma_{SL} = \gamma_{SV} - \gamma_{LV}\cos\theta \qquad \text{Equation (5.6)}$$

Here γ_{SL}, γ_{SV}, γ_{LV} denote the liquid-vapour, solid-liquid and solid-vapour surface energy respectively, and θ the contact angle between liquid and solid, i.e. the wetting angle. When $\gamma_{SL} > \gamma_{SV}$, the θ is greater than 90^{o}, no spreading occurs, i.e. the liquid drop tends to spheroidise. In contrast, when $\gamma_{SL} < \gamma_{SV}$, the θ is smaller than 90^{o}, the solid surface will be covered by a thin film of liquid, spreading along the surface of solid.

Studies show that for pure copper, the wetting angles are well above 90^{o} on the surface of carbon and silicon carbide at temperature up to 1150 ^{o}C [116] and 1400 ^{o}C [117] respectively. This fact implies that pure copper exiting in the transferred material can no longer be bonded with SiC and C on the composites surface, even if at a high temperature up to 1150 ^{o}C. In the joining sector, however, a lot of studies have been carried out to improve the wetting ability of copper through alloying active elements, most of them are IV-B elements such as Ti, Zr, Hf, and others such as Ni, Be, Cr, V, In and Co (a range of references on development of active filler metal are available from a review paper on advances in brazing of ceramics[118]). These active elements can reduce the wetting angle to less than 90^{o}. However, in this research, EDX analysis either in SEM or TEM did not detect such active elements. This fact indicates that even if a high temperature up to 1150^{o}C is available on the interface, the copper existing in the transferred materials cannot wet the carbon and silicon carbide.

However, the wetting angle between Cu and Si is significantly smaller than 90^{o}. For instance, it was shown that, at 1100^{o}C, the wetting angle can quickly drop to 6^{o} from initial 45^{o} [119]. This should be the reason why copper was enriched on the Si surface and a strong bond was developed between the friction transfer layer and the Si regions.

Based on the above analysis, it could be conclude that bonding between transferred materials and constituents in C_f/C-SiC composites can happen between transferred materials and silicon through fusion and/or brazing joining under the current testing condition. Bonding is not able to occur between transferred materials and SiC, and between transferred materials and carbon. Potential bonding of transferred materials-SiC and transferred materials-carbon could occur by integrating active elements into Cu to improve the wetting ability of copper alloys on SiC and C constituents.

5.2.2 Mechanical damage in the near surface of the C_f/C-SiC composite

Under the current dynamometer testing conditions, no visible fracture damage was found on silicon substrate. However, the surfaces in both SiC and C_f/C regions were subjected to breaking damage from the very early brakings, as shown in (Figure 4-27- Figure 4-29). The appearance of significant contacting damage in both silicon carbide and carbon regions implies one possibility that the critical energy releasing rates of silicon carbide (G_{SiC}^{C}) and carbon (G_{C}^{C}) could be lower than that of silicon (G_{Si}^{C}) in this composite, i.e. $G_{SiC}^{C} < G_{Si}^{C}$ and $G_{C}^{C} < G_{Si}^{C}$.

Fracture releasing rate, G^C, is a parameter used to gauge the fracture tolerance of a material under loading condition. It should have the following relationship with the Young's modulus, E, and fracture toughness, K_{IC}, of a material

$$G^{C} = \frac{(1-\nu^{2})K_{IC}^{2}}{E} \qquad \text{Equation (5.7)}$$

where ν is its Poisson ratio. By re-arranging equation 5.7, the following linear relationship between logarithm of modulus and fracture toughness should be obtained.

$$\log_{10} K_{IC} = \tfrac{1}{2}\log_{10}\left(\frac{E}{1-\nu^{2}}\right) + \log_{10}(G^{C})^{\frac{1}{2}} \qquad \text{Equation (5.8)}$$

In a $\log_{10}(E/1-\nu^2)$ – $\log_{10}(K_{1c})$ chart, the intercepts on the K_{IC} axis of parallel linear dashed lines with a slope of ½ represent the values of G^C. A group of such lines have been drawn in Figure 5-1(a), with specific values are labelled for the fracture strain rates. When materials sit on the same line, it indicates that they should have same fracture strain rate; materials near the top left corner should have larger fracture strain rate than those closer to the bottom right corner. Data drawn from Cambridge Materials Selection database[120] have been marked in this chart for these ceramics that could be comparable with the ceramic constituents observed in this composite: silicon, sintered SiC, nitride bonded SiC, vapour deposited SiC, pure graphite, isotropic carbon fibre. Three carbon fibre reinforced carbon composites (CCC1, CCC2 and CCC3) have also been included[121]. As shown in Figure 5-1(a), silicon and graphite have the similar

fracture strain rate, but much lower than any SiC ceramics and CCC. This implies that cracking damage would not have occurred in SiC and C_f/C regions when no cracking is observed in silicon. The discrepancy between the experimentally observed and theoretically predicted on the fracture resistance of the ceramic constituents during braking may imply that K_{IC} values measured from ceramics might have over-estimated, when these data are intended to be applied to measure the micro-cracking resistance of the constituents on the friction surface during braking. In fact, fracture resistance of polycrystalline ceramics could increase with crack extension, i.e. the well-known R-curve behaviour, and the magnitude of this increase could be in excess of a factor of three [122]. For ceramics with complex microstructure, like polycrystalline and composites, this difference would become more significant[123].

Recently, Leatherbarrow and Wu[124] estimated Young's modulus and K_{IC} of Si and SiC in the C_f/C-SiC composites from nano-indentation test. The C_f/C-SiC composite used in their research was the same as the one used in this study. K_{IC} measured by nano-indentaion test is 0.7 MPa.$m^{1/2}$, which is much smaller than typical cited value of approximately 3 MPa.$m^{1/2}$ for polycrystalline SiC. By using Young's modulus and K_{IC} measured from their research, G^c of SiC and Si should be 1.27 and 1.67 J/m^2 (Table 5-1). This result indicates that SiC is more fragile than Si under the same loading conditions. Therefore, cracking damage could occur in SiC even through no cracking was observed in silicon. It seems that the fracture toughness derived from nano-indentation test, which may only be appropriate to gauge the crack initiation resistance, should be useful to understand tribology related damaging. Most of fracture toughness values from database may not be suitable for estimating the micro-cracking resistance in ceramic, because these measured fracture toughness values are the maximum resistance of the crack propagation, which could only be reached after the cracks propagate with sufficient length. This view has been demonstrated in a study on the wear resistance of alumina, where the damage resistance has little relationship with large crack propagation resistance, i.e. K_{IC} measured by most methods, but a strong relationship with short crack energy releasing rate[125].

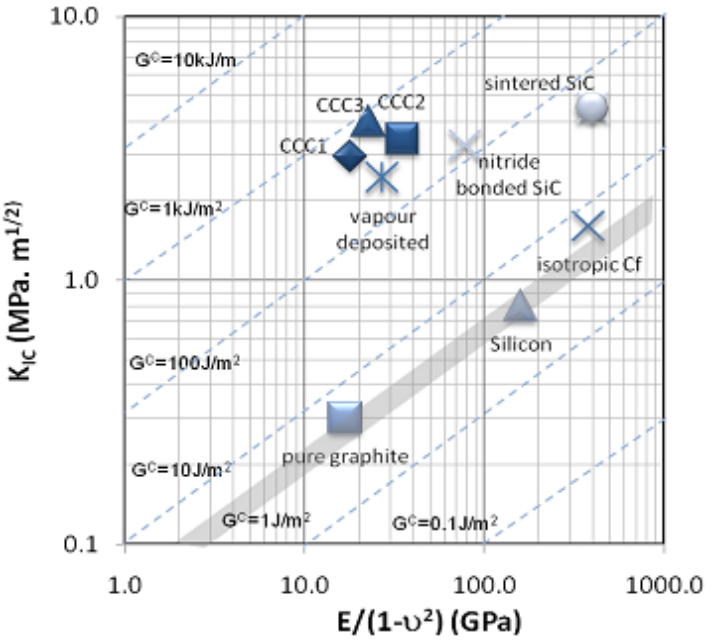

(a)

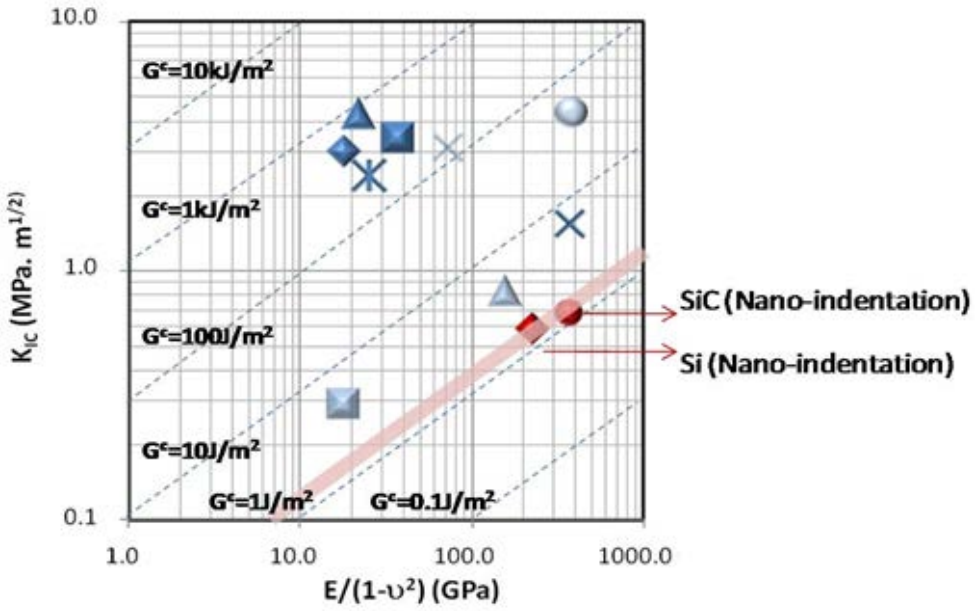

(b)

Figure 5-1 Fracture toughness of ceramics (K_{IC}) plotted against Young's modulus ($E/(1-v^2)$). The family of lines are of critical energy releasing rate (G^C). (a) The shaded band shows that pure graphite, silicon and isotropic carbon fibres have similar fracture energy by using K_{IC} and E borrowed from database in calculation; any ceramics above this band are more resistant to cracking than those on/below the band (b) The shade band shows that SiC and Si have similar fracture energy by using K_{IC} and E measured from nano-indentation in calculation.

It is believe that the following possible physical aspects inside the silicon carbide might have led its surface more fragile than silicon: (a) the silicon carbide regions in the composite might have been weakly bonded as the grain boundaries were not purposely engineered in the LSI process; (b) large residual tensile stress could exist on the grains boundaries due to the constraint on the growth of silicon carbide grains in LSI process and the thermal strains generated during cooling down from the silicon impregnation temperature, which are featured through the appearance of stacking faults inside the SiC grains[126] .

Table 5-1 Fracture toughness and critical energy releasing rate derived from nano-indentation hardness test at room temperature[124]

	υ	Young's modulus E (GPa)	Fracture toughness (K_{IC}) ($MPa.m^{1/2}$)	Critical energy releasing rate (G^c) (J/m^2)
SiC	0.188	375	0.7	1.27
Si	0.27	200	0.6	1.67

The same analysis can apply to C_f/C region where the short-crack energy releasing rate, particularly along the interface between carbon-fibre and carbon matrix, should be significantly smaller than those measured from C_f/C composites, since in the design of most fibre reinforced composites, the fibre/matrix interfaces are deliberately weakened to improve the fracture tolerance[127], which is why the three CCC composites, shown in Figure 5-1(a), are sitting above all SiC ceramics. Unfortunately little experimental measurement is available on the interface or grain boundary fracture energy, as an addition in Figure 5-1 to exhibit the picture more clearly. However, according to Figure 5-1(b), it can be anticipated that the fracture toughness for the initiation of microcracks in C_f/C should be less than $0.2MPa.m^{1/2}$, in order to give smaller fracture energy release rate than Si.

It is convinced through the analysis that short crack initiating resistance must be improved for the ceramic matrix, including all interfaces in these composites in order to promote the development of a steady friction surface during braking for the aim of

maintaining the friction and engineering performance of the composites, in addition to improve the adhesion of the transferred materials on the friction surface.

During friction, the friction heat induces the thermal expansion of C_f/C-SiC composites. Because the constituents in C_f/C-SiC composites (C_f, CVI C, Si and SiC) have various coefficients of thermal expansion, an internal thermal stress builds up in the C_f/C-SiC disc due to the thermal expansion mismatch. Apart from the mechanical force, the author believes that the substrate damage could be induced by internal thermal stress if the thermal stress is over the fracture strength of material. As a result of the thermal mechanical damage, the development of transfer layer on friction surface of C_f/C-SiC composite becomes unstable.

For a homogeneous material, under uniform temperature, the thermal stress can be calculated by knowing the temperature difference, the modulus of material and the coefficient of thermal expansion. However, the calculation of thermal stress could be rather complex if the temperature distribution along the thickness of material is non-uniform; the temperature distribution on the in-plane surface is non-uniform; or the material is heterogeneous. The heat flow and temperature distribution in the heterogeneous C_f/C-SiC composite disc are not able to be monitored by the current laboratory scale dynamometer and the calculation of the thermal stress in C_f/C-SiC composite disc is beyond the scope of this thesis. Nevertheless, the thermal stress could be a potential issue which influences the development of transfer layer on C_f/C-SiC as discussed above.

5.3 Deformation of SiC in C_f/C-SiC composite disc

TEM cross section on SiC revealed that twins or micro-twins existed in SiC substrate below the friction surface. These twins could be a result of deformation twining of SiC

by friction. The deformation twining of SiC is usually produced as a result of different mobility of Si partial dislocation and C partial dislocation[128 129 130]. It is confirmed that the kinks developed on the friction surface were associated with the deformation twining of SiC, as kinks on the friction surface always developed at the positions where twins or micro-twins were observed in the substrate (Figure 4-24). According to the experimental observation, a mechanism is proposed here to explain the deformation of the SiC friction surface, as schematically shown in Figure 5-2.

Figure 5-2(a) schematically shows the cross section of SiC friction surface before friction. A Si layer exists underneath the SiC crystal. At the early stage of friction, the deformation twining of SiC occurred under the brake load. Due to the deformation of the crystal lattice, a kink developed on SiC when twining occurred (Figure 5-2(b)). Once the SiC twin generated in the parent SiC substrate, slipping of the twin could take place along twinning boundaries, under the brake load. Consequently, the Si underneath SiC twin could be compressed down by the slipping of SiC, such that a terrace step produced on the Si/SiC interface (Figure 5-2(c)).

One condition must be satisfied for deformation of SiC without fracture damage: materials existing underneath SiC should be soft enough to accommodate the kink developed on SiC and the slipping of SiC twin. In the C_f/C-SiC composite, these types of materials are Si and C_f/C.

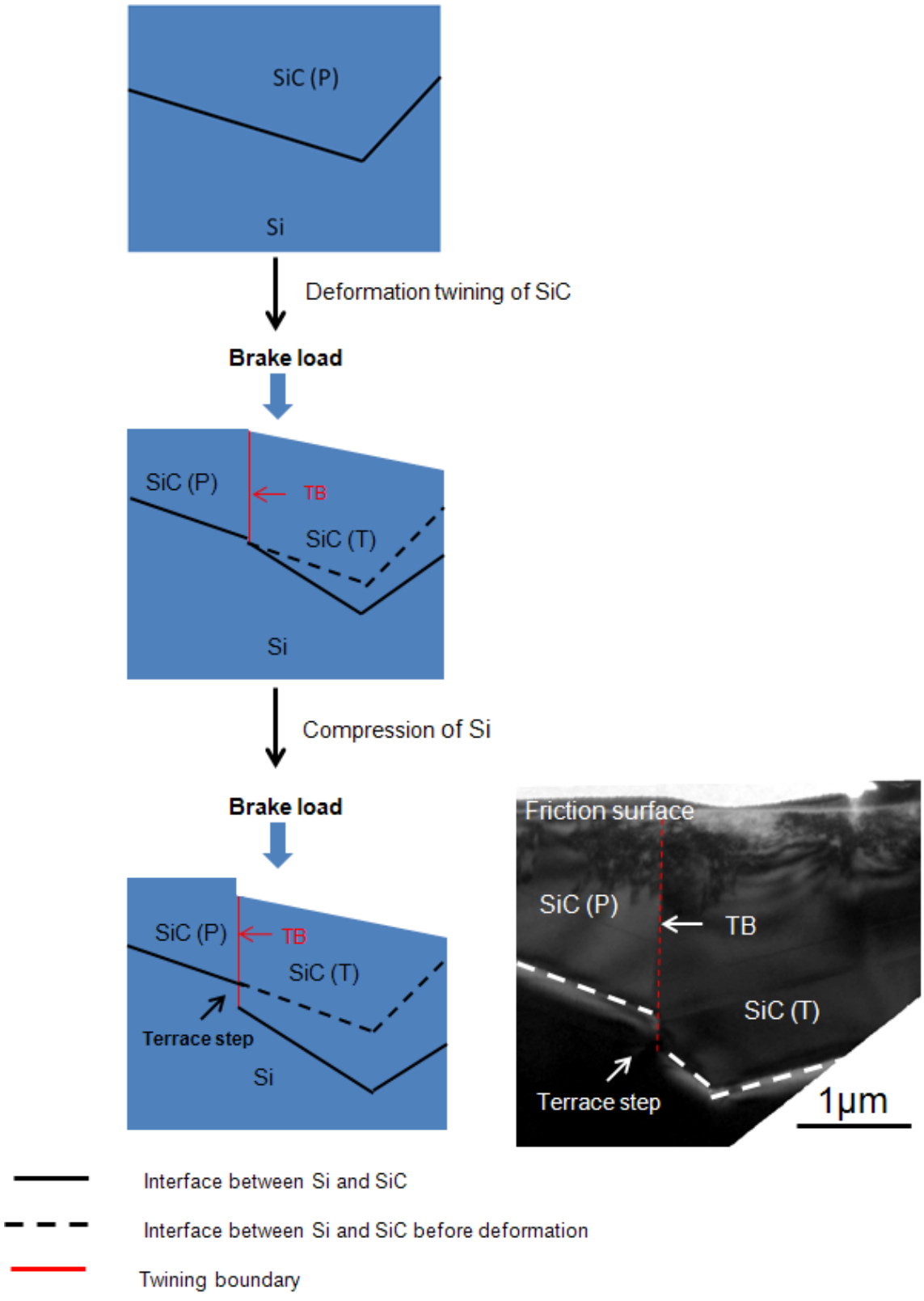

Figure 5-2 Schematic illustration of the development of kinks on the friction surface of SiC. SiC(P) stands for SiC parent, SiC(T) stands for SiC twin. (a) SiC before deformation, (b) generation of kinks by deformation twining, (c) slipping of SiC twins along twining boundary

5.4 Correlationship between coefficient of friction and transfer layer development

The development of the three types of friction surfaces on the C_f/C-SiC composite disc could make a direct impact on the measurements of coefficient of friction and its stabilization. Generally, the growth of the transfer layer with the addition of further brakings increases the contact area between the disc and the pad; such an increment should lead to an improvement of the measured COFs (Figure 4-6, in observation Ⅲ-Ⅸ). Once the development of the transfer layer is stabilised, the COF would reach to a constant value, where it is generally regarded as the completion of bedding process. However, this stabilisation has not yet been seen under the current dynamometer testing regime. Judging from the development of the transfer layer on different regions, the author believes that those on the silicon regions could give a stabilised state very swiftly (Figure 4-8). Whereas the development process of transferred material on SiC and C_f/C region is very dynamic (Figure 4-19, Figure 4-27 and Figure 4-29).The transfer material, developed in pervious friction stage, could be stripped off in following friction process. The stable COF could be only achieved when the formation and removing process of transferred materials reached to a dynamic balanced state. Compared with quick and continuous development process of transfer layer on Si, a longer time is required to reach the dynamic balance states for transferred material developed on SiC and C_f/C region. Therefore, development of unstable type II friction surface could be the key factor that leaves a longer bedded-in time for friction pair of organic pad/C_f/C-SiC disc. To sum up, the growth of type I likely lead to a stable friction, and type II and type III to a longer braking to approach a stable level.

Chapter 6 Summary

1. The development process of transfer layer was studied on the friction surface of C_f/C-SiC composite when the composite disc was coupled with an organic pad. The development of transfer layer during friction was strongly dependant on the adhesion between the transferred materials and the constituents in the C_f/C-SiC composite, as well as the steadiness of the composite surface. Three types of friction surface were identified on the composite's surface: type I– the transfer layer had a steady relationship with the matrix and good longevity; type II –the transferred material had an unstable relationship with the matrix and poor durability; type III – the transferred material had a steady relationship with the matrix but short lifetime. It appeared that type I existed on all silicon regions and some silicon carbide regions; type II on all C_f/C regions and most of silicon carbide regions; type III in large voids and cracks/crevices. Type I likely lead to steady COF vales quickly, but the type II surface and type III to a longer braking time to approach a stable level. One of the controlling factors for type II friction surface should be the fracture resistance of the matrix, apart from the adhesion strength between the transferred materials and the composite. To avoid the appearance of type II surface, it is necessary to increase the critical strain rate of short crack propagation of silicon carbide and C_f/C regions in the composites.

2. The transfer layer developed on Si region was composed of constituents from pad, metal oxides and metal silicides which were generated by oxidation of metals and alloying of Si and metals during friction. The bonding between transfer layer and silicon substrate was developed on the interface through melting fusion and/or brazing joining. The interfacial bonding between transfer layer and silicon substrate is believed to be the key factor for the formation of a stable transfer layer on Si. Inside silicon substrate, the precipitates with high oxygen content were developed.

3. The transferred material was only observed in craters of SiC region which were produced by fracture-induced chipping-off of SiC. Under current testing conditions, interface bonding was not found between transferred material and SiC. Kinks were widely developed on the friction surface of SiC. It is believed that these were produced by deformation twinning of SiC, followed by slipping of SiC twins or microtwins along twinning boundary.

4. Transfer layer was not developed on the surface of carbon fibres, although a thin amorphous film was developed on top of carbon fibre. Wear debris penetrated into the interfaces between carbon fibres and carbon matrix. It is believed that the chipping-off of carbon fibres along the carbon fibre-carbon matrix interface was resulted from microcracks developed along the interface between carbon fibres and carbon matrix.

Chapter 7 Further work

- Based on the analysis of friction surface of C_f/C-SiC composites, it is impossible to maintain surface integration due to the cracking damage inside SiC and C_f/C region, which has a negative effect on achieving stabilised friction performance. Therefore, there is a need to redesign the microstructure of C_f/C-SiC composite to reduce the surface damage and maintain integration of friction surface. On the other hand, the constituents in pad need to be optimised for developing a well bonded transfer layer across the whole friction surface of C_f/C-SiC.

- The influence of testing condition, e.g. brake pressure, brake load, number of stops, on the development of transfer layer on C_f/C-SiC composite disc need to be investigated in further study.

- The current study of transfer layer development on the as-polished C_f/C-SiC disc. The influence of surface roughness on the development of transfer layer need to be investigated in further study.

Publications

Yuan Wang and Houzheng Wu, Friction surface evolution of carbon fibre reinforced carbon/silicon carbide (Cf/C-SiC) composites, *Journal of the European Ceramic Society*, **30** (2010), 3187-3201

Yuan Wang and Houzheng Wu, Friction Surface Development on Carbon Fibre Reinforced Carbon-Silicon Carbide, *Proceedings of the 7th International Conference on High Temperature Ceramic Matrix Composites (HTCMC-7),*2010

Houzheng Wu, Yuan Wang, Friction Surface Damage of Carbon-Fibre Reinforced Carbon-Silicon Carbide Composites (C_f/C-SiC), *key engineering materials*, **484** (2011), 32-35

Houzheng Wu, Yuan Wang, David Pindar, Phil Ferdani, Interaction between ceramic matrix composites and organic pad materials and its impact on the friction performance, *SAE international,* 2011, 11BC-0048

Yuan Wang, Houzheng Wu, Microstructure of friction surface developed on carbon fibre reinforced carbon – silicon carbide (C_f/C-SiC), *Journal of the European Ceramic Society,* 2012*,* Article in Press

Reference

[1] T. Liu, S.K Rhee, et al, A study of wear rates and transfer films of friction materials, *Wear*, **60**(1980),1–12

[2] W. Krenkel, B. Heidenreich, et al, C/C-SiC composites for advanced friction system, *Advanced Engineering Materials*, **4** (2002), 427-436

[3] J. Y. Paris, L. Vincent, et al, High-speed tribological behaviors of carbon/silicon-carbide composite, *Composites Science and Technology*, **61**(2001), 417-423

[4] N. M. Kinkaid, O. M. O'Reilly, et al, Review automotive disc brake squeal, *Journal of Sound and Vibration,* **267** (2003), 105–166

[5] http://repairpal.com/brake-drum

[6] G. A. Harper, Brakes and Friction Materials: the history and Development of the technology, Mechanical Engineering Publications limited, London, England,1998

[7] J. D. Halderman and C. D. Mitchell, Automotive brake systems (2nd Edition ed.), Prentice-Hall, Upper Saddle River, NJ (2000)

[8] F.W. Lanchester, Improvements in the brake mechanism of power-propelled road vehicles, G.B. Patent No. **26407**, 1902

[9] D. C. Barton, M. J. Haigh, The second international seminar on automotive braking recent development and future trends, professional Engineering Publish Limited, Bury St Edmund and London, UK

[10] G. R. Devi, K. R. Rao, Carbon-carbon composites – an overview, *Defence Science Journal*, **43** (1993), 369-383

[11] B. J. Chapman, G. Mannion, Titanium-bearing cast iron for automotive braking applications, *Foundry Trade Journal*. **25** (1982), 232-246

[12] S. Kalpakjian, S. R. Schmid, Manufacturing Engineering and Technology Fourth Edition, Pearson Education Limited, United Kingdom, 2003

[13] J. D. Holme, Disc brake rotor with a grey cast iron composition, European Patent **EP1034317**, 2002

[14] M. Macnaughta, Cast iron brakes – a brief history of their development and metallurgy, Technical Report, Foundryman, 1998, 321-324

[15] D. C. Barton, Advances in automotive braking technology, Mechanical Engineering Publications Limited, England, 1996

[16] M. Ihm, Introduction to gray cast iron brake rotor metallurgy, SAE tutorial

[17] http://www.hitcoracing.com/

[18] F. Smeacetto , M. Ferraris, et al., Protective coatings for carbon bonded carbon fibre composites, *Ceramic international*, **34**(2008), 1297-1301

[19] C.M.Ma, N.Tai, et al., Microstructure and oxidation resistance of SiC coated carbon-carbon composites via pressureless reaction sintering, *Journal of Materials Science*, **31**(1996),649-654

[20] S. Fan, L. Zhang, et al., Microstructure and properties of 3D needle-punched carbon/silicon carbide brake materials, *Composites Science and Technology*, **67**(2007), 2390-2398

[21] http://www.sglgroup.com

[22] P. J. Blau, Composites, functions, and testing of friction brake materials and their additives, ORNL/TM-2001/64, 2011

[23] J. Bijwe, Composites as friction materials: recent developments in non-asbestos fiber reinforced friction materials—a review, *Polymer Composite*, **18**(1997), 378-396

[24] D.Chan, G.W. Stachowiak, Review of automotive brake friction materials, *Proceedings of the Institution of Mechanical Engineers, part D: Journal of automotive engineering*, **218** (2004), 953-966

[25] A. Anderson, Friction and wear of automotive brakes, In: P. J. Blau, ed., Friction, lubrication and wear technology, *ASM handbook*, **18**, 569-577

[26] R. Naslain, CVI-composites, In: R. Warren, ed., *Ceramic matrix composites*, Glasgow, 1992, 199–244

[27] R. Naslain, R. Pailler, et al., Synthesis of highly tailored ceramic matrix composites by pressure-pulsed CVI, *Solid State Ionics*, **141–142** (2001), 541–548

[28] J. Ma, Y. Xu, et al., Preparation and mechanical properties of C/SiC composites with carbon fiber woven preform, *Materials Letters*, **61**(2007), 312–315

[29] F. Lamouroux, X. Bourrat, and R. Naslain, Silicon carbide infiltration of porous C–C composites for improving oxidation resistance, *Carbon*, **33**(1995), 525–535

[30] Y. Xu, Y. Zhang, et al, Preparation and friction behavior of carbon fibre reinforced silicon carbide matrix composites, *Ceramic international*, **33** (2007), 439-445

[31] G. B. Zheng, H. Sano, et al., The properties of carbon fibre/SiC composites fabricated through impregnation and pyrolysis of polycarbosilane, *Journal of Materials Science*, **34** (1999), 827–834

[32] M. F. Gonon, S. Hampshire, Comparison of two processes for manufacturing ceramic matrix composites from organometallic precursors, *Journal of the European Ceramic Society*, **19** (1999), 285–291

[33] K. Masaki, T. Inoue, et al., , Consolidation of polymer-derived SiC matrix composites: process and microstructure, *Composite science and technology*, **62**(2002), 2179–2188

[34] J. Zhong, S. Qiao, et al, Rapid fabrication of C/C/SiC composite by PIP of HMDS, *Journal of Materials Processing Technology*, **190** (2007), 358–362

[35] F. I. Hurwitz, Pyrolytic conversion of methyl- and vinylsilanepolymers to Si-C ceramics, *Journal of materials science*, **30** (1995), 3130-3136

[36] Z. F. Zhang, F. Babonneau, *et al.,* Poly(methylsilane) — a high ceramic yield precursor to silicon carbide, *Journal of the American Ceramic Society,* **74** (1991) 670-673

[37] O. Delverdier, M. Monthioux, et al., Thermal behavior of polymer-derived ceramics. I. Si-C and Si-C-O systems from both commercial and new polycarbosilane (PCS) precursors *, Journal of the European Ceramic Society,* **12** (1993) 27-41

[38] M. Kawase, T. Tago, et al. Chemical vapor infiltration and deposition to produce a silicon carbide-carbon functionally gradient material, *Chemical Engineering Science*, **54** (1999), 3327-3334

[39] W. Krenkel, Carbon fibre reinforced CMC for high performance structures*, International Journal of applied ceramic technology*, **1**(2004), 188-200

[40] C. Zuber, B. Heidenreich, Development of a net shape manufacturing method for ventilated brake discs in single piece design, *Materialwiss. u. Werkstofftech.* **37**(2006),301-308

[41] S. Fan, L. Zhang, et al., Microstructure and tribological properties of advanced carbon/silicon carbide aircraft brake materials, *Composites science and technology*, **68** (2008), 3002-3009

[42] J. Nie, Y. Xu, et al., Microstructure, thermophysical and ablative performances of a 3D needled Cf/C-SiC composite, *International Journal of applied ceramic technology*, **7**(2010), 197-206

[43] H. A. El-Hija, W. Krenkel, et al., Development of Cf/C-SiC brake pads for high performance elevator*, International Journal of applied ceramic technology*, **2**(2005), 105-113

[44] G. H. Jang, K. H. Cho, et al., Tribological properties of Cf/C-SiC composites for brake discs, *Metal and materials international*, **16**(2010), 61-66

[45] P. Delhaes, Chemical vapor deposition and infiltration processes of carbon materials, *Carbon*, **40** (2002), 641–657

[46] X. Wei, L. Cheng, et al., Numerical simulation of effect of methyltrichlorosilane flux on isothermal chemical vapor infiltration process of C/SiC composites, *Journal of the American Ceramic Society*, **89**(2006), 2762–2768

[47] R. Naslain, Design, Preparation and properties of non-oxide CMCs for application in engines and nuclear reactors: an overview, *Composites Science and Technology,* **64** (2004) 155–170

[48] S. K. Rhee, M. G. Jacko and P. H. S. Tsang, The role of friction film in friction, wear and noise of automotive brakes, *Wear*, **146** (1991), 89-97

[49] A. Wirth, D. Eggleston, R. Whitaker, A fundamental tribochemical study of the third body layer formed during automotive friction braking, *Wear,* **179** (1994) 75–81.

[50] M. Eriksson, F. Bergman, S. Jacobson, Surface characterization of brake pads after running under silent and squealing conditions, *Wear*, **232** (1999) 163–167

[51] M. Eriksson, S. Jacobson, Tribological surfaces of organic brake pads, *Tribolgy International,* **33** (2000), 817–827

[52] M. G. Jacko, P. H. S. Tsang, S. K. Rhee, Wear debris compaction and friction film formation of polymer composites, *Wear*, **133** (1989), 23–38.

[53] Z. Li, P. Xiao, et al., Microstructure and properties of carbon fibre reinforced C/SiC dual matrix composites, *New carbon materials*, **25**(2010), 225-231

[54] P. J. Blau, H. M. Meyer, Characterization of wear particles produced during friction tests of conventional and unconventional disc brake material, *wear*, **255** (2003), 1261-1269

[55] M. Godet, The third-body approach: a mechanical view of wear, *Wear*, **100** (1984), 437–452

[56] S. F. Scieszka, Tribological phenomena in steel-composite brake material friction pairs, *Wear*, **64** (1980), 367–378

[57] W. Österle, I. Urban, et al., Correlations between surface modification and tribological performance of brake pads, *Surface Engineering,* **17** (2001), 123–125

[58] W. Österle, M. Griepentrog, et al., Chemical and microstructural changes induced by friction and wear of brakes, *Wear*, **251** (2001), 1469–1476.

[59] M. Eriksson, F. Bergman, et al., On the nature of tribological contact in automotive brakes, *Wear*, **252** (2002), 26–36

[60] P. Filip, M. A. Wright, Characterization of composite materials for automotive braking industry, *Practical Metallography,* **30** (1999), 449–456

[61] P. Filip, Z. Weiss, et al., On friction layer formation in polymer-matrix composite materials for brake applications, *Wear,* **252** (2002), 189–198.

[62] W. Österle, I. Urban, Friction layers and friction films on PMC brake pads, *Wear*, **257** (2004), 215–226

[63] W. Österle, I. Urban, Third body formation on brake pads and rotor, *tribology international*, **39** (2006), 402-408

[64] W. Österle, H. Kloss, et al., Towards a better understanding of brake friction materials, *Wear*, **263** (2007), 1189-1201

[65] M.Terheci, R.R. Manory, et al., The friction and wear of automotive grey cast iron under dry sliding conditions, part 2.-friction and wear-particle generation mechanisms and their progress with time, *Wear*, **185** (1995), 119-124

[66] T. A. Libsch and S. K. Lee, Microstructural changes in semimetallic disc brake pads created by low temperature dynamometer testing, *Wear*, **46**(1978), 203-212

[67] S. K. Rhee and R. T. Ducharme, The friction surface of grey cast iron brake rotor , *Wear*, **23** (1973), 271-273

[68] R. Hinrichs, M. A. Z. Vasconcellos, et al., A TEM snapshot of magnetite formation in brakes: The role of the disc's cast iron graphite lamellae in third body formation, *Wear*, **270**(2011), 365-370

[69] T. Liu and S. K. Rhee, High temperature wear of semimetallic disc brake pads. In W.A. Glaeser, K.C. Ludema, et al., preceding of internal conference on wear of materials, St. Louis, MO, April 25-28, 1977, American Society of Mechanical Engineers, New York, 1977, 552-554

[70] S. Zhang , F. Wang, Comparison of friction and wear performances of brake materials containing different amounts of ZrSiO4 dry sliding against SiCp reinforced Al matrix composites, *Materials Science and Engineering A,* **443** (2007) , 242–247

[71] S. Zhang, F. Wang, Comparison of friction and wear performances of brake material dry sliding against two aluminium matrix composites reinforced with different SiC particles, *Journal of Materials Processing Technology*, **182** (2007), 122–127

[72] A. T. Alpas and J. Zhang, Effect of SiC particulate reinforcement on the dry sliding wear of aluminium-silicon alloys (A356), *Wear*, **155** (1992), 83-104

[73] H. Nakanishi, Development of aluminum metal matrix composites (Al-MMC) brake rotor and pad , *JSAE Review*, **23** (2002), 365–370

[74] X. Y. Li and K. N. Tandon, Microstructural characterization of mechanically mixed layer and wear debris in sliding wear of an Al alloy and an Al based composite, *Wear*, **245** (2000), 148–161

[75] S. C. Tjong, S. Q. Wu, et al., Wear behavior of an Al-12% Si alloy reinforced with a low volum fraction of SiC particles, *Composites Science and Technology*, **57** (1997), 1551-1558

[76] I. Sallit, C. Richard, et al., Characterization methodology of a tribological couple: metal matrix composite/brake pads, *Materials characterization,* **40** (1998), 169-188

[77] R. K. Uyyuru, M. K. Surappa, et al., Tribological behavior of Al-Si-SiCp composites/automobile brake pad system under dry sliding condition, *Tribology international*, **20**(2007) 365-373

[78] G. Straffelini, M. Pellizzari, et al., Influence of load and temperature on the dry sliding behaviour of Al-based metal-matrix-composites against friction material, *Wear*, **256** (2004), 754–763

[79] K. Laden, J. D. Guérin, et al., Frictional characteristics of Al-SiC composite brake discs, *Tribology letter*, **8**(2000), 237-247

[80] G. J. Howell, A. Ball, Dry sliding wear of particulate-reinforced aluminium alloys against automobile friction materials, *Wear,* **181-183** (1995), 379-390

[81] H. Kasem, Fiber–matrix unbonding and plastic deformation in C/C composites under tribological loading, *Wear*, **269** (2010), 104–111

[82] H. Kasem, B. Sylvie, et al., Interdependence between wear process, size of detached particles and CO2 production during carbon/carbon composite friction, *Wear*, **263** (2007) 1220–1229

[83] S. Ozcan, P. Filip, Microstructure and Wear mechanisms in C/C composites, *Wear* **259**(2005), 642-650

[84] T. Chen, W. Gong, et al., Effect of fiber-type on braking behaviour of carbon-carbon composites, *Materials science and engineering A*, **441**(2006), 73-78

[85] S. Awashi, J. L. wood, C/C composites-materials for aircraft brakes, *Advanced ceramic material*, **3**(1998), 449-451

[86] T. J. Hutton, B. McEnaney, et al., Structural studies of wear debris from carbon–carbon composite aircraft brakes, *Carbon*, **37** (1999), 907–916

[87] C. P. Ju, K. J. LEE, low energy wear behaviour of polyacrylonitrile fiber-reinforced, pitch-matrix, carbon-carbon composites, *Carbon*, **32**(1994), 971-977

[88] N. Murdie, C. P. Ju, Microstructure of worn pitch/resin/CVI C-C composites, *Carbon*, **29**(1991), 335-342

[89] J. D. Chen, J. H. Chern Lin, C. P. Ju, Effect of humidity on the tribological behavior of carbon-carbon Composites, *Wear*, **249**(2011), 240-249

[90] J. D. Chen and C. P. Ju, Friction and wear of PAN/pitch, PAN/CVI and pitch/resin/CVI based carbon/carbon composites, *Wear,* **174** (1994) 129-135

[91] K. J. Lee, M. J. Tsai**,** et al.**,** Effect of densification parameters on the low-energy tribological behavior of carbon/carbon composites, *Carbon*, **48**(2010), 1353-1361

[92] T. Chen, W. Gong, et al., effect of fibre-types on braking behavior of carbon-carbon composites, *Materials Science and Engineering A,* **441**(2006), 73-78

[93] J. D. Chen, C. P. Ju, Effect of sliding speed on the tribological behavior of a PAN-pitch carbon-carbon composite, *Materials Chemistry and Physics*, **39**(1995), 174-179

[94] T. J. Hutton, D. Johnson et al., Effect of fibre orientation on the tribology of model carbon-carbon composite, *Wear*, **249** (2001), 647-655

[95] B. K. Yen, T. Ishihara, On temperature-dependent tribological regimes and oxidation of carbon-carbon composites up to 1800^{o}C, *Wear*, **196** (1996), 254-262

[96] K. J. Lee, J. H. Chern Lin and C. P. Ju, Electron Microscopic Study of worn PAN-Pitch based carbon-carbon composite, *Carbon*, **35**(1997), 613-620

[97] G. P. Ostermeyer, On the dynamics of the friction coefficient, *Wear*, **254**(2003), 852–858

[98] W. Österle, I. Urban, et al., Characterization and evaluation of the formation of friction layers during braking with conventional PMC friction material against a cast iron rotor. Proceedings 14th International Colloquium Tribology, Esslingen, German, in:

W. Bartz, Editor, *Technische Akademie Esslingen, Esslingen, Germany*, **1** (2004), 483–489

[99] M. Eriksson, J. Lord, et al., Wear and contact conditions of brake pads — dynamical in-situ studies of pad on glass. *Wear*, **249** (2001), 272-278

[100] M. H. Cho, K. H. Cho, et al., The roles of transfer layers on friction characteristics in the sliding interface between friction materials against gray cat iron brake discs, *Triology Letters*, **20** (2005), 101-108

[101] Z. Stadler, K. Krnel, et al., Friction behaviour of sintered metallic brake pads on a C/C-SiC composite brake disc, *Journal of European Ceramic Society*, **27**(2007), 1411-1417

[102] P. J. Blau, Friction and wear transitions of materials, U.S.A. Noyes Publications, Park Ridge, New Jersy, 1989

[103] B. Bhushan, Introduction to Tribology, John Wiley& Sons, New York, Inc. 2002

[104] K. W. Hee, P. Filip, Performance of ceramic enhanced phenolic matrix brake lining materials for automotive brake linings, *Wear*, **259** (2005), 1088-1096

[105] L. Gudmand-Høyer, A. Bach, et al., Tribological properties of auto motive disc brakes with solid lubricants, *Wear*, **232** (1999), 168-175

[106] A. Ravikiran and M. K. Surappa, Osillations in coefficient of friction during dry sliding of A356 Al-30% wt SiC- MMC against steel, *Scripta Mataialia*, **36** (1997), 95-98,

[107] H. J. Zhou, S. M. Dong, et al., Friction and wear properties of 3D carbon/silicon carbide composites prepared by liquid silicon infiltration, *Tribology Letters*, **37** (2010), 337–341

[108] C. Zollfrank, H. Sieber, Microstructure evolution and reaction mechanism of Biomorphous SiSiC Ceramic, *Journal of the American Ceramic Society*, **88**(2005), 51-58

[109] A. Leatherbarrow, H. Wu, Understanding the development of the microstructure inside C_f/C-SiC composites manufactured by liquid silicon infiltration, *Proceeding in the 7th International Conference on High Temperature Ceramic Matrix Composite (HT-CMC7)*, Bayreuth, Germany, 2010, 308-313

[110] A. Leatherbarrow, H. Wu, The nature of silicon carbide phases developed from different carbonaceous sources and its impact on the microstructure of C_f/C-SiC composites, In: *34th Advanced Processing and Manufacturing Technologies for Structural and Multifunctional Materials: Ceramic Engineering and science proceeding,* **31** (2010), 73-83

[111] JCPDS International center for diffraction data, Powder diffraction file, JCPDS International centre for diffraction data, Swarthmore

[112] R. T. Downs, M. Hall-Wallace, The american mineralogist crystal structure database, *American Mineralogist*, **88** (2003), 247-250

[113] T. B. Massalski, Binary alloy phase diagrams, 2nd edition, ASM International, Materials Park, Ohio (1990)

[114] Phase equalibria diagrams database version 3.1, National institute of standards and technology (NIST)

[115] A. Blomberg, An electron microscopy study of worn ceramic surfaces, *Tribology International*, **26** (1993), 369-381

[116] A. Mortimer, M. Nicholas, The wetting of carbon by copper and copper alloys, *Journal of Materials Science*, **5** (1970), 149-155

[117] P. Nikolopoulos, S. Agathopoulos, et al., Wettability and interfacial energies in SiC-liquid metal systems, *Journal of Materials Science*, **27** (1992), 139-145

[118] O. M. Akselsen, Review advances in brazing of ceramics, *Journal of Materials Science,* **27**(1992), 1989-2000

[119] P. Protsenko, O. Kozlova, et al., Dissolution wetting of Si by molten Cu*, Journal of Materials Science,* **43** (2008), 5669–5671

[120] Cambridge Engineering Selector Version 5.1.0., Granta Design Ltd., 2009.

[121] K. H. J. Buschow, R. W. Cahn et al., Encyclopaedia of materials: science and technology, Elsevier Science Ltd., 2001, 952–967

[122] R. F. Cook, B. R. Lawn, C. J. Fairbanks, Microstructure-strength properties in ceramics: I, Effect of crack size on toughness. *Journal of the American Ceramic Society,* **68**(1985), 604–615

[123] S. J. Bennison, B. R. Lawn, Role of interfacial grain-bridging sliding friction in the crack-resistance and strength properties of nontransforming ceramics. *Acta Metalialia*, **37**(1989), 2659–2671

[124] A. Leatherbarrow, H. Wu, Mechanical behaviour of the constituents inside carbon-fibre/carbon-silicon carbide composites characterized by nano-indentation, *Journal of the European Ceramic Society*, **32**(2011), 579-588

[125] S. J. Cho, B.J. Hockey, et al., Grain-size and R-curve effects in the abrasive wear of alumina, *Journal of the American Ceramic Society,* **72**(1989), 1249–1252

[126] B. R. Lawn, Fracture of brittle solids 2nd ed, Cambridge University Press, Cambridge, U.K, 1993, 319–324

[127] D. Hull, T. W. Clyne, An introduction to composite materials, Cambridge solid state science series 2nd ed., Cambridge University Press, Cambridge,1996,147–153

[128] P. Porouz, P. M. Hazzleding, Cross-slip and twining in semiconductors, *Scripta Metallurgica,* **25**(1991), 1167-1172

[129] P. Porouz, Deformation mode in Si, slip or twining? *Scripta Metallurgica,* **21**(1987), 1463-1468

[130] P. Porouz, J. W. Yang, Polytypic transformation in SiC: the role of TEM, *Ultramicroscopy*, **51**(1993), 189-214